Human Papillomavirus Hijacks the Dual Endosome-Golgi Membrane Systems During Cell Entry

by

Mara Calypso Harwood

A dissertation submitted in partial fulfillment
of the requirements for the degree of
Doctor of Philosophy
(Cellular and Molecular Biology)
in the University of Michigan
2023

Doctoral Committee:

Professor Billy Tsai, Chair
Associate Professor Diane Fingar
Professor Emerita Roberta Fuller
Associate Professor Andrew Tai

Mara Calypso Harwood

mcalypso@umich.edu

ORCID iD: 0000-0003-4976-8400

Dedication

To the viruses of my youth.

Acknowledgements

Thanks to Dr. Billy Tsai for always being there (literally… always in the lab). Bill's approachable excitement for science and ability to explain anything as a sketch on the whiteboard is hard to beat. There are many lessons Bill has taught me. Some that come to mind:

1. Don't over complicate things.
2. One can never have too much grant money.
3. Always celebrate accomplishments with a big lab lunch.
4. An entire email can be written in the subject line (see number 1).
5. How to layer the perfect sucrose gradient.
6. You can mope for one day, then get back to work.
7. Don't worry about what other people think, they probably aren't thinking about you.
8. It's not a party without an extreme obstacle course.
9. Always draw a model (see number 1).
10. Don't hold a grudge (unless it's reviewer #1).
11. If something isn't working, move on and try another approach tomorrow.
12. Khaki shorts are appropriate 8 months of the year in Michigan (see number 1).

As the above list suggests, Bill sets an example by being unapologetically himself. He is rarely intimidating (although I hear he is a black belt?), and I've felt comfortable asking him many silly questions without fear of sounding stupid. Thank you, Bill, for giving me a safe place to try new things that cost thousands of dollars, for listening to my unsolicited opinions, and for literally always being there.

Thanks to Team HPV: Dr. Takamasa Inoue, Dr. Allison Dupzyk, Kaitlyn Speckhart, and Dr. Tai-Ting Woo. I truly couldn't ask for better teachers and teammates. This dissertation would not be possible without the four of you. Also thank you to Dr. Dan DiMaio and his lab,

especially Dr. Yuka Takeo, for their HPV expertise, experimental contributions, and persistence with getting our papers submitted!

To every single Tsai Lab member I have been lucky enough to overlap with: Dr. Yu-Jie (Jay) Chen, Dr. Tai-Ting Woo, Jeffrey Williams, Jeffrey Knupp, Madison Pletan, Kaitlyn Speckhart, Grace Cha, Ethan Houck, and Dr. Riya Sarkar; and former members: Dr. Chelsey Spriggs, Dr. Allison Dupzyk, Dr. Corey Cunningham, Dr. Parikshit Bagchi, Dr. Xiaofang Liu, Aaron Chang, and Ellen James. You have all helped in your own ways: answering my little lab questions, de-stressing over coffee, making birthday cupcakes, diluting Bill's attention when I didn't have data, laughing through socially-distanced mid-pandemic drinks in the park, always telling me my dogs are cute, and generally making sure the lab doesn't completely fall apart!

Thank you to Dr. Jared Young for inviting me into your lab and believing in me when I was an undergraduate student at Mills College. Your patience and graciousness are unmatched! I am so lucky to call you my first research mentor – you were the first person to describe what getting a PhD in biology might actually be like, and to tell me I would be good at it. Thank you for writing regularly and honestly to this day. The team of undergraduate scientists you helped lead at Mills is still one of the best teams I've been a part of.

Thank you to my parents: you have supported my education every single step of the way. Thank you for telling me to be brave, and always funding a plane ticket when I needed one. Mom, thank you for sending cross-country care packages I insist on not needing (I need them). Dad, thank you for visiting me every spring break and putting the best dad-jokes in the family chat. You both instilled in me a love for nature and the sense of awe that comes from studying natural sciences.

Casey and Deema, I probably wouldn't be at Michigan without you! Casey, you gave me permission to apply to grad school instead of taking the MCAT, and were always an amazing big brother even when I was being a brat. Deema, you were my first friend in Michigan and helped me get through some tough times with zero-judgement. If I make a mistake, I can always count on one of you knowing how to fix it, with all your many, many tools.

To Dr. Alexander Kukreja: I know what FRET is now. You sat through every practice talk, read every paper, listened to every complaint, and celebrated every success with me. More importantly, you helped foster my sense-of-self outside of grad school. Thank you for taking me to concerts, trudging along my hikes, trading podcasts, being a goofball, sharing my secrets, and most recently helping shatter the mold for what a loving cross-Atlantic partnership can look like.

Last of all, thank you to Ruby Roo and Eddie Vedder. Because you can't read, I'll leave it at this: with dogs you are never alone. I love you.

Chapters 1, 2, and 3 are all multi-author publications with contributions by Dr. Chelsey Spriggs, Dr. Allison Dupzyk, Dr. Takamasa Inoue, Dr. Tai-Ting Woo, Dr. Yuka Takeo, and Dr. Daniel DiMaio. Specific data contributions are indicated in the Author Contributions section of each chapter. Funding sources are indicated in the Acknowledgements section of each chapter.

Table of Contents

List of Tables

List of Figures

Abstract

Human papillomavirus (HPV) is a common human pathogen, infecting the majority of individuals by adulthood. Although most HPV infections resolve spontaneously, persistent infection with certain HPV types contributes to cervical, anogenital, and oropharyngeal cancers, and is also responsible for a wide variety of warts. Despite the significant impact of HPV on human health, many details of its cellular entry mechanism remain a mystery.

From the host cell surface, HPV is internalized by endocytosis, delivered to the endosome, and then transported to the Golgi apparatus. Upon mitosis, HPV exits the Golgi and enters the nucleus during mitotic nuclear envelope breakdown. Once in the nucleus, the viral genome is delivered to the nucleoplasm and replication ensues. Throughout this process, HPV remains largely protected within organelles and transport vesicles, presumably to avoid detection by the host cell. How then does HPV direct itself along the proper route for infection? This dissertation provides a mechanistic roadmap for how HPV transits two distinct organelles – the endosome and the Golgi – en route to the nucleus to establish infection, with particular focus on the oncogenic HPV type 16 (HPV16).

Specifically, this dissertation demonstrates how the cytosolic protein p120 catenin targets HPV to the endosomal membrane protein γ-secretase. This is a critical step because γ-secretase promotes insertion of the viral capsid protein L2 across the endosome membrane. Membrane insertion exposes a portion of L2 to the cytosol, enabling this viral protein to recruit cytosolic sorting factors that target the virus to the Golgi en route for infection. Hence, these studies

identify a new host factor, p120 catenin, that facilitates the recruitment of a viral protein to the host γ-secretase, a key event that drives the virus along a productive entry pathway.

Upon Golgi arrival, HPV must transit this complex organelle to cause infection. This dissertation reveals the mechanism by which HPV transits the Golgi apparatus – by directly engaging the COPI sorting complex. Direct binding of HPV to the COPI retrograde sorting complex is essential for HPV to exit the Golgi and reach the nucleus. Though COPI is a highly conserved cellular complex, this is the first evidence of a virus that acts as a cargo for COPI during viral entry. These studies provide mechanistic insight into how HPV hijacks classic retrograde trafficking machinery to support its own vesicular transport through the Golgi.

CHAPTER 1:
An Introduction to How HPV Hijacks Host Machineries to Cause Infection

With permission from the publisher, portions of this chapter have been adapted from a previous publication:

How non-enveloped viruses hijack host machineries to cause infection

Chelsey C. Spriggs[†], Mara C. Harwood[†], and Billy Tsai. (2019).

Advances in virus research, 104, 97–122. https://doi.org/10.1016/bs.aivir.2019.05.002;

[†]co-first authors

1.1 Abstract

Viruses must navigate the complex endomembranous network of the host cell to cause infection. In the case of a non-enveloped virus that lacks a surrounding lipid bilayer, internalization across the plasma membrane is not sufficient to cause infection. Rather, the virus must traverse organelle membranes along its intracellular journey towards the nucleus. One critical step of this process is exposure of the virus to the cytosol. This cytosolic exposure is achieved by viral penetration across a host endomembrane, ultimately enabling subsequent trafficking steps and nuclear delivery of the virus to initiate infection. Precisely how this is accomplished varies between distinct non-enveloped DNA viruses, with each exploiting slightly different machinery for membrane penetration and intracellular trafficking. These processes not

only illuminate a highly-coordinated interplay between non-enveloped viruses and their host, but may provide new strategies to combat non-enveloped virus-induced diseases.

1.2 Introduction

To cause infection, a virus typically binds to a receptor displayed on the surface of the host cell (*1, 2*). This engagement triggers receptor-mediated endocytosis, initiating a complex journey for the viral particle through the highly inter-connected cellular endomembrane network (*3*). Transport via this network, which includes the endosome, lysosome, Golgi, and endoplasmic reticulum (ER), can lead to either non-productive or productive infection. In a non-productive infection, the virus is delivered to an organelle where it is either trapped or becomes degraded by a protease. By contrast, for productive infection to take place, the virus instead must be directed down a pathway that enables it to penetrate a membrane barrier so that it can reach the cytosol or the nucleus, which is essential for successful infection (*4*). The strategies devised by viruses as they exploit the myriad of host intracellular transport machineries and membrane penetration apparatus to promote infection, which are unique and vary widely, are often dependent on the physical properties of the viral particle.

One critical property of a virus that governs its productive entry route is the presence or absence of a lipid bilayer surrounding the viral particle. A virus encased within a lipid bilayer is called an enveloped virus, while a virus lacking this bilayer is called a non-enveloped virus. An enveloped virus, such as the human immunodeficiency virus (HIV) (*5*) or influenza virus (*6*), penetrates at either the plasma membrane or the endosome membrane of the host. Membrane penetration is accomplished when the viral and host membrane fuse, thereby delivering the core viral particle into the cytosol to promote infection (*7, 8*).

By contrast, as a lipid bilayer does not surround a non-enveloped virus, its membrane penetration mechanism must be fundamentally distinct from an enveloped virus. Although the precise molecular basis by which a non-enveloped virus penetrates a host membrane remains

enigmatic, a more coherent understanding of this process is emerging (*9-11*). The first step is delivery of the viral particle to the membrane penetration site. For a non-enveloped virus, this typically begins with receptor-mediated endocytosis to deliver the virus from the cell surface into an endocytic compartment. The virus then co-opts intracellular transport machineries to reach the proper organelle it will penetrate, such as the endosome, Golgi, or ER. Next, upon reaching the specific membrane penetration site, cellular cues such as low pH, receptors, proteases, or chaperones, impart critical conformational changes to the virus (*12*). This results in formation of a hydrophobic viral intermediate capable of penetrating the limiting membrane (*13-16*). In some cases, the viral particle may interact with host factors to facilitate membrane penetration (*17, 18*), or the virus may release lytic factors to aid in its membrane penetration (*19*). In the final step, depending on the specific penetration site, host factors are recruited to extract the virus into the cytosol or nucleus to complete the penetration process (*20, 21*).

This dissertation focuses on clarifying the molecular entry mechanisms of human papillomavirus (HPV), a common non-enveloped DNA virus. HPV membrane penetration occurs in two steps. Following endocytosis to the endosome, HPV first initiates membrane penetration by partially inserting a viral capsid protein across the endosomal membrane. With a portion of the virus exposed to the cytosol, HPV is further targeted to the Golgi apparatus. During mitosis, Golgi membrane fragmentation generates Golgi-derived vesicles (GDVs) harboring HPV. These GDVs in turn gain access to the nucleus due to nuclear envelope breakdown at the onset of mitosis. Within the nucleus, HPV completes membrane penetration across the GDV membrane, fully depositing the viral particle into the nucleoplasm to enable infection.

1.3 Human papillomavirus is a common disease-associated infection

HPV is the most common sexually transmitted infection in the United States (*22*). To date, there are 229 HPV types documented by the International HPV Reference Center (*23*). HPV types are classified by the sequence homology of the viral capsid protein L1, with each type having at least 10% sequence dissimilarity in the L1 gene (*24, 25*).

There are at least 14 oncogenic "high-risk" HPV types (HPV16, 18, 31, 33, 35, 39, 45, 51, 52, 56, 58, 59, 66, 68), as defined by their ability to infect mucosal epithelia of the oral and anogenital tract and their carcinogenic potential (*26, 27*). While most HPV infections resolve within 2 years, persistent infection with high-risk HPV types can cause cervical, anogenital, and oropharyngeal cancers (*28*).

The vast majority of HPV types are considered "low-risk", or non-oncogenic (*29*). These HPV types primarily infect cutaneous epithelial cells and are responsible for nearly all cases of warts, including plantar warts, palmar warts, and anogenital warts (*30*). However, some low-risk HPV types are associated with cancer if infection is not resolved, such as in the case of persistent laryngeal papillomas caused by HPV11 (*29*). Other pathologies linked to HPV include epidermodyplasia verruciformis (EV), a rare skin condition associated with HPV5 (*31*). Some skin cancers are also linked to HPV infections, while many HPV types have no known clinical manifestations (*30*).

High-risk HPV causes cellular transformation primarily through the persistent expression of the viral oncoproteins E6 and E7, which bind and degrade the cellular tumor suppressors p53 and pRb respectively (*28*), driving cell cycle entry and cellular proliferation (*30*). Although low risk HPVs also express E6 and E7, they bind weakly to p53 and pRb and do not degrade these proteins, producing limited effects on cellular transformation pathways (*28, 30*).

Comparative studies of high-risk and low-risk HPVs have focused largely on E6 and E7 oncoproteins (*32*). However, entry and trafficking mechanisms mediated by the viral capsid proteins may also differ between high- and low-risk HPV types (*33*). Despite HPV's significant impact on human health, there is limited understanding of how different HPV types enter cells to establish infection. Because HPV16 is responsible for the majority of HPV associated cancer (*28, 30*), this dissertation focuses on HPV16 cellular entry events, and key experimental data are further validated using HPV18 and HPV5.

1.4 Hijacking the dual endosome-Golgi membrane systems during HPV cell entry

1.4.1 Cell surface binding and entry to the endosome

Structurally, HPV is composed of the L1 and L2 capsid proteins. The L1 major capsid protein forms an icosahedral outer shell of 72 pentamers. Harbored within the L1 pentamers is the L2 minor coat protein. These viral proteins encapsulate an 8-kilobase-pair, double-stranded DNA genome (*34*). The viral genome encodes eight genes, some of which are necessary for cellular transformation (*35*).

Through miniscule wounds or abrasions, HPV infects the basal epithelial cells of cutaneous and mucosal tissues (*35*). To initiate infection, L1 directly binds to heparin sulfate proteoglycans (HSPGs) expressed at the surface of the host cell (*36, 37*). Following HSPG binding, L1 is cleaved by the serine protease KLK8, and L2 interacts with the peptidylprolyl isomerase cyclophilin B (*38, 39*). These steps result in exposure of L2 to the capsid surface, revealing a furin cleavage site at its N-terminus (*40*). While extracellular furin cleavage of L2 does not appear to be immediately essential for cell surface events, it is required to engage factors important at later steps of viral entry (*40*). Ultimately, the conformational changes of the viral capsid allow for transfer to an unknown entry receptor at the plasma membrane (Figure 1.1, step 1) (*41, 42*). The identity of the entry receptor and mode of endocytosis remains a point of contention. Numerous putative factors are thought to support cellular uptake of HPV, including integrins α6 and β4, as well as tetraspanins CD63 and CD151 (*43-46*). Annexin A2 and epidermal growth factor receptors have also been implicated in viral entry, though their contributions are less clear (*47-49*).

Further complicating the process, emerging evidence suggests that endocytosis of HPV is independent of clathrin-, caveolin-, cholesterol-, or dynamin-mediated endocytic mechanisms

(*50, 51*). Rather, HPV internalization appears to be guided by an actin-dependent mechanism related to macropinocytosis. In vitro, endocytosis of HPV occurs in a highly asynchronous fashion, with virions continually internalized from 2 to 20h after addition of virus to cell culture (*50*). This asynchrony may be a result of the multiple conformational changes and extracellular processing events required for HPV entry. In addition, this asynchrony suggests the presence of a secondary entry receptor as a limiting factor of viral uptake.

1.4.2 Membrane penetration

Upon internalization, HPV is delivered to the endosome. As the endosome matures and acidifies, L1 and L2 begin to dissociate in a pH-dependent manner (*13*). Proper dissociation and early endocytic trafficking of the virus also appears to involve cyclophilin B (*52*), tetraspanin CD63, syntenin-1, and the ESCRT protein ALIX (*53*), as well as interaction with sorting nexin 17 (*54*). The extent to which L1-L2 disassembles at the endosome is unclear, as emerging evidence suggests that a subset of L1 remains associated with L2 and the viral genome through later trafficking steps (*55*).

The initial membrane penetration of HPV to the cytosol occurs at the endosomal membrane. HPV differs from other non-enveloped DNA viruses in that the entire viral particle never reaches the cytosol; instead, HPV exposes the C-terminal portion of its L2 capsid protein to the cytosol, while its N-terminal portion remains complexed to the viral DNA within the endosomal lumen (Figure 1.1, step 2) (*56, 57*). To achieve this topology, L2 must physically insert into the endosomal membrane. Although this topology is in principle possible because L2 contains a cell-penetrating peptide (CPP) and a transmembrane-like domain, how L2 is inserted into the endosomal membrane remains largely mysterious (*14, 58*).

A clue to this enigma was recently revealed when the transmembrane protease γ-secretase was shown to act as a chaperone, promoting insertion of L2 into the endosomal membrane in a pH-dependent manner (*17*). Proper membrane insertion of L2 by γ-secretase is a critical step, as mutation of L2's transmembrane-like domain, or of γ-secretase itself, terminates productive infection (*17, 58*). The molecular basis by which γ-secretase promotes membrane penetration of L2 remains unclear. Despite the well-established proteolytic activity of this transmembrane protease, cleavage of L2 by γ-secretase is not required to promote HPV infection—only γ-secretase-induced membrane insertion of L2 is essential (*17*). Thus, HPV appears to exploit a novel chaperone function of γ-secretase, a phenomenon further explored in Chapter 2 of this dissertation.

γ-secretase-dependent insertion of L2 is a decisive step of HPV infection, as it diverts the virus away from the non-productive lysosomal pathway and instead targets HPV along the productive route (*17, 59*). Specifically, with a portion of L2 now exposed to the cytosol, it engages the cytosolic retromer sorting complex (*60, 61*). Retromer normally functions to sort a cellular cargo from the endosome to the Golgi apparatus. HPV hijacks this retrograde transport function of the retromer, allowing for the endosome-localized virus to be delivered to the Golgi apparatus (Figure 1.1, step 3) (*59, 61, 62*).

1.4.3 Golgi transit

Upon reaching the Golgi, the viral DNA remains shielded from the cytosol within the Golgi lumen, with only L2 protruding into the cytosolic space. HPV remains in the Golgi until the onset of mitosis, when this organelle fragments to form Golgi-derived vesicles (GDVs) (*63, 64*). HPV takes advantage of Golgi fragmentation by budding off into GDVs, thus escaping the

Golgi while still remaining protected within a membrane (Figure 1.1, step 4) (*65*). As mitosis progresses, the HPV-harboring vesicles are transported towards the nuclear region, where the virus appears to colocalize with the centrosome (*65, 66*). This trafficking step is thought to involve dynein-mediated transport, though additional evidence is required to support this observation (*67, 68*). Chapter 3 of this dissertation further investigates the mechanism by which HPV achieves Golgi transit and the nature of the Golgi-derived vesicles.

1.4.4 Nuclear import

With the concomitant nuclear envelope breakdown (NEB) during mitosis (*64*), the HPV-harboring vesicles gain entry to the nucleus (*63, 66*). In this manner, HPV is thought to accesses the nucleus without engaging the nuclear pore complex. The virus-harboring vesicles associate with the condensed chromosomes of the host cell (*65, 66*). During this highly dynamic process, it is unclear how HPV anchors itself in the nucleus. One possibility is that the virus directly binds to the mitotic chromosomes through a chromatin binding domain on L2 (*66, 69*). Alternatively, L2 might actively target the viral DNA to promyelocytic leukemia nuclear bodies of the host cell (*21, 70*). As a third option, an unidentified nuclear host factor may help target and retain the viral complex at the nucleus during specific stages of mitosis. Though L2 appears to contain nuclear localization signals (NLSs) (*71*), the functional significance of these signals during infection remains to be addressed.

Upon completion of mitosis, when the nuclear envelope reforms, the HPV-harboring vesicle is effectively trapped within the nucleus (*65, 66, 72*). How L2 and the viral genome fully translocate across the protective vesicular membrane into the nucleoplasm is entirely unknown

(Figure 1.1, step 5). In fact, the presence of cargo-transport vesicles within the nucleus is itself a unique phenomenon, with no previously described examples.

What mechanism might translocate and expose the viral genome to the nucleoplasm? There is minimal evidence that nuclear phospholipases could play a role in degrading the vesicular membrane (*60, 63*). Furthermore, whether L2 executes a function in exposing the viral DNA is not known. Coordinating nuclear entry and viral DNA translocation with mitotic NEB appears to be unique to HPV among non-enveloped viruses, though some enveloped viruses such as the murine-leukemia virus are known to rely on NEB as well (*73*). Regardless, upon nuclear exposure of HPV's genome, host cell machinery initiates viral transcription and replication, thereby promoting infection.

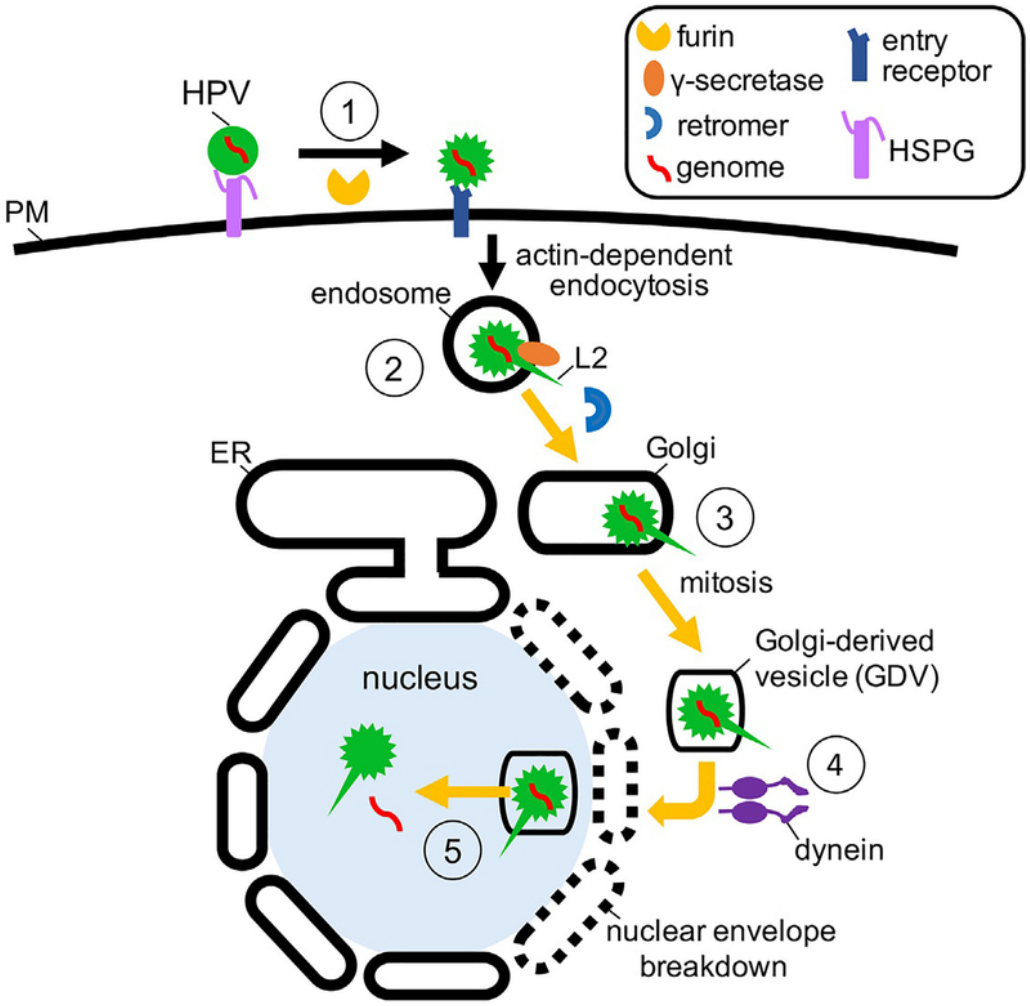

Figure 1.1: Hijacking the dual endosome-Golgi membrane systems during HPV cell entry
*To initiate infection, HPV attaches to HSPGs on the cell surface, resulting in conformational changes to the virus that enable furin-cleavage of L2 and subsequent transfer of the virus to an unknown entry receptor (**step 1**). The virus is then endocytosed by an actin-dependent mechanism to reach the endosome. As the endosome matures, the viral capsid proteins dissociate in a pH-dependent manner, and L2 engages γ-secretase. The C-terminus of L2 is then inserted across the endosomal membrane by γ-secretase, with the N-terminus remaining complexed to the viral DNA within the endosomal lumen (**step 2**). From here, the cytosolic portion of L2 engages retromer, and the virus is trafficked to the Golgi apparatus (**step 3**). Golgi fragmentation during mitosis generates HPV-harboring vesicles, which are thought to undergo dynein-mediated transport toward the nucleus (**step 4**). With the concomitant breakdown of the nuclear envelope during mitosis, the HPV-harboring vesicles enter the nucleus, where they remain intact until completion of mitosis and nuclear envelope reformation. Through an unknown mechanism, the viral genome is exposed to the nucleoplasm, and viral replication ensues (**step 5**).*

1.5 Conclusion and future directions

In order to cause infection, viruses must navigate the complex intracellular environment of their host cells to reach the cytosol or nucleus where replication occurs. How this is achieved can vary greatly among non-enveloped DNA viruses. In the case of HPV, the virus must insert a portion of its viral capsid protein across the host endosomal membrane so that it may access cytosolic sorting factors, which aid in subsequent trafficking steps.

The study of how non-enveloped viruses co-opt cellular membrane penetration apparatus and transport machineries has revealed much about how these viruses infect cells, but several questions remain. For instance, how does HPV hijack γ-secretase activity to promote penetration of the endosome membrane? Probing these phenomena will provide critical insights into the trafficking functions of both HPV and γ-secretase. Although it is not the only non-enveloped DNA virus to pass through the Golgi during entry (*74*), HPV is unique in its method of budding from the Golgi in Golgi-derived vesicles. How is this achieved, and what is the nature of these vesicles? Furthermore, HPV's genome remains in a protective vesicle throughout nuclear entry. How the viral genome egresses from the transport vesicles into the nucleoplasm remains largely unexplored.

The leveraging of both new and traditional techniques will be instrumental in addressing these outstanding questions. For instance, with increasing advances in high-resolution microscopy techniques, these state-of-the-art imaging approaches could be used to resolve the formation and structure of the HPV-containing Golgi-derived vesicles. Along the same lines, sophisticated microscopy methods may illuminate how γ-secretase mediates HPV insertion, as well as how the viral DNA is translocated across the limiting membrane upon arrival in the nucleus. Because identifying additional host factors involved in viral entry is a critical objective

in clarifying the infection mechanisms of non-enveloped viruses, ongoing proteomic advances may aid in this endeavor. For example, biotin-proximity labeling (BioID) can be used to screen for relevant protein-protein interactions, and if coupled with mass-spectrometry, may reveal even the most transient of associations (*75, 76*). In addition to modern methods, however, the use of classical biochemical techniques is still very much needed. In particular, developing in vitro assays to reconstitute viral entry events will clarify the precise molecular mechanisms of these processes, which is imperative for answering these questions.

Even still, perhaps the greatest and most deliberated question remains. Why has HPV devised its unique and specific entry strategy to reach the nucleus to cause infection? It is possible that the unique characteristics of the HPV viral particle necessitate a selective path during entry: acidification in the endosome to allow for interaction with γ-secretase, a cell-penetrating motif to allow for membrane penetration of the capsid protein, or perhaps a Golgi-dependent action that has yet to be uncovered. While we can only speculate on the reasons, one thing that is certain is that after many years of viral evolution, these distinctions provide us the best clues to understanding and preventing virus infection and are only waiting to be discovered.

1.6 Acknowledgements

M.C.H. is supported by NIH (T32-GM007315). C.C.S. is supported by the National Institutes of Health (NIH) (T32-AI007528). B.T. is funded by the NIH (RO1-AI064296).

With permission from Elsevier, portions of this chapter have been adapted from an original publication: *How non-enveloped viruses hijack host machineries to cause infection. Chelsey C. Spriggs†, Mara C. Harwood†, and Billy Tsai. (2019). Advances in virus research, 104, 97–122. https://doi.org/10.1016/bs.aivir.2019.05.002; †co-first authors.*

1.7 References

1. A. Helenius, Virus Entry: Looking Back and Moving Forward. *J Mol Biol* **430**, 1853-1862 (2018).

2. J. Mercer, M. Schelhaas, A. Helenius, Virus entry by endocytosis. *Annu Rev Biochem* **79**, 803-833 (2010).

3. J. Staring, M. Raaben, T. R. Brummelkamp, Viral escape from endosomes and host detection at a glance. *J Cell Sci* **131**, (2018).

4. U. F. Greber, Virus and Host Mechanics Support Membrane Penetration and Cell Entry. *J Virol* **90**, 3802-3805 (2016).

5. G. B. Melikyan, HIV entry: a game of hide-and-fuse? *Curr Opin Virol* **4**, 1-7 (2014).

6. S. T. Smrt, J. L. Lorieau, Membrane Fusion and Infection of the Influenza Hemagglutinin. *Adv Exp Med Biol* **966**, 37-54 (2017).

7. J. J. Skehel, D. C. Wiley, Receptor binding and membrane fusion in virus entry: the influenza hemagglutinin. *Annu Rev Biochem* **69**, 531-569 (2000).

8. W. Weissenhorn *et al.*, Structural basis for membrane fusion by enveloped viruses. *Mol Membr Biol* **16**, 3-9 (1999).

9. C. S. Kumar, D. Dey, S. Ghosh, M. Banerjee, Breach: Host Membrane Penetration and Entry by Nonenveloped Viruses. *Trends Microbiol* **26**, 525-537 (2018).

10. C. L. Moyer, G. R. Nemerow, Viral weapons of membrane destruction: variable modes of membrane penetration by non-enveloped viruses. *Curr Opin Virol* **1**, 44-49 (2011).

11. B. Tsai, Y. Ye, T. A. Rapoport, Retro-translocation of proteins from the endoplasmic reticulum into the cytosol. *Nat Rev Mol Cell Biol* **3**, 246-255 (2002).

12. Y. Yamauchi, U. F. Greber, Principles of Virus Uncoating: Cues and the Snooker Ball. *Traffic* **17**, 569-592 (2016).

13. J. L. Smith, S. K. Campos, A. Wandinger-Ness, M. A. Ozbun, Caveolin-1-dependent infectious entry of human papillomavirus type 31 in human keratinocytes proceeds to the endosomal pathway for pH-dependent uncoating. *J Virol* **82**, 9505-9512 (2008).

14. P. Zhang, G. Monteiro da Silva, C. Deatherage, C. Burd, D. DiMaio, Cell-Penetrating Peptide Mediates Intracellular Membrane Passage of Human Papillomavirus L2 Protein to Trigger Retrograde Trafficking. *Cell* **174**, 1465-1476 e1413 (2018).

15. E. K. Rainey-Barger, B. Magnuson, B. Tsai, A chaperone-activated nonenveloped virus perforates the physiologically relevant endoplasmic reticulum membrane. *J Virol* **81**, 12996-13004 (2007).

16. K. Chandran, D. L. Farsetta, M. L. Nibert, Strategy for nonenveloped virus entry: a hydrophobic conformer of the reovirus membrane penetration protein micro 1 mediates membrane disruption. *J Virol* **76**, 9920-9933 (2002).

17. T. Inoue *et al.*, gamma-Secretase promotes membrane insertion of the human papillomavirus L2 capsid protein during virus infection. *J Cell Biol* **217**, 3545-3559 (2018).

18. P. Bagchi, X. Liu, W. J. Cho, B. Tsai, Lunapark-dependent formation of a virus-induced ER exit site contains multi-tubular ER junctions that promote viral ER-to-cytosol escape. *Cell Rep* **37**, 110077 (2021).

19. C. M. Wiethoff, H. Wodrich, L. Gerace, G. R. Nemerow, Adenovirus protein VI mediates membrane disruption following capsid disassembly. *J Virol* **79**, 1992-2000 (2005).

20. A. Dupzyk, B. Tsai, Bag2 Is a Component of a Cytosolic Extraction Machinery That Promotes Membrane Penetration of a Nonenveloped Virus. *J Virol* **92**, (2018).

21. L. Guion, M. Bienkowska-Haba, S. DiGiuseppe, L. Florin, M. Sapp, PML nuclear body-residing proteins sequentially associate with HPV genome after infectious nuclear delivery. *PLoS Pathog* **15**, e1007590 (2019).

22. C. L. Satterwhite *et al.*, Sexually transmitted infections among US women and men: prevalence and incidence estimates, 2008. *Sex Transm Dis* **40**, 187-193 (2013).

23. International Human Papillomavirus Reference Center. "Human papillomavirus reference clones." *International Human Papillomavirus Reference Center,* Karolinska Institutet, https://www.hpvcenter.se/human_reference_clones/. Accessed 03-22-2023.

24. E. M. de Villiers, C. Fauquet, T. R. Broker, H. U. Bernard, H. zur Hausen, Classification of papillomaviruses. *Virology* **324**, 17-27 (2004).

25. H. U. Bernard *et al.*, Classification of papillomaviruses (PVs) based on 189 PV types and proposal of taxonomic amendments. *Virology* **401**, 70-79 (2010).

26. W. Arman, K. Munger, Mechanistic Contributions of lncRNAs to Cellular Signaling Pathways Crucial to the Lifecycle of Human Papillomaviruses. *Viruses* **14**, (2022).

27. E. Meites, J. Gee, E. R. Unger, L. E. Markowitz, Chapter 11: Human Papillomavirus, in *Epidemiology and Prevention of Vaccine-Preventable Diseases (Pink Book),* Centers for Disease Control and Prevention. Chap. 11, pp. 165-178 (2021).

28. M. Schiffman *et al.*, Carcinogenic human papillomavirus infection. *Nat Rev Dis Primers* **2**, 16086 (2016).

29. N. Egawa, J. Doorbar, The low-risk papillomaviruses. *Virus Res* **231**, 119-127 (2017).

30. J. Doorbar, N. Egawa, H. Griffin, C. Kranjec, I. Murakami, Human papillomavirus molecular biology and disease association. *Rev Med Virol* **25 Suppl 1**, 2-23 (2015).

31. S. J. de Jong *et al.*, Epidermodysplasia Verruciformis: Inborn Errors of Immunity to Human Beta-Papillomaviruses. *Front Microbiol* **9**, 1222 (2018).

32. A. J. Klingelhutz, A. Roman, Cellular transformation by human papillomaviruses: lessons learned by comparing high- and low-risk viruses. *Virology* **424**, 77-98 (2012).

33. N. Mistry, C. Wibom, M. Evander, Cutaneous and mucosal human papillomaviruses differ in net surface charge, potential impact on tropism. *Virol J* **5**, 118 (2008).

34. C. B. Buck *et al.*, Arrangement of L2 within the papillomavirus capsid. *J Virol* **82**, 5190-5197 (2008).

35. J. Doorbar, The papillomavirus life cycle. *J Clin Virol* **32 Suppl 1**, S7-15 (2005).

36. T. Giroglou, L. Florin, F. Schafer, R. E. Streeck, M. Sapp, Human papillomavirus infection requires cell surface heparan sulfate. *J Virol* **75**, 1565-1570 (2001).

37. K. F. Richards, M. Bienkowska-Haba, J. Dasgupta, X. S. Chen, M. Sapp, Multiple heparan sulfate binding site engagements are required for the infectious entry of human papillomavirus type 16. *J Virol* **87**, 11426-11437 (2013).

38. M. Bienkowska-Haba, H. D. Patel, M. Sapp, Target cell cyclophilins facilitate human papillomavirus type 16 infection. *PLoS Pathog* **5**, e1000524 (2009).

39. C. Cerqueira, P. Samperio Ventayol, C. Vogeley, M. Schelhaas, Kallikrein-8 Proteolytically Processes Human Papillomaviruses in the Extracellular Space To Facilitate Entry into Host Cells. *J Virol* **89**, 7038-7052 (2015).

40. R. M. Richards, D. R. Lowy, J. T. Schiller, P. M. Day, Cleavage of the papillomavirus minor capsid protein, L2, at a furin consensus site is necessary for infection. *Proc Natl Acad Sci U S A* **103**, 1522-1527 (2006).

41. P. M. Day, D. R. Lowy, J. T. Schiller, Heparan sulfate-independent cell binding and infection with furin-precleaved papillomavirus capsids. *J Virol* **82**, 12565-12568 (2008).

42. H. C. Selinka *et al.*, Inhibition of transfer to secondary receptors by heparan sulfate-binding drug or antibody induces noninfectious uptake of human papillomavirus. *J Virol* **81**, 10970-10980 (2007).

43. P. Aksoy, C. Y. Abban, E. Kiyashka, W. Qiang, P. I. Meneses, HPV16 infection of HaCaTs is dependent on beta4 integrin, and alpha6 integrin processing. *Virology* **449**, 45-52 (2014).

44. M. Evander *et al.*, Identification of the alpha6 integrin as a candidate receptor for papillomaviruses. *J Virol* **71**, 2449-2456 (1997).

45. K. D. Scheffer *et al.*, Tetraspanin CD151 mediates papillomavirus type 16 endocytosis. *J Virol* **87**, 3435-3446 (2013).

46. G. Spoden *et al.*, Clathrin- and caveolin-independent entry of human papillomavirus type 16--involvement of tetraspanin-enriched microdomains (TEMs). *PLoS One* **3**, e3313 (2008).

47. A. Dziduszko, M. A. Ozbun, Annexin A2 and S100A10 regulate human papillomavirus type 16 entry and intracellular trafficking in human keratinocytes. *J Virol* **87**, 7502-7515 (2013).

48. Z. Surviladze, A. Dziduszko, M. A. Ozbun, Essential roles for soluble virion-associated heparan sulfonated proteoglycans and growth factors in human papillomavirus infections. *PLoS Pathog* **8**, e1002519 (2012).

49. J. R. Taylor *et al.*, Heterotetrameric annexin A2/S100A10 (A2t) is essential for oncogenic human papillomavirus trafficking and capsid disassembly, and protects virions from lysosomal degradation. *Sci Rep* **8**, 11642 (2018).

50. M. Schelhaas *et al.*, Entry of human papillomavirus type 16 by actin-dependent, clathrin- and lipid raft-independent endocytosis. *PLoS Pathog* **8**, e1002657 (2012).

51. G. Spoden *et al.*, Human papillomavirus types 16, 18, and 31 share similar endocytic requirements for entry. *J Virol* **87**, 7765-7773 (2013).

52. M. Bienkowska-Haba, C. Williams, S. M. Kim, R. L. Garcea, M. Sapp, Cyclophilins facilitate dissociation of the human papillomavirus type 16 capsid protein L1 from the L2/DNA complex following virus entry. *J Virol* **86**, 9875-9887 (2012).

53. L. Grassel *et al.*, The CD63-Syntenin-1 Complex Controls Post-Endocytic Trafficking of Oncogenic Human Papillomaviruses. *Sci Rep* **6**, 32337 (2016).

54. M. Bergant Marusic, M. A. Ozbun, S. K. Campos, M. P. Myers, L. Banks, Human papillomavirus L2 facilitates viral escape from late endosomes via sorting nexin 17. *Traffic* **13**, 455-467 (2012).

55. S. DiGiuseppe, M. Bienkowska-Haba, L. G. M. Guion, T. R. Keiffer, M. Sapp, Human Papillomavirus Major Capsid Protein L1 Remains Associated with the Incoming Viral Genome throughout the Entry Process. *J Virol* **91**, (2017).

56. S. DiGiuseppe *et al.*, Topography of the Human Papillomavirus Minor Capsid Protein L2 during Vesicular Trafficking of Infectious Entry. *J Virol* **89**, 10442-10452 (2015).

57. N. Kamper *et al.*, A membrane-destabilizing peptide in capsid protein L2 is required for egress of papillomavirus genomes from endosomes. *J Virol* **80**, 759-768 (2006).

58. M. P. Bronnimann, J. A. Chapman, C. K. Park, S. K. Campos, A transmembrane domain and GxxxG motifs within L2 are essential for papillomavirus infection. *J Virol* **87**, 464-473 (2013).

59. W. Zhang, T. Kazakov, A. Popa, D. DiMaio, Vesicular trafficking of incoming human papillomavirus 16 to the Golgi apparatus and endoplasmic reticulum requires gamma-secretase activity. *mBio* **5**, e01777-01714 (2014).

60. A. Lipovsky *et al.*, Genome-wide siRNA screen identifies the retromer as a cellular entry factor for human papillomavirus. *Proc Natl Acad Sci U S A* **110**, 7452-7457 (2013).

61. A. Popa *et al.*, Direct binding of retromer to human papillomavirus type 16 minor capsid protein L2 mediates endosome exit during viral infection. *PLoS Pathog* **11**, e1004699 (2015).

62. P. M. Day, C. D. Thompson, R. M. Schowalter, D. R. Lowy, J. T. Schiller, Identification of a role for the trans-Golgi network in human papillomavirus 16 pseudovirus infection. *J Virol* **87**, 3862-3870 (2013).

63. I. Aydin *et al.*, Large scale RNAi reveals the requirement of nuclear envelope breakdown for nuclear import of human papillomaviruses. *PLoS Pathog* **10**, e1004162 (2014).

64. L. Champion, M. I. Linder, U. Kutay, Cellular Reorganization during Mitotic Entry. *Trends Cell Biol* **27**, 26-41 (2017).

65. S. DiGiuseppe *et al.*, Incoming human papillomavirus type 16 genome resides in a vesicular compartment throughout mitosis. *Proc Natl Acad Sci U S A* **113**, 6289-6294 (2016).

66. C. M. Calton *et al.*, Translocation of the papillomavirus L2/vDNA complex across the limiting membrane requires the onset of mitosis. *PLoS Pathog* **13**, e1006200 (2017).

67. L. Florin *et al.*, Identification of a dynein interacting domain in the papillomavirus minor capsid protein l2. *J Virol* **80**, 6691-6696 (2006).

68. M. A. Schneider, G. A. Spoden, L. Florin, C. Lambert, Identification of the dynein light chains required for human papillomavirus infection. *Cell Microbiol* **13**, 32-46 (2011).

69. I. Aydin *et al.*, A central region in the minor capsid protein of papillomaviruses facilitates viral genome tethering and membrane penetration for mitotic nuclear entry. *PLoS Pathog* **13**, e1006308 (2017).

70. P. M. Day, C. C. Baker, D. R. Lowy, J. T. Schiller, Establishment of papillomavirus infection is enhanced by promyelocytic leukemia protein (PML) expression. *Proc Natl Acad Sci U S A* **101**, 14252-14257 (2004).

71. S. Mamoor *et al.*, The high risk HPV16 L2 minor capsid protein has multiple transport signals that mediate its nucleocytoplasmic traffic. *Virology* **422**, 413-424 (2012).

72. P. M. Day *et al.*, Human Papillomavirus 16 Capsids Mediate Nuclear Entry during Infection. *J Virol* **93**, (2019).

73. S. Cohen, S. Au, N. Pante, How viruses access the nucleus. *Biochim Biophys Acta* **1813**, 1634-1645 (2011).

74. B. P. Dhungel, C. G. Bailey, J. E. J. Rasko, Journey to the Center of the Cell: Tracing the Path of AAV Transduction. *Trends Mol Med* **27**, 172-184 (2021).

75. D. I. Kim *et al.*, Probing nuclear pore complex architecture with proximity-dependent biotinylation. *Proc Natl Acad Sci U S A* **111**, E2453-2461 (2014).

76. D. I. Kim *et al.*, An improved smaller biotin ligase for BioID proximity labeling. *Mol Biol Cell* **27**, 1188-1196 (2016).

CHAPTER 2:
p120 Catenin Recruits HPV to γ-Secretase to Promote Virus Infection

With permission from the publisher, this chapter is adapted from a previous publication:

p120 catenin recruits HPV to γ-secretase to promote virus infection

Mara C. Harwood[†], Allison J. Dupzyk[†], Takamasa Inoue, Daniel DiMaio, and Billy Tsai. (2020).

PLoS pathogens, 16(10), e1008946. https://doi.org/10.1371/journal.ppat.1008946;

[†]co-first authors

2.1 Abstract

During internalization and trafficking, human papillomavirus (HPV) moves from the cell surface to the endosome where the transmembrane protease γ-secretase promotes insertion of the viral L2 capsid protein into the endosome membrane. Protrusion of L2 through the endosome membrane into the cytosol allows the recruitment of cytosolic host factors that target the virus to the Golgi en route for productive infection. How endosome-localized HPV is delivered to γ-secretase, a decisive infection step, is unclear. Here we demonstrate that cytosolic p120 catenin, likely via an unidentified transmembrane protein, interacts with HPV at early time-points during viral internalization and trafficking. In the endosome, p120 is not required for low pH-dependent disassembly of the HPV L1 capsid protein from the incoming virion. Rather, p120 is required for HPV to interact with γ-secretase – an interaction that ensures the virus is transported along a

productive route. Our findings clarify an enigmatic HPV infection step and provide critical insights into HPV infection that may lead to new therapeutic strategies against HPV-induced diseases.

2.2 Introduction

Human papillomavirus (HPV) infects nearly 80 million U.S. adults (*1*) and is the primary cause of cervical, anogenital, and oropharyngeal cancers (*2*). While efficacious prophylactic vaccines exist against 9 types of HPV (*2*), the vaccines have not been efficiently utilized, with over half the target population remaining unvaccinated in the U.S. (*3*). One consequence of underutilized HPV vaccines is the alarming increase in the number of HPV-associated oropharyngeal cancers, surpassing that of cervical cancers in the U.S. in recent years (*4*). Despite HPV's significant impact on human health, there is limited understanding of its cellular entry mechanisms leading to infection. Thus, identifying host factors essential for HPV infection may reveal novel targets for anti-viral therapy and remains an important objective in combating HPV-induced diseases.

Structurally, HPV is a nonenveloped virus composed of the viral capsid proteins L1 and L2 which encase the viral DNA genome (*5*). At the plasma membrane, L1 binds to extracellular heparin sulfate proteoglycans, resulting in a series of conformational changes to the viral capsid (*6-14*). The N-terminus of the L2 protein is then cleaved by furin at the cell surface (*15-17*), and the virus is subsequently transferred to an unknown entry receptor (*10, 18*). Through an unknown mechanism, the virus is then endocytosed (*19-21*). Immediately after endocytosis, HPV is delivered to the endosome, where some of the L1 and L2 molecules are disassembled from the incoming virus particle (*22, 23*).

In the endosome, the viral particle is targeted to a critical factor – the transmembrane protease γ-secretase (*24-27*). In addition to its well-characterized protease function (*28, 29*), our labs recently discovered that the catalytic subunit of γ-secretase, presenilin-1 (PS1), harbors a novel chaperone activity that promotes insertion of the C-terminus of L2 into the endosome

membrane (*24*). This insertion event enables this segment of L2 to protrude into the cytosol, a step mediated by a cell-penetrating peptide (CPP) on the C-terminus of the L2 protein (*30, 31*). Subsequently, host factors such as retromer and SNX17 are recruited to the cytosolic segment of L2, and the virus is guided to the Golgi en route to the nucleus for infection (*32-34*).

Targeting of HPV to γ-secretase for membrane insertion is a critical step because it directs HPV along an infectious route (*24*). However, it is not known how HPV is targeted to γ-secretase to engage this tightly-controlled host factor (*28*). One possible scenario is that HPV is recruited to γ-secretase by hijacking pre-existing "γ-secretase adaptors" (*28, 29*). One such factor is the cytosolic host protein p120 catenin (p120), which is known to target cell surface transmembrane proteins to γ-secretase for proteolytic processing (*35, 36*).

We report here that HPV interacts with cytosolic p120, likely via a transmembrane receptor, at the cell surface. Upon reaching the endosome, the virus undergoes low pH-dependent disassembly of the L1 protein in a step that does not require p120 or γ-secretase. However, p120 is essential for HPV to associate with γ-secretase. This allows for membrane insertion of L2 into the endosome membrane, a requisite step for productive trafficking. These findings provide important new insight into HPV entry, revealing how the virus hijacks γ-secretase – along with its adaptor – to promote infection.

2.3 Results

2.3.1 p120 binds to HPV16 and promotes virus infection

To study HPV internalization and trafficking, we used a well-established HPV pseudovirus (PsV) system consisting of wild-type (WT) viral capsid proteins L1 and L2 and a reporter plasmid expressing GFP protein with a C-terminal S-tag (GFP-S) or secreted luciferase (Luc) in place of the viral genome (Supplementary Figure 2.1A) (*37, 38*). A 3xFLAG epitope tag appended to the C-terminus of L2 (termed "L2F") allows for detection of the virus particle throughout the trafficking events (*25*). Importantly, key trafficking steps of the HPV PsV resemble that of HPV produced by stratified keratinocyte raft cultures (*37*). For instance, both raft-derived virus and PsV require γ-secretase for infection (*25-27*).

We recently used an immunoprecipitation-mass spectrometry (IP-MS) approach and found that WT HPV16.L2F (Luc) binds to γ-secretase during entry (*24*). In addition, the cytosolic host factor p120 catenin (p120) was significantly enriched in the virally-associated proteins identified by this approach, compared to proteins pulled down from uninfected cell extracts incubated with highly purified PsV (Figure 2.1A); the full IP-MS data set can be found in Supplementary Table 2.1. Interestingly, p120 is a known binding-partner of γ-secretase (*35, 36*). To confirm this IP-MS result (*24*), we used anti-FLAG antibody to immunoprecipitate the HPV16 L2 minor capsid protein and showed by immunoblotting that p120 co-immunoprecipitated with L2 in extracts from HPV16 PsV-infected HeLa cells but not from uninfected cells (Figure 2.1B); as a negative control, an isotype-matched IgG control antibody did not precipitate p120 or the C-terminal fragment of the catalytic γ-secretase subunit PS1 from extracts of WT HPV16.L2F (Luc)-infected cells (Supplementary Figure 2.1B). These results indicate that p120 is a direct or indirect binding partner of L2 during HPV infection.

We next asked if the p120-HPV16 interaction requires L2, or if L1 is sufficient to bind to p120. To test this, we used an HPV virus-like particle (VLP) containing only L1 (HPV16 L1 VLP). Immunoprecipitation of endogenous p120 co-immunoprecipitated L1 in cells infected with HPV16 L1 VLP or with WT HPV16.L2F (Luc), which contains both L1 and L2 (Figure 2.1C); as a negative control, an isotype-matched IgG control antibody did not pull down L1 or L2 from extracts of WT HPV16.L2F (Luc)-infected cells (Supplementary Figure 2.1C). These results demonstrate that capsids consisting of only HPV L1 are sufficient to associate with p120. Thus, L1 may in fact mediate an indirect interaction between L2 and p120.

To probe whether p120 plays a role in HPV infection, p120 was depleted by using three unique p120-targeting siRNAs (*39, 40*), and HPV infection was measured by immunoblotting for expression of a GFP-S reporter construct contained within the HPV16 PsV [WT HPV16.L2F (GFP-S)]. p120 knockdown was confirmed by immunoblotting. We found that p120 depletion by each of the p120 siRNAs in HeLa cells inhibited HPV infection by ~80% compared to scrambled siRNA-treated cells (Figure 2.1D). As expected, perturbing γ-secretase (by either knockdown of PS1 or treatment with the γ-secretase inhibitor XXI) potently blocked infection (*24-27*). p120 depletion similarly inhibited HPV infection in SiHa cervical cancer cells (HPV-positive) (Figure 2.1E) and SCC-47 (*41*) oropharyngeal cancer cells (HPV-positive) (Figure 2.1F). Three different siRNAs were used because some cell lines were more responsive to specific siRNAs than others.

We further confirmed these results using a WT HPV16 PsV harboring a luciferase reporter plasmid [WT HPV16.L2F (Luc)], which again revealed a ~80% reduction in infection in response to p120 knockdown in HeLa cells (Figure 2.1G). Importantly, these p120-depleted cells were also markedly resistant to infection by HPV5 or HPV18 pseudovirus (Figure 2.1G); XXI treatment or PS1 knockdown also blocked HPV5 and HPV18 infection. Partial depletion of p120

in the HPV-negative C33A and HaCaT cells also decreased HPV16 PsV infection as assessed by luciferase activity (Supplementary Figures 2.1G-H). As controls, we found that depletion of p120 had no effect on cell viability as measured by trypan blue staining (Supplementary Figure 2.1D) or cell doubling time as assessed by direct counting of the cell number (Supplementary Figure 2.1E). Furthermore, the p120-depleted cells were susceptible to infection by the polyomavirus SV40, another non-enveloped DNA virus which does not require γ-secretase for infection (Supplementary Figure 2.1F). These results confirm that cell toxicity or proliferation was not a confounding factor in the p120 siRNA knockdown experiments. Together, our data demonstrate that p120 promotes infection of different HPV types in multiple biologically-relevant cell-types, including the SCC-47 oropharyngeal cells previously untested for HPV infection (*41*).

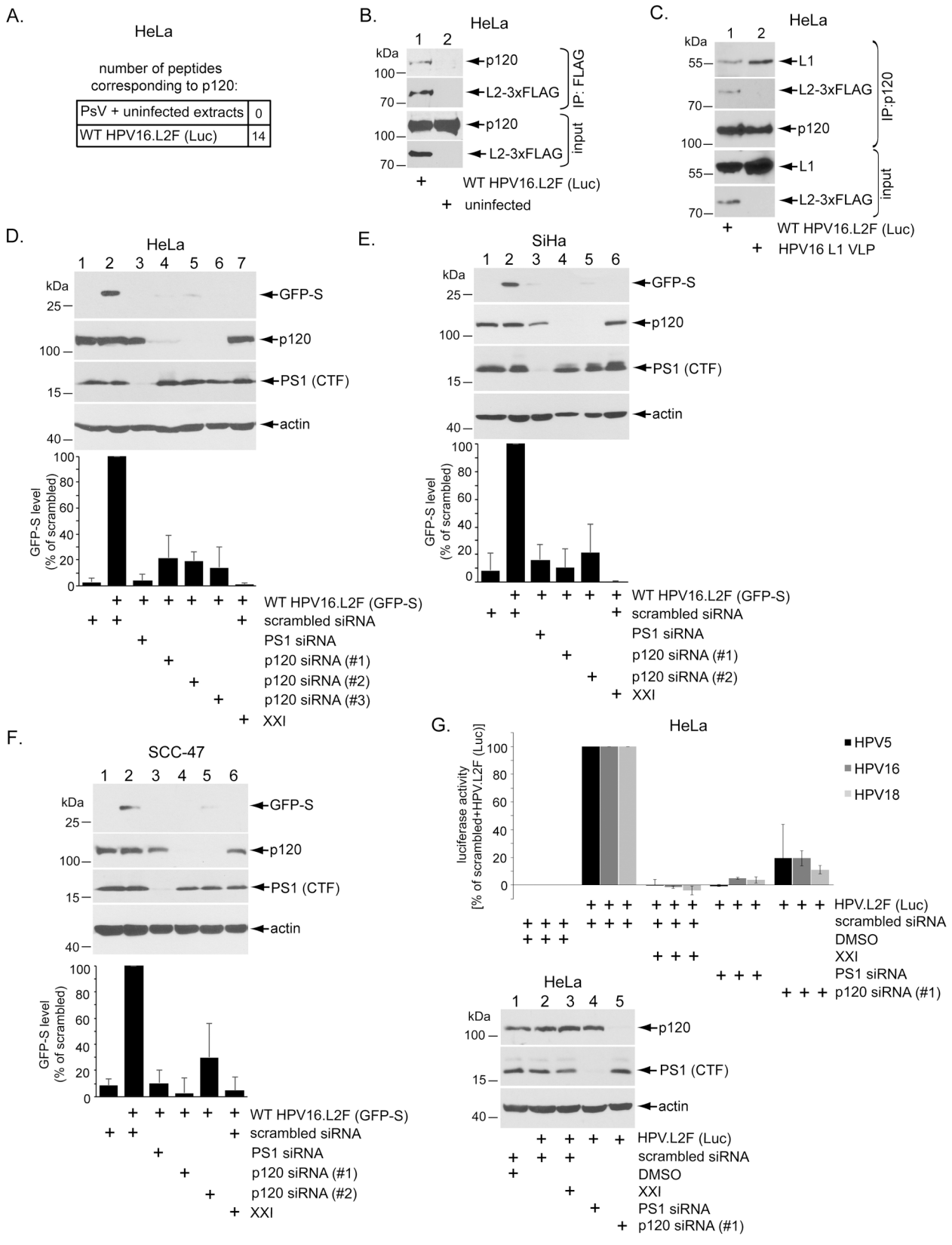
A.
HeLa
number of peptides corresponding to p120:
PsV + uninfected extracts 0
WT HPV16.L2F (Luc) 14
B.
HeLa
kDa
p120
L2-3xFLAG
IP: FLAG
input
WT HPV16.L2F (Luc)
uninfected
C.
HeLa
L1
L2-3xFLAG
p120
IP:p120
input
WT HPV16.L2F (Luc)
HPV16 L1 VLP
D.
HeLa
GFP-S
p120
PS1 (CTF)
actin
GFP-S level (% of scrambled)
WT HPV16.L2F (GFP-S)
scrambled siRNA
PS1 siRNA
p120 siRNA (#1)
p120 siRNA (#2)
p120 siRNA (#3)
XXI
E.
SiHa
GFP-S
p120
PS1 (CTF)
actin
GFP-S level (% of scrambled)
WT HPV16.L2F (GFP-S)
scrambled siRNA
PS1 siRNA
p120 siRNA (#1)
p120 siRNA (#2)
XXI
F.
SCC-47
GFP-S
p120
PS1 (CTF)
actin
GFP-S level (% of scrambled)
WT HPV16.L2F (GFP-S)
scrambled siRNA
PS1 siRNA
p120 siRNA (#1)
p120 siRNA (#2)
XXI
G.
HeLa
luciferase activity [% of scrambled+HPV.L2F (Luc)]
HPV5
HPV16
HPV18
HPV.L2F (Luc)
scrambled siRNA
DMSO
XXI
PS1 siRNA
p120 siRNA (#1)
HeLa
p120
PS1 (CTF)
actin
HPV.L2F (Luc)
scrambled siRNA
DMSO
XXI
PS1 siRNA
p120 siRNA (#1)

Figure 2.1: p120 binds to HPV16 and promotes virus infection

A. *Summary of L2 immunoprecipitation-mass spectrometry performed on samples of HeLa cells infected for 16 hrs or uninfected cell extract incubated with purified HPV16 PsV as described in Inoue et al., 2018.*

B. *HeLa cells infected with or without WT HPV16.L2F (Luc) for 6 hrs were lysed and the resulting extract subjected to immunoprecipitation using a FLAG antibody. The precipitated material was analyzed by SDS-PAGE and immunoblotting using the indicated antibodies. Samples labelled input were not immunoprecipitated. See Supplementary Figure 2.1B for IgG control.*

C. *HeLa cells were infected with HPV16.L2F (Luc) or HPV16 L1 VLP (virus-like particles containing L1 only). 2.5 hpi, cells were lysed and the resulting extract subjected to immunoprecipitation using an antibody against p120. The precipitated material was subjected to SDS-PAGE and immunoblotting using antibodies recognizing the indicated proteins. Samples labelled input were not immunoprecipitated. See S1C Fig for IgG control.*

D. *HeLa cells transfected with the indicated siRNA were infected with WT HPV16.L2F (GFP-S), with or without γ-secretase inhibitor XXI. 48 hpi, cells were lysed and the resulting extract subjected to SDS-PAGE and immunoblotting using the indicated antibodies. Graph shows data normalized against WT HPV16.L2F (GFP-S)-infected cells treated with scrambled siRNA, and further normalized against the actin level. Data represent the mean ± SD of at least three independent experiments.*

E. *As in D, except the human SiHa cervical cancer cells were used.*

F. *As in D, except the human SCC-47 oropharyngeal cancer cells were used.*

G. *HeLa cells transfected with the indicated siRNA were infected with HPV5, HPV16, or HPV18 pseudovirus harboring a luciferase reporter plasmid, with or without γ-secretase inhibitor XXI. 48 hpi, luciferase activity was measured from the cell culture media. Graph shows luciferase activity normalized against scrambled siRNA-treated cells with and without HPV. Data represent the mean ± SD of at least three independent experiments. The immunoblot reveals the extent of p120 (or PS1) depletion.*

2.3.2 A γ-secretase mutant that cannot bind to p120 inefficiently supports HPV infection

p120 is an established γ-secretase adaptor, binding to the C-terminal fragment of the PS1 subunit of γ-secretase and recruiting substrates to the enzyme (Figure 2.2A) (*28, 29, 35, 36*). We therefore asked whether the ability of γ-secretase to bind to p120 is crucial for HPV infection. To test this, we used a γ-secretase mutant that cannot bind to p120 (*35*); this mutant contains a deletion of amino acids 330-360 in the γ-secretase PS1 subunit (Δ330-360 PS1). To confirm that the PS1 mutant does not interact with p120, HeLa cells lacking endogenous PS1 due to CRISPR-mediated knockout (HeLa PS1 CRISPR KO #1 cells) (*24*) were transfected with WT PS1 or Δ330-360 PS1. Only the full-length PS1 is shown in the blot, although both WT PS1 and Δ330-360 PS1 can undergo endoproteolytic processing, generating an N-terminal fragment and a C-terminal fragment of PS1 (*28, 35*). As expected, immunoprecipitation of p120 pulled down WT PS1 (Figure 2.2B, lane 3) but not Δ330-360 PS1 (Figure 2.2B, lane 6). As a control, we found that expression of WT or mutant PS1 did not significantly affect cell doubling in the HeLa PS1 CRISPR KO cells (Figure 2.2D).

We then tested the ability of Δ330-360 PS1 to support HPV infection. Consistent with previous data (*24*), HeLa PS1 CRISPR KO cells did not support HPV infection (Figure 2.2C, lane 1), as assessed by expression of the GFP-S reporter protein. When WT PS1 was expressed in these cells, HPV infection was restored (Figure 2.2C, lane 2; quantified in right graph), as previously reported (*24, 25*). However, expression of Δ330-360 PS1 inefficiently restored infection, even though the mutant protein was efficiently expressed (Figure 2.2C, lane 3; quantified in right graph). Because this PS1 deletion mutant was previously shown to remain catalytically active (*35*) and can still undergo endoproteolytic cleavage into an N-terminal fragment and a C-terminal fragment, its inability to fully restore HPV infection is unlikely to be

due to a defect in global misfolding. The residual ~30% of infection that is achieved in the presence of the PS1 deletion mutant suggests that there may be a p120-independent mechanism to target HPV to PS1, possibly through other γ-secretase adaptors. These data therefore demonstrate that γ-secretase binding to p120 is required for HPV infection, and along with the loss-of-function results further establish p120 as an important host factor during HPV entry.

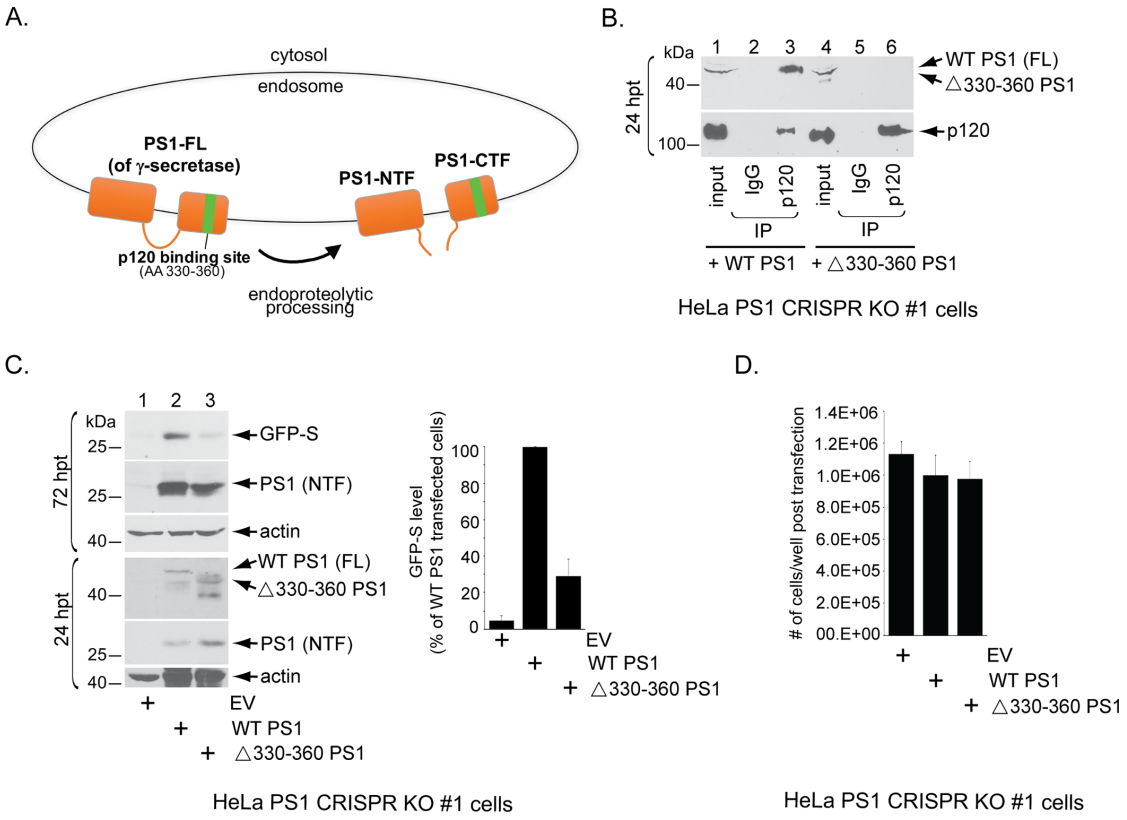

Figure 2.2: A γ-secretase mutant that cannot bind to p120 inefficiently supports HPV16 infection

A. *A model depicting the p120-binding site in the PS1 subunit of γ-secretase. p120 binds to amino acid (AA) 330–360 of PS1. "FL", full-length; "NTF", N-terminal fragment; "CTF", C-terminal fragment*

B. *HeLa PS1 CRISPR knockout cells were transfected with a plasmid expressing either WT PS1 or PS1 deleted of amino acids 330–360 (Δ330–360 PS1). 24 hrs post-transfection (hpt), cells were lysed and the resulting extract was subjected to immunoprecipitation using either a control IgG antibody or an antibody against p120. The precipitated material was subjected to SDS-PAGE and immunoblotting using antibodies recognizing p120 or FLAG-tagged L2. Only the full-length (FL) PS1 (prior to endoproteolytic processing) is shown.*

C. *(Upper panels, 72 hrs post-transfection, hpt) HeLa PS1 CRISPR knockout cells were transfected with empty vector (EV), WT PS1, or Δ330–360 PS1 for 24 hrs, and then infected with WT HPV16.L2F (GFP-S). 48 hpi, cells were lysed and the resulting extract subjected to SDS-PAGE and immunoblotting using the indicated antibodies. The levels of GFP-S were quantified as in Fig 1. Data are normalized against infected cells transfected with WT PS1, and further normalized against the actin levels. Data represent the mean ± SD of three independent experiments. (Lower panels, 24 hrs post-transfection, hpt) A pool of cells were harvested 24 hrs post-transfection with the indicated DNA in the absence of PsV. The resulting cell extract was subjected to SDS-PAGE and immunoblotting using antibodies recognizing the indicated proteins to visualize protein levels at the time of infection. Both the full-length PS1 and the N-terminal fragment of PS1 (due to endoproteolytic processing) are observed at the 24 hpt time point.*

D. *HeLa PS1 CRISPR KO #1 cells were seeded at equal amounts in a 6-well plate and transfected with empty vector (EV), WT PS1, or Δ330–360 PS1 for 24 hrs. 72 hours after transfection, cells were harvested and the total number of cells per condition were counted by hemocytometer. Data represent the mean ± SD of three independent experiments.*

2.3.3 HPV16 binds to p120 prior to engaging γ-secretase

We next performed a time-course experiment to determine when p120 binds to HPV during entry. To this end, we infected HeLa cells with the WT HPV16.L2F (Luc) and immunoprecipitated 3xFLAG-tagged L2 at different time points across 16 hrs of infection. We found that p120 associates with HPV L2 soon after addition of virus. Maximal association occurred at 0.25-2 hrs post-infection (hpi), and this association is decreased by 4 hpi and lost by 7-10 hpi (Figure 2.3A). Although we initially identified p120 by using the IP-MS approach performed at 16 hpi (Figure 2.1A), immunoblotting did not detect HPV-associated p120 at this time point, likely because the MS approach is a much more sensitive method than immunoblotting. By contrast, association of HPV L2 to the γ-secretase PS1 subunit was first detectable at 4-6 hpi (Figure 2.3B), similar to a previous report (*24*). These data demonstrate that HPV16 binds to p120 before the virus engages γ-secretase and that the loss of p120 binding is roughly coincident with the acquisition of γ-secretase binding. Of note is the appearance of a minor <70 kDa L2 protein species correlating with association of the virus with PS1 (Figure 2.3B). We have previously characterized this species to be the γ-secretase-cleaved form of the L2 protein (*24*), and determined that cleavage of L2 by γ-secretase is not essential for the function of γ-secretase during HPV infection.

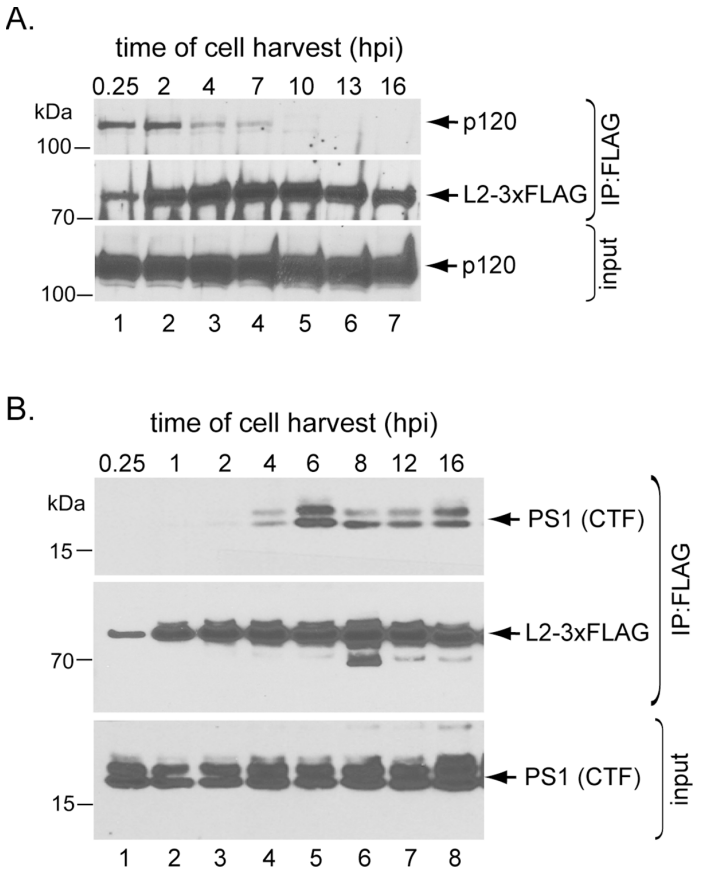

Figure 2.3: HPV16 binds to p120 prior to engaging γ-secretase
A-B. *HeLa cells infected with HPV16.L2F (Luc) for the indicated time points were lysed and the resulting extract subjected to immunoprecipitation using FLAG antibody. The precipitated material was analyzed by SDS-PAGE and immunoblotting using antibodies recognizing p120 or FLAG-tagged L2 (panel A) or PS1 or FLAG-tagged L2 (panel B).*

2.3.4 Low pH initiates partial L1 capsid disassembly via a p120 and γ-secretase-independent mechanism

Previous studies suggested that HPV undergoes low pH-dependent partial disassembly of L1 in the endosome during entry (*19, 22, 23*). Our observation that p120 loses its interaction with HPV 7-10 hpi (Figure 2.3A), time points when HPV is in the endosome (*24*), prompted us to ask whether p120 might be required for HPV to undergo pH-dependent capsid disassembly. To test this, cells were infected with HPV16.L2F (Luc), harvested at various times after infection, and the resulting cell extract subjected to a virus capsid disassembly assay based on sucrose gradient centrifugation and SDS-PAGE (Figure 2.4).

At 0.5 hpi when HPV is bound at the cell surface primed for endocytosis, both L1 and L2 are found in the most dense sucrose fraction (fraction 8), suggesting that the viral particles have not experienced significant disassembly – we refer to these viral particles in fraction 8 as largely intact (Figure 2.4A, 0.5 hpi, fraction 8). The L1 levels in fraction 8 representing the intact virus and fractions 1-7 representing disassembled virus are quantified in the right graph. Consistent with previously published imaging data (*42-44*), L2 remains associated with the viral DNA throughout infection. However, at 8 hpi when some of the virus has arrived at the endosome, a small pool of L1 sedimented more slowly (Figure 2.4A, 8 hpi, fractions 1-7; quantified in the right graph), indicating that a minority of molecules of L1 have disassembled from the capsid. At 16 hpi, when the bulk of the virus is endocytosed, a greater portion of L1 sedimented slowly (Figure 2.4A, 16 hpi, fractions 1-7; quantified in the right graph). Furthermore, when endosomal acidification was blocked by bafilomycin A1 (BafA1), L1 disassembly was significantly inhibited (Figure 2.4B, fraction 8; quantified in the right graph). By contrast, addition of the chemical denaturant SDS fully disrupts the virus, including dissociation of L2 which was not

seen under physiological conditions (Figure 2.4B). While these data suggest that under normal conditions, L1 undergoes pH-dependent partial disassembly during HPV internalization and trafficking, it is evident that not all L1 proteins have dissociated from the L2-viral genome complex. Even at 16 hpi, some L1 is clearly seen in the heaviest sucrose fraction, suggesting that it remains intact with L2 and the viral genome (Figure 2.4A). This is consistent with reports that a portion of L1 reaches the nucleus along with L2 and the viral genome (*44, 45*).

Importantly, upon p120 knockdown, L1 disassembly is observed at 16 hpi (Figure 2.4C, fractions 1-7; quantified in the right graph), indicating that p120 is not required for HPV to undergo pH-mediated disassembly. Likewise, knockdown of PS1 had no effect on virus disassembly (Figure 2.4D, fractions 1-7; quantified in the right graph), as expected since γ-secretase is not known to be involved in endosomal arrival of HPV. Together, these data indicate that p120 (and γ-secretase) are not required for L1 capsid disassembly. Additionally, the finding that HPV still undergoes disassembly in cells depleted of p120 (or γ-secretase) but not in cells in which endosome acidification is blocked indicate that p120 and γ-secretase do not promote initial endosome entry of HPV, despite the fact that p120 binds to HPV at early timepoints during infection. This is consistent with our earlier report that γ-secretase knockdown or inhibition do not block localization of HPV to endosomes at 8 hpi (*24, 25*).

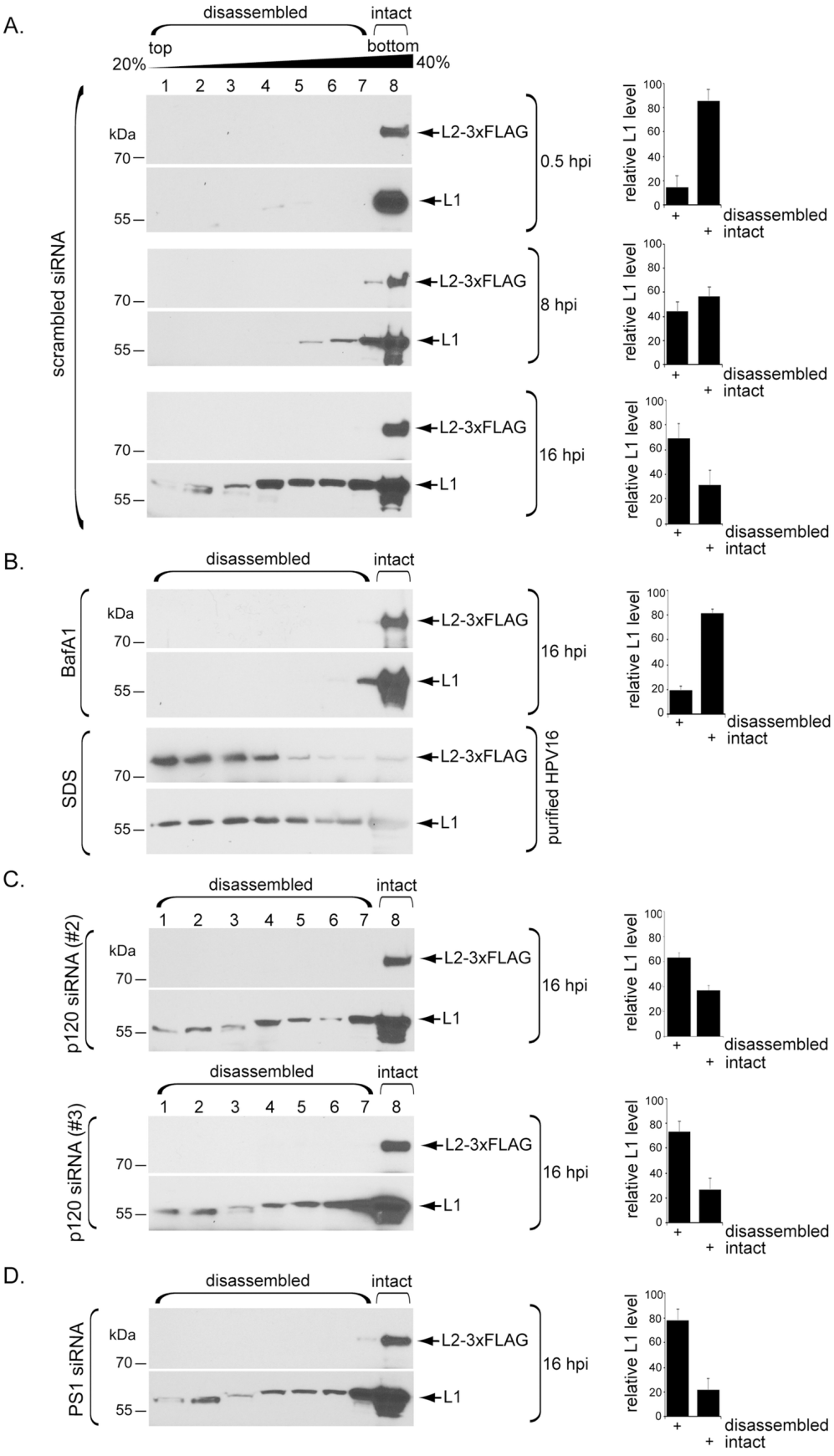
A.
disassembled
intact
top
bottom
20%
40%
1 2 3 4 5 6 7 8
kDa
70
55
L2-3xFLAG
L1
0.5 hpi
8 hpi
16 hpi
scrambled siRNA
relative L1 level
100
80
60
40
20
0
+
disassembled
+
intact
B.
BafA1
SDS
purified HPV16
C.
p120 siRNA (#2)
p120 siRNA (#3)
D.
PS1 siRNA

Figure 2.4. Low pH initiates partial L1 capsid disassembly via a p120- and γ-secretase-independent mechanism
A. *HeLa cells transfected with scrambled siRNA were infected with WT HPV16.L2F (Luc). At the indicated time point post infection, cells were lysed and the resulting extract layered on top of a discontinuous 20–40% sucrose gradient. Following centrifugation, fractions were collected and subjected to SDS-PAGE and immunoblotting using antibodies recognizing L1 or FLAG-tagged L2. The levels of L1 in fractions 1–7 (disassembled) and fraction 8 (intact) were quantified. Data represent the mean ± SD of at least three independent experiments.*
B. *(upper panels) HeLa cells were treated with bafilomycin A1 (BafA1) for 24 h, then infected, processed, and quantified as in A. Data represent the mean ± SD of at least three independent experiments. (lower panels) Purified WT HPV16.L2F (Luc) was treated with the chemical denaturant SDS, and the sample processed as in A.*
C. *HeLa cells transfected with the indicated p120 siRNA were infected, processed, and quantified as in A. Data represent the mean ± SD of at least three independent experiments.*
D. *HeLa cells transfected with the PS1 siRNA were infected, processed, and quantified as in A. Data represent the mean ± SD of at least three independent experiments.*

2.3.5 p120 promotes L2 binding to γ-secretase and membrane insertion

Although p120 is not essential for low pH-dependent disassembly of the L1 capsid protein in the endosome, p120 might play a critical role in targeting HPV to γ-secretase since p120 is known to deliver cellular substrates to γ-secretase (*35, 36, 46*). To test whether p120 was required for association between HPV and γ-secretase, we depleted p120 and used coimmunoprecipitation to probe the level of HPV-γ-secretase binding. We found that knockdown of p120 disrupted the HPV-γ-secretase interaction (Figure 2.5A; quantified in the right graph), suggesting that p120 is required for HPV to engage γ-secretase.

When HPV is recruited to γ-secretase, the viral L2 protein is inserted into the endosome membrane via the chaperone activity of γ-secretase. Thus, we asked if p120 is essential for γ-secretase-dependent membrane insertion of L2. A robust alkali resistance assay was previously developed to monitor insertion of L2 into the endosome membrane (*24*). In this approach, L2 remains in the alkali-resistant final "pellet" (P) fraction if it is inserted into the membrane. We found that upon p120 knockdown, the level of L2 in the alkali-resistant pellet fraction was markedly reduced (Figure 2.5B; quantified in the right graph), indicating that p120 is essential for γ-secretase to engage and insert L2 into the endosome membrane.

A.

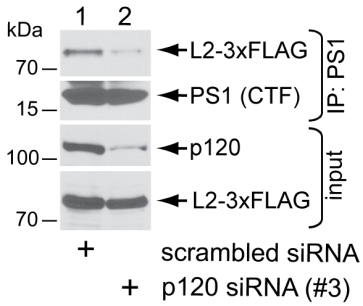
1 2
kDa
70
15
100
70
L2-3xFLAG
PS1 (CTF)
p120
L2-3xFLAG
IP: PS1
input
+ scrambled siRNA
+ p120 siRNA (#3)

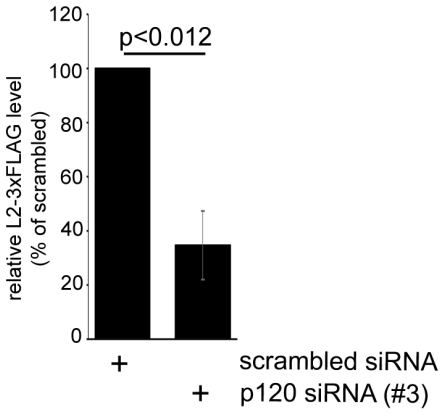
p<0.012
relative L2-3xFLAG level (% of scrambled)
120
100
80
60
40
20
0
+ scrambled siRNA
+ p120 siRNA (#3)

B.

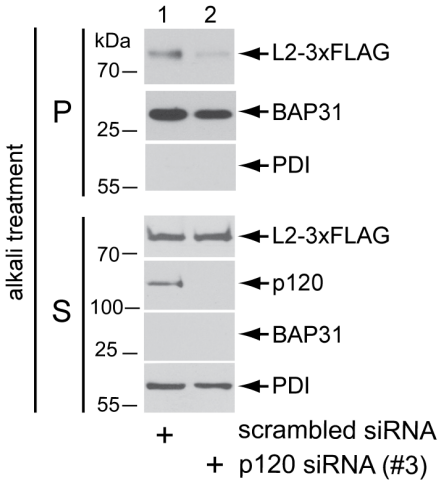
1 2
kDa
alkali treatment
P
S
70
25
55
70
100
25
55
L2-3xFLAG
BAP31
PDI
L2-3xFLAG
p120
BAP31
PDI
+ scrambled siRNA
+ p120 siRNA (#3)

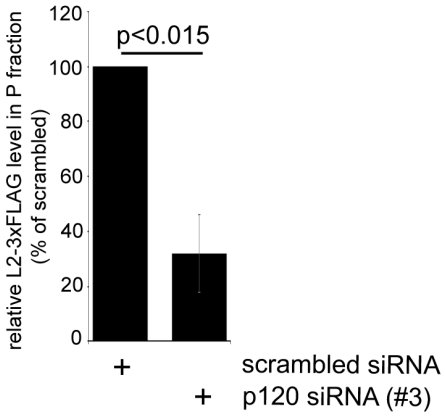
p<0.015
relative L2-3xFLAG level in P fraction (% of scrambled)
120
100
80
60
40
20
0
+ scrambled siRNA
+ p120 siRNA (#3)

C.

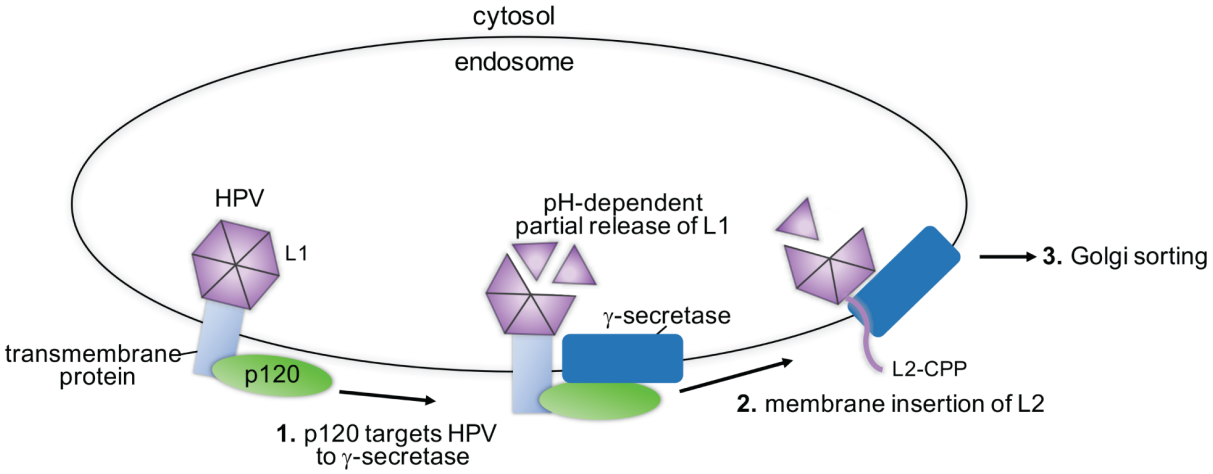
cytosol
endosome
HPV
L1
transmembrane protein
p120
pH-dependent partial release of L1
γ-secretase
L2-CPP
3. Golgi sorting
2. membrane insertion of L2
1. p120 targets HPV to γ-secretase

Figure 2.5: p120 promotes L2 binding to γ-secretase and membrane insertion
A. *HeLa cells transfected with the indicated siRNA were infected with WT HPV16.L2F (Luc) for 16 hrs. Cells were lysed and the resulting extract subjected to immunoprecipitation using an antibody against PS1. The precipitated material was subjected to SDS-PAGE and immunoblotting antibodies recognizing the indicated proteins. The level of immunoprecipitated L2-3xFLAG is quantified in the right graph. Data represent the mean ± SD of at least three independent experiments. A two-tailed t test was used to determine statistical significance.*
B. *HeLa cells infected with WT HPV16.L2F (Luc) for 16 hrs were mechanically homogenized and processed to generate a membrane fraction (see Materials and Methods), which was treated with alkali reagents and recentrifuged to generate a pellet fraction (which contains transmembrane proteins) and a supernatant fraction (which harbors soluble proteins). Both fractions were subject to SDS-PAGE and immunoblotting with antibodies recognizing the indicated proteins. Presence of the membrane protein BAP31 in the pellet fraction and soluble protein PDI in the supernatant fraction confirm proper fractionation. The level of L2-3xFLAG in the pellet fraction is quantified in the right graph. Data represent the mean ± SD of at least three independent experiments. A two-tailed t test was used to determine statistical significance.*
C. *Proposed model for p120-dependent targeting of HPV16 to γ-secretase. In the endosome, HPV L1 partially dissociates from L2 in a pH-dependent manner. p120 bound to HPV, presumably via a transmembrane protein, targets the virus to γ-secretase (step 1). This is a critical step as γ-secretase promotes insertion of the viral capsid protein L2 into the endosome membrane (step 2). Membrane protrusion mediated by the cell-penetrating peptide (CPP) on the C-terminus of L2 then exposes the retromer binding site to the cytosol, which in turn recruits host factors that direct the virus along an infectious route through the Golgi apparatus and to the nucleus (step 3).*

2.4 Discussion

This study clarifies an important HPV entry event. Upon endosomal arrival, HPV is delivered to the transmembrane protease γ-secretase which promotes insertion of L2 into the endosome membrane and CPP-mediated protrusion of a segment of L2 into the cytosol (Figure 2.5C, step 2) (*24, 25, 30, 31*). The L2 C-terminus in the cytosol in turn recruits cytosolic sorting factors (such as the retromer) which delivers HPV to the Golgi en route for successful infection (Figure 2.5C, step 3) (*32-34*). Without γ-secretase-induced membrane insertion of L2, the virus does not enter the retrograde transport pathway and infection cannot proceed). Hence, the delivery of HPV to γ-secretase in the endosome represents a decisive HPV infection event, although how this is accomplished is unknown.

We used an unbiased IP-mass-spectrometry screen (*24*) to identify p120 as a host factor that binds to HPV during viral internalization and trafficking; whether the L1 and L2 viral proteins both participate in binding to p120 is unclear, but capsids consisting of L1 alone are sufficient for this interaction. We then confirmed with genetic knockdowns that p120 is essential for productive infection of multiple HPV types in several cell types, including oropharyngeal SCC-47 cells (*41*). As the prevalence of HPV-associated oropharyngeal cancers has recently surpassed that of HPV-induced cervical cancers in the U.S. (*4*), the use of these cells may provide a relevant model to study HPV-associated oropharyngeal cancer.

What specific HPV entry step is mediated by p120? Our data revealed that the HPV-p120 interaction occurs early during HPV infection, prior to the virus reaching the endosome and associating with γ-secretase. Importantly, depletion of p120 blocked interaction of HPV with γ-secretase and membrane insertion of L2 by this transmembrane protease. However, depletion of p120 did not block low pH-induced disassembly of the virus in the endosome. Based on these

results, we propose that p120 acts to target HPV to γ-secretase independently of capsid disassembly (Figure 2.5C, step 1). The observation that p120 depletion does not block L1 disassembly from the viral capsid strongly suggests that the action of p120 is not dependent on low pH-induced L1 disassembly. Hence, in this scenario, L1 disassembly can still continue at 16 hpi even though p120 is no longer interacting with HPV.

The model that p120 acts to target HPV to γ-secretase (Figure 2.5C, step 1) is in agreement with the established role of p120 in targeting cellular transmembrane proteins to γ-secretase (*28, 29, 35, 36, 46*). By associating with p120, HPV simply exploits this pathway to reach γ-secretase. Our model further suggests that γ-secretase must engage p120 so that γ-secretase can capture HPV and insert the L2 protein into the endosome membrane – this idea is indeed supported by the finding that a γ-secretase mutant that cannot bind to p120 failed to efficiently promote HPV infection. However, there was some residual infection in cells expressing the p120 mutant or knocked-down for p120, suggesting the presence of a p120-independent mechanism to target HPV to PS1. For example, there may be other γ-secretase adaptors that facilitate this virus targeting step.

Because p120 is a cytosolic factor, and the non-enveloped HPV is in the endosome lumen after endocytosis and does not become exposed to the cytosol until after interaction with γ-secretase, a critical question is how p120 engages HPV before reaching γ-secretase. One possibility is that the HPV-p120 interaction is bridged by an unidentified transmembrane protein. As p120 binds to HPV early during infection, a cell surface receptor of HPV might in fact be this transmembrane protein. In this regard, several cell surface receptors including integrins, growth factor receptors, tetraspanins, and annexin A2 have been implicated as HPV receptors (*7, 21, 47-53*); whether these receptors physically link HPV to p120 are unknown.

p120 is a well-established binding-partner of the cell-cell adhesion transmembrane protein cadherin (*35, 36, 46, 54*). Because p120 has also been shown to deliver cadherins to γ-secretase (*28, 29, 35, 36*), an intriguing scenario is that HPV binds to the cadherin component of the cadherin-p120 complex at the cell surface. When p120 delivers cadherins to γ-secretase, which itself spans the membrane, HPV is concomitantly recruited to γ-secretase. However, no functional data have been reported regarding a role of cadherins during HPV infection. Clearly, identifying the transmembrane protein(s) coupling HPV to p120 will be a fruitful area for future investigation. In sum, our findings here provide further mechanistic insights into a critical HPV entry step, illuminating how the virus hijacks the action of an adaptor of the critical host component γ-secretase to promote infection.

2.5 Materials & Methods

2.5.1 Antibodies & Inhibitors

Antibodies and inhibitors used in this study are as follows:

Table 2.1: List of Antibodies & Inhibitors

Antibodies			
Antigen	**Species**	**Cat # / Source**	**Application**
FLAG M2	Mouse mono	F3165; Sigma	WB, IP
P120	Mouse mono	sc-23873; Santa Cruz	WB, IP
HPV16 L1	Mouse mono	MAB885; Sigma	WB
S-tag	Rabbit poly	ab180958; Abcam	WB
PS1 C-terminal	Rabbit mono	5643S; Cell Signaling	WB
PS1 N-terminal fragment	Rabbit poly	811101; BioLegend	WB
HSP90	Mouse mono	sc-13119; Santa Cruz	WB
β-actin	Rabbit mono	4967S; Cell Signaling	WB
Bap31	Rat mono	MA3-002; Invitrogen	WB
PDI	Mouse mono	ab2792; Abcam	WB
SV40 T Ag	Mouse mono	sc-147; Santa Cruz	IF
Inhibitors			
Compound	**Solvent**	**Source**	**Concentration**
XXI	DMSO	565790; Millipore	1 μM
Bafilomycin A1 (Ba	DMSO	508409; Millipore	30 nM

IP, immunoprecipitation; WB, Western blot; IF, immunofluorescence

2.5.2 DNA Constructs

The p16sheLL, p5sheLL, and p18sheLL plasmids were gifts from Dr. John Schiller (National Cancer Institute, Rockville, MD; Addgene plasmids #37320, #46953, and #37321). These plasmids were used as in Zhang et al., 2014 (*25*) to produce the WT HPV16.L2F, HPV5.L2F, and HPV18.L2F pseudoviruses (PsVs) with FLAG tagged L2, and WT L1. The WT PS1 pCDNA3.1(-) construct used was generated in Inoue et al., 2018 (*24*). Δ330-360 PS1 was subcloned from the pMX-IRES-GFP retroviral expression vector (*35, 55*) (a gift from Dr. Nikolaos Robakis, Mount Sinai School of Medicine) and inserted into pcDNA3.1(-) for mammalian transfection.

2.5.3 Cells

HeLa cells were purchased from American Type Culture Collection. The 293TT cells were a generous gift from Dr. Christopher Buck (National Cancer Institute, Rockville, MD). SCC-47 cells were a gift from Dr. Thomas Carey (University of Michigan). HeLa PS1 CRISPR KO #1 cells were generated as in Inoue et al., 2018. SiHa, C33A, and HaCaT cells were supplied by Dr. Dan DiMaio (Yale University). All cells were cultured in DMEM (Thermo Fisher Scientific) and 10% fetal bovine serum (Corning) containing 10 µg/ml streptomycin and 10 U/ml penicillin (Thermo Fisher Scientific).

2.5.4 HPV Pseudovirus Production

WT HPV16.L2F, WT HPV18.L2F, and WT HPV5.L2F pseudoviruses were produced according to Inoue et al., 2018 (*24*) and as described in (*56*). Briefly, 293TT cells were co-transfected with p16sheLL.L2F, p18sheLL.L2F, or p5sheLL.L2F along with indicated reporter construct (phGluc expressing secreted *Gaussia* luciferase, or pcDNA3.1 expressing GFP with a

C-terminal S-tag) with polyethyleneimine (Polysciences Inc.). After 48 hrs, cells were lysed in a buffer containing 0.5% Triton X-100, 10 mM $MgCl_2$, and 5 mM $CaCl_2$. The lysate was incubated overnight at 37 ˚C with 250 U/mL Benzonase Nuclease (Millipore) and 10 U/mL Plasmid-Safe DNase (Lucigen). The resulting extract was centrifuged on an OptiPrep gradient of 27, 33, and 39% at 300,000 g for 4 hrs at 16 ˚C in a SW55 Ti rotor. Purity of the pseudovirus preparations was analyzed by subjecting the virus to SDS-PAGE and Coomassie staining (Invitrogen) (Supplementary Figure 2.1A). We estimated the amount of L1 to be ~1000 ng/µL by performing SDS-PAGE and Coomassie blue staining on purified pseudovirus preparations and comparing the amount of L1 to protein standards electrophoresed in parallel. HPV16.L1 (L1 only VLP) was a gift from Pengwei Zhang, Yale University.

2.5.5 siRNA Transfection

siRNAs used in this study were generated by Sigma-Aldrich as follows:

Table 2.2: List of siRNAs

siRNA			
Name	**Sequence**	**Conc.**	**Source**
PS1	5’-UCAAGUACCUCCCUGAAUG-3’	25 – 100 nM	Inoue et al., 2018 (*24*)
p120 siRNA #1	5'-AACGAGGUUAUCGCUGAGAAC-3'	100 nM	Xiao et al., 2003 (*40*)
p120 siRNA #2	5'-GCGAUUGCUUCGAAAGGCUCGUGAU-3'	100 nM	Zhu et al., 2012 (*39*)
p120 siRNA #3	5’-GCUAUGAUGACCUGGAUUA-3’	100 nM	predesigned by Sigma-Aldrich

As a negative control, Allstar siRNA (Qiagen) was used. HeLa cells were seeded and simultaneously reverse transfected with 100 nM siRNA using Lipofectamine RNAi MAX (Thermo Fisher Scientific) and OPTI-MEM (Gibco) and incubated for at least 48 hrs prior to infection or biochemical assays.

2.5.6 Immunoprecipitation mass-spectrometry

The IP mass-spectrometry results shown in Figure 2.1 and Supplementary Table 2.1 are from Inoue et al., 2018 (*24*). Briefly, HeLa cells were asynchronously infected with WT HPV16.L2F at a concentration of ~12.5pg L1/cell for 16 hrs or uninfected. The cells were harvested, and lysed in 3 mL of a buffer containing 50 mM Hepes (pH 7.5), 150 mM NaCl (HN buffer), 1% Triton X-100, and 1 mM phenylmethylsulfonyl fluoride (PMSF). Centrifugation of the resulting extract at 16,100x g generated a supernatant fraction that was incubated with FLAG M2 antibody (0.3 μg/ml) at 4ºC for 2 h. The immune complex was then captured with protein G-coated magnetic beads (Thermo Fisher Scientific). The HeLa cell extract derived from uninfected cells were mixed with OptiPrep-isolated HPV16.L2F prior to incubation with FLAG M2 antibody and was used as a background control to determine post-lysis binding proteins. The bound proteins were eluted with 0.1 mg/ml 3xFLAG peptide (Sigma) and precipitated by trichloroacetic acid (TCA). The TCA-precipitated materials were subjected to mass-spectrometry analysis (Taplin Mass Spectrometry Core Facility, Harvard Medical School).

2.5.7 Immunoprecipitation

HeLa cells were plated at approximately 5 x 10^6 in 10 cm plates and incubated for 16-24 hrs (until ~80-90% confluent). Cells were then infected with WT HPV16.L2F at a concentration of ~5.7pg L1/cell for indicated times before lysis in 1% Decyl Maltose Neopenyl Glycol

(DMNG) (Anatrace) in HN buffer (50 mM Hepes + 150 mM NaCl) and 1 mM PMSF. Lysed cells were centrifuged at 16,100 g for 10 min and the resulting supernatant was incubated with antibody against M2 FLAG, PS1 C-terminal fragment, p120, or an equal concentration of IgG control antibody overnight at 4˚C. Protein G magnetic Dynabeads (Thermo Fisher) were then added to the sample for 1 hr at 4˚C. Beads were washed 3X in 0.1% DMNG in HN buffer, and incubated at 95˚C for 10 minutes with 5X SDS sample buffer plus 2-mercaptoethanol (BME) and subjected to SDS-PAGE and immunoblotting as indicated. In Figure 2.1B, HeLa cells were infected with HPV16.L2F at a concentration of ~6.25 pg L1/cell for 6 hrs before treatment as above. In Figure 2.1C, HeLa cells were infected with HPV16.L2F or HPV16.L1 at a concentration of ~6.25 pg L1/cell for 2.5 hrs before treatment as above (L1 only VLP, provided by Pengwei Zhang, Yale University). In Figure 2.5A, cells were seeded and reverse transfected with the indicated siRNAs for 24 hrs and infected at a concentration of ~6.25 pg L1/cell for 16 hrs before treatment as above. In Figure 2.2B, HeLa PS1 CRISPR KO #1 cells were seeded in 10 cm plates. Cells were grown to ~80% confluency (about 1 day) and transfected with 5 ug WT PS1 or Δ330-360 PS1 using polyethyleneimine (Polysciences Inc.) for 24 hrs. Immunoprecipitation was then performed as above, except that cells were lysed in 0.5% NP-40 (Sigma) in 100 mM Hepes and 1 mM PMSF, and the beads were washed in 0.05% NP-40 in 100 mM Hepes.

2.5.8 HPV16 infection studies

All infections were performed asynchronously. In Figure 2.1D-F, the indicated cell types were seeded with approximately $4x10^5$ cells per well in 6-well plates and reverse transfected with 100nM of the indicated siRNAs for 72 hrs, followed by infection with WT HPV16.L2F (GFP-S) at a concentration of ~4.2-8.4 pg L1/cell. Cells were treated with DMSO (Sigma) or

compound XXI (1 μM) at time of infection. 48 hpi, cells were harvested in 1% Triton X-100 in HN buffer and 1 mM PMSF. Lysed cells were centrifuged at 16,100 g for 10 min and the resulting supernatant was incubated at 95˚C for 10 minutes with 5X SDS sample buffer plus BME and subjected to SDS-PAGE and immunoblotting with the indicated antibodies. In Figure 2.1G and Supplementary Figures 2.1G-H, cells were instead infected with WT HPV16 pseudovirus containing a luciferase reporter genome (Luc) a concentration of ~4.2-8.4 pg L1/cell. 48 hpi, 20 μl of media supernatant was collected from each well and luciferase activity was measured using BioLux Gaussia Luciferase Assay Kit (NEB) according to manufacturer's instructions. In Figure 2.2C, HeLa PS1 CRISPR KO #1 cells were seeded in 6-well plates. Cells were grown to ~80% confluency (about 1 day) and transfected with 2 ug of plasmid expressing WT PS1 or Δ330-360 PS1 using polyethyleneimine (Polysciences Inc.) the following day. Cells were plated in duplicate, and one set was harvested at 24 hrs post-transfection to evaluate protein expression levels. The other set of cells were infected with WT HPV16.L2F (GFP-S) and incubated for an additional 48 hrs prior to harvesting and processing for SDS-PAGE as above.

2.5.9 Trypan Blue Assay

In Supplementary Figure 2.1D, HeLa cells were seeded with approximately $4x10^5$ cells per well in 6-well plates and simultaneously reverse transfected with 100 nM of the indicated siRNA for 72 hrs. Cells were then trypsinized, resuspended in PBS, and diluted at a 1:1 ratio in 0.4% Trypan Blue Solution (Thermo Fisher). The solution was loaded on a hemocytometer and the number of blue-staining cells was quantified relative to the number of total cells. Three biological replicates were performed for a total of ~300 cells per condition. Bars represent the means ± SD. Statistical significance was determined by the student's *t* test.

2.5.10 Cell Doubling Assay

In Supplementary Figure 2.1E, HeLa cells were seeded with approximately $4x10^5$ cells per well of a 6-well plate and simultaneously reverse transfected withs 100 nM of the indicated siRNA for 72 hrs. Cells were then trypsinized, resuspended in media, loaded on a hemocytometer, and the total number of cells per well was counted for each condition. In Figure 2.2C, HeLa PS1 CRIPSR KO#1 cells were seeded with $4x10^5$ cells per well of a 6-well plate. The next day, cells were transfected with 2 ug of the indicated DNA using PEI. 24 hpt, cells were trypsinized, resuspended in media, loaded on a hemocytometer, and the total number of cells per well was counted for each condition.

2.5.11 SV40 Infection Assay

In Supplementary Figure 2.1F, HeLa cells seeded on glass coverslips in a 6-well plate (with approximately 7.5 X 10^5 cells per well) were simultaneously reverse transfected with the indicated siRNAs. Cells were incubated for 72 hrs, then infected with SV40 (MOI ~25). Cells were then fixed in 1% paraformaldehyde and permeabilized in 0.2% Triton X-100 in PBS, incubated with anti-SV40 T antigen primary antibody, followed by an anti-mouse 594 fluorophore. Coverslips were mounted on slides using prolong Gold plus DAPI mounting agent and cells were visualized using fluorescent microscopy. The number of cells expressing large T antigen was scored relative to the total number of cells. Approximately 500 cells were counted per condition per replicate.

2.5.12 Disassembly Assay

In Figure 2.4, HeLa cells were seeded in 6-cm plates with approximately 6.4 X 10^5 cells per plate and simultaneously reverse transfected with indicated siRNA against p120 (100 nM),

PS1 (25 nM), or with control Allstar siRNA (100 nM). After 24 hrs of siRNA-mediated knockdown, cells were infected with WT HPV16.L2F (GFP-S) at a concentration of ~6.25 pg L1/cell. Infection was allowed to proceed for the indicated time, followed by lysis in 50 µl of 1% Triton X-100 in HN buffer with 100X PMSF. Cells were lysed at 4˚C for 10 min, followed by centrifugation at 4˚C for 10 min at 16,100 X g. The resulting extract was layered on top of a discontinuous 20-40% sucrose gradient and centrifuged at 50,000 X g for 30 min at 4˚C. After centrifugation, individual sucrose layers were collected and incubated at 95˚C for 10 min with 5X SDS running buffer plus BME. Fractions were subjected to SDS-PAGE and immunoblotting as indicated. For the SDS-treated samples, purified WT HPV16L2.F (GFP-S) was treated with 1% SDS in HN buffer for 10 min at 4˚C. For the BafA1-treated samples, cells were treated with 1 nM BafA1 for 2 hrs prior to 16 hr infection with WT HPV16.L2F (GFP-S). For quantification, the L1 band densities in fractions 1-7 (disassembled) or fraction 8 (intact) were divided by total amount of L1. Bars represent the means ± SD of at least three independent biological replicates.

2.5.13 Alkali Extraction Assay

Data in Figure 2.5B were generated as in Inoue et al., 2018 (*24*). Briefly, HeLa cells were seeded at 2.0 x 10^6 cells in 6-cm plates, grown to 80-90% confluency (approximately 1 day), and infected with WT HPV16.L2F (GFP-S) a concentration of ~6.25 pg L1/cell for 16 hrs. After 16 hrs, cells were collected and resuspended in HN buffer before being homogenized in 10 µm clearance ball bearing homogenizer (Isobiotech). The cell homogenate was then centrifuged at 16,100 x g at 4˚C for 10 min. The resulting supernatant was centrifuged at 50,000 rpm 4˚C for 30 min in a TLA 100.3 rotor (Beckman). Pellet was treated with 25 µl of 10 mM Tris-HCl (pH 7.5), 150 mM NaCl, 2 mM $MgCl_2$, 5 mM DTT, and 50 units of Benzonase. The sample was then incubated at 37˚C for 30 min. After 30 min, 225 µl of 0.1M Na_2CO_3 and 2 M Urea was added

and incubated at 4˚C for 10 min. Next the samples were centrifuged at 50,000 rpm at 4˚C for 10 min. The supernatant fraction was collected, and the pellet was rinsed in HN buffer, and re-centrifuged. The pellet and supernatant fractions were incubated at 95˚C for 10 min with 5X SDS running buffer plus BME, then subjected to SDS-PAGE and immunoblotting with the indicated antibodies. For quantification in Figure 2.5B, bars represent the relative values of L2-FLAG in the pellet fraction normalized against the L2-FLAG level in the pellet fraction of scrambled siRNA treated cells. The values were further normalized against the BAP31 band intensities. Bars represent the means ± SD of at least three biological replicates. Statistical significance was determined using the student's *t* test.

2.6 Acknowledgements

The authors would like to thank Mac Crite (Yale) for critical reading of this manuscript. This work was funded by grants from the National Institutes of Health (R01AI150897 and AI064296) to BT, and R01AI150897 to DD. MCH was funded by NIH T-32-GM007315.

With permission from the publisher, this chapter is adapted from an original publication: *p120 catenin recruits HPV to γ-secretase to promote virus infection. non-enveloped viruses hijack host machineries to cause infection. Mara C. Harwood†, Allison J. Dupzyk†, Takamasa Inoue, Daniel DiMaio, and Billy Tsai. (2020). PLoS pathogens, 16(10), e1008946. https://doi.org/10.1371/journal.ppat.1008946; †co-first authors.*

2.7 Author Contributions

Contributions for each figure are as follows:

Mara C. Harwood

- Figures 2.1D, 2.1E, 2.1F, 2.1G, 2.2A, 2.2B, 2.2C, 2.2D, 2.3A, 2.4A, 2.5C
- Supplementary Figures 2.1A, 2.1B, 2.1C, 2.1D, 2.1E, 2.1F, 2.1G, 2.1H

Allison J. Dupzyk

- Figures 2.1B, 2.1C, 2.3A, 2.4A, 2.4B, 2.4C, 2.4D, 2.5A, 2.5B
- Supplementary Figure 2.1A

Takamasa Inoue

- Figures 2.1A, 2.3B
- Supplementary Table 2.1

2.8 Supplemental Material

2.8.1 Supplementary Figures

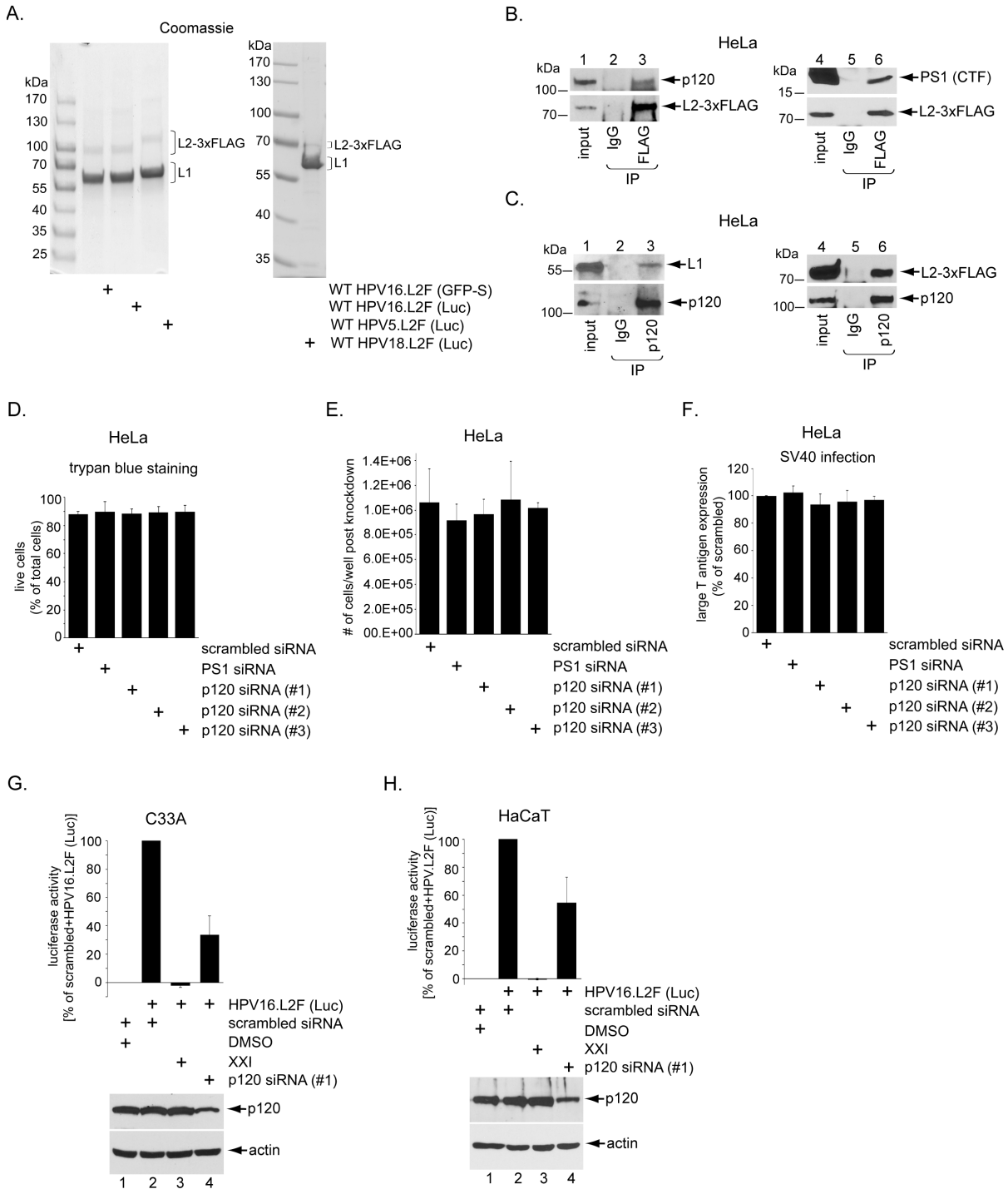

Supplementary Figure 2.1: Additional data characterizing a role of p120 during HPV16 infection (related to Figure 2.1)
A. *Purified WT HPV16.L2F (GFP-S), WT HPV16.L2F (Luc), WT HPV5.L2F (Luc), and WT HPV18.L2F (Luc) used in this study. Samples were subjected to SDS-PAGE and staining with Coomassie blue. The positions of L1 and FLAG-tagged L2 are indicated.*
B. *HeLa cells infected with WT HPV16.L2F (Luc) for 6 hrs were lysed and the resulting extract subjected to immunoprecipitation using a FLAG antibody, or an equal concentration of IgG control antibody. The precipitated material was analyzed by SDS-PAGE and immunoblotting using the indicated antibodies. Samples labelled input were not immunoprecipitated.*
C. *HeLa cells were infected with HPV16.L2F (Luc). 2.5 hpi, cells were lysed and the resulting extract was subjected to immunoprecipitation using an antibody against p120, or an equal concentration of IgG control antibody. The precipitated material was analyzed by SDS-PAGE and immunoblotting using the indicated antibodies. Samples labelled input were not immunoprecipitated.*
D. *HeLa cells transfected with the indicated siRNA were treated with trypan blue 72 hours after transfection to stain dead cells. Data represent the mean ± SD of three independent experiments.*
E. *HeLa cells were seeded at equal amounts and transfected with the indicated siRNA. 72 hours after transfection, cells were harvested and the total number of cells per condition were counted by hemocytometer. Data represent the mean ± SD of three independent experiments.*
F. *HeLa cells transfected with the indicated siRNA were infected with SV40 and subjected to immunofluorescence staining using an antibody against SV40 large T antigen. Data are the percent of cells expressing large T antigen, as assessed by fluorescent microscopy, normalized against SV40-infected cells treated with scrambled siRNA and represent the mean ± SD of three independent experiments.*
G. *C33A cells transfected with the indicated siRNA were infected with or without WT HPV16.L2F (Luc). 48 hpi, luciferase activity was measured from the cell culture media. Graph shows luciferase activity normalized against scrambled siRNA-treated cells with and without HPV. Data represent the mean ± SD of at least three independent experiments. The immunoblot reveals the extent of p120 depletion.*
H. *As in G, except HaCaT cells were used.*

2.8.2 Supplementary Tables

Supplementary Table 2.1: Potential HPV16-interacting host factors
Download complete table (Excel file): https://doi.org/10.1371/journal.ppat.1008946.s002
Full results from Inoue et al., 2018 (24) of L2 immunoprecipitation-mass spectrometry performed on samples of HeLa cells infected with WT HPV26.L2F for 16 hrs or uninfected cell extract incubated with purified HPV16 PsV (called mock-infected in table). The total number of peptides corresponding to the mock or HPV-infected cells are bolded. The results for p120 are highlighted in green.

2.9 References

1. C. L. Satterwhite *et al.*, Sexually transmitted infections among US women and men: prevalence and incidence estimates, 2008. *Sex Transm Dis* **40**, 187-193 (2013).

2. CDC, "Cancers Associated with Human Papillomavirus, United States—2014–2018," *USCS Data Brief, no. 26* (Atlanta, GA: Centers for Disease Control and Prevention, US Department of Health and Human Services, 2021).

3. T. Y. Walker *et al.*, National, Regional, State, and Selected Local Area Vaccination Coverage Among Adolescents Aged 13-17 Years - United States, 2017. *MMWR Morb Mortal Wkly Rep* **67**, 909-917 (2018).

4. L. E. Markowitz, J. Gee, H. Chesson, S. Stokley, Ten Years of Human Papillomavirus Vaccination in the United States. *Acad Pediatr* **18**, S3-S10 (2018).

5. C. B. Buck *et al.*, Arrangement of L2 within the papillomavirus capsid. *J Virol* **82**, 5190-5197 (2008).

6. K. F. Richards, M. Bienkowska-Haba, J. Dasgupta, X. S. Chen, M. Sapp, Multiple heparan sulfate binding site engagements are required for the infectious entry of human papillomavirus type 16. *J Virol* **87**, 11426-11437 (2013).

7. A. B. Raff *et al.*, The evolving field of human papillomavirus receptor research: a review of binding and entry. *J Virol* **87**, 6062-6072 (2013).

8. J. G. Joyce *et al.*, The L1 major capsid protein of human papillomavirus type 11 recombinant virus-like particles interacts with heparin and cell-surface glycosaminoglycans on human keratinocytes. *J Biol Chem* **274**, 5810-5822 (1999).

9. C. Cerqueira *et al.*, Heparin increases the infectivity of Human Papillomavirus type 16 independent of cell surface proteoglycans and induces L1 epitope exposure. *Cell Microbiol* **15**, 1818-1836 (2013).

10. M. Becker, L. Greune, M. A. Schmidt, M. Schelhaas, Extracellular Conformational Changes in the Capsid of Human Papillomaviruses Contribute to Asynchronous Uptake into Host Cells. *J Virol* **92**, (2018).

11. C. Cerqueira, P. Samperio Ventayol, C. Vogeley, M. Schelhaas, Kallikrein-8 Proteolytically Processes Human Papillomaviruses in the Extracellular Space To Facilitate Entry into Host Cells. *J Virol* **89**, 7038-7052 (2015).

12. T. Giroglou, L. Florin, F. Schafer, R. E. Streeck, M. Sapp, Human papillomavirus infection requires cell surface heparan sulfate. *J Virol* **75**, 1565-1570 (2001).

13. M. Knappe *et al.*, Surface-exposed amino acid residues of HPV16 L1 protein mediating interaction with cell surface heparan sulfate. *J Biol Chem* **282**, 27913-27922 (2007).

14. J. Dasgupta *et al.*, Structural basis of oligosaccharide receptor recognition by human papillomavirus. *J Biol Chem* **286**, 2617-2624 (2011).

15. R. M. Richards, D. R. Lowy, J. T. Schiller, P. M. Day, Cleavage of the papillomavirus minor capsid protein, L2, at a furin consensus site is necessary for infection. *Proc Natl Acad Sci U S A* **103**, 1522-1527 (2006).

16. L. Cruz, J. Biryukov, M. J. Conway, C. Meyers, Cleavage of the HPV16 Minor Capsid Protein L2 during Virion Morphogenesis Ablates the Requirement for Cellular Furin during De Novo Infection. *Viruses* **7**, 5813-5830 (2015).

17. P. M. Day, D. R. Lowy, J. T. Schiller, Heparan sulfate-independent cell binding and infection with furin-precleaved papillomavirus capsids. *J Virol* **82**, 12565-12568 (2008).

18. R. C. Kines, C. D. Thompson, D. R. Lowy, J. T. Schiller, P. M. Day, The initial steps leading to papillomavirus infection occur on the basement membrane prior to cell surface binding. *Proc Natl Acad Sci U S A* **106**, 20458-20463 (2009).

19. M. Schelhaas *et al.*, Entry of human papillomavirus type 16 by actin-dependent, clathrin- and lipid raft-independent endocytosis. *PLoS Pathog* **8**, e1002657 (2012).

20. G. Spoden *et al.*, Human papillomavirus types 16, 18, and 31 share similar endocytic requirements for entry. *J Virol* **87**, 7765-7773 (2013).

21. G. Spoden *et al.*, Clathrin- and caveolin-independent entry of human papillomavirus type 16--involvement of tetraspanin-enriched microdomains (TEMs). *PLoS One* **3**, e3313 (2008).

22. M. Bienkowska-Haba, C. Williams, S. M. Kim, R. L. Garcea, M. Sapp, Cyclophilins facilitate dissociation of the human papillomavirus type 16 capsid protein L1 from the L2/DNA complex following virus entry. *J Virol* **86**, 9875-9887 (2012).

23. J. L. Smith, S. K. Campos, A. Wandinger-Ness, M. A. Ozbun, Caveolin-1-dependent infectious entry of human papillomavirus type 31 in human keratinocytes proceeds to the endosomal pathway for pH-dependent uncoating. *J Virol* **82**, 9505-9512 (2008).

24. T. Inoue *et al.*, gamma-Secretase promotes membrane insertion of the human papillomavirus L2 capsid protein during virus infection. *J Cell Biol* **217**, 3545-3559 (2018).

25. W. Zhang, T. Kazakov, A. Popa, D. DiMaio, Vesicular trafficking of incoming human papillomavirus 16 to the Golgi apparatus and endoplasmic reticulum requires gamma-secretase activity. *mBio* **5**, e01777-01714 (2014).

26. B. Karanam *et al.*, Papillomavirus infection requires gamma secretase. *J Virol* **84**, 10661-10670 (2010).

27. H. S. Huang, C. B. Buck, P. F. Lambert, Inhibition of gamma secretase blocks HPV infection. *Virology* **407**, 391-396 (2010).

28. G. Barthet, A. Georgakopoulos, N. K. Robakis, Cellular mechanisms of gamma-secretase substrate selection, processing and toxicity. *Prog Neurobiol* **98**, 166-175 (2012).

29. A. J. Beel, C. R. Sanders, Substrate specificity of gamma-secretase and other intramembrane proteases. *Cell Mol Life Sci* **65**, 1311-1334 (2008).

30. P. Zhang, G. Monteiro da Silva, C. Deatherage, C. Burd, D. DiMaio, Cell-Penetrating Peptide Mediates Intracellular Membrane Passage of Human Papillomavirus L2 Protein to Trigger Retrograde Trafficking. *Cell* **174**, 1465-1476 e1413 (2018).

31. P. Zhang, R. Moreno, P. F. Lambert, D. DiMaio, Cell-penetrating peptide inhibits retromer-mediated human papillomavirus trafficking during virus entry. *Proc Natl Acad Sci U S A* **117**, 6121-6128 (2020).

32. A. Popa *et al.*, Direct binding of retromer to human papillomavirus type 16 minor capsid protein L2 mediates endosome exit during viral infection. *PLoS Pathog* **11**, e1004699 (2015).

33. A. Lipovsky *et al.*, Genome-wide siRNA screen identifies the retromer as a cellular entry factor for human papillomavirus. *Proc Natl Acad Sci U S A* **110**, 7452-7457 (2013).

34. P. M. Day, C. D. Thompson, R. M. Schowalter, D. R. Lowy, J. T. Schiller, Identification of a role for the trans-Golgi network in human papillomavirus 16 pseudovirus infection. *J Virol* **87**, 3862-3870 (2013).

35. Z. Kouchi *et al.*, p120 catenin recruits cadherins to gamma-secretase and inhibits production of Abeta peptide. *J Biol Chem* **284**, 1954-1961 (2009).

36. A. Kiss, R. B. Troyanovsky, S. M. Troyanovsky, p120-catenin is a key component of the cadherin-gamma-secretase supercomplex. *Mol Biol Cell* **19**, 4042-4050 (2008).

37. C. B. Buck, D. V. Pastrana, D. R. Lowy, J. T. Schiller, Efficient intracellular assembly of papillomaviral vectors. *J Virol* **78**, 751-757 (2004).

38. C. L. Young, Z. T. Britton, A. S. Robinson, Recombinant protein expression and purification: a comprehensive review of affinity tags and microbial applications. *Biotechnol J* **7**, 620-634 (2012).

39. Y. T. Zhu, H. C. Chen, S. Y. Chen, S. C. Tseng, Nuclear p120 catenin unlocks mitotic block of contact-inhibited human corneal endothelial monolayers without disrupting adherent junctions. *J Cell Sci* **125**, 3636-3648 (2012).

40. K. Xiao *et al.*, Cellular levels of p120 catenin function as a set point for cadherin expression levels in microvascular endothelial cells. *J Cell Biol* **163**, 535-545 (2003).

41. J. C. Brenner *et al.*, Genotyping of 73 UM-SCC head and neck squamous cell carcinoma cell lines. *Head Neck* **32**, 417-426 (2010).

42. C. M. Calton *et al.*, Translocation of the papillomavirus L2/vDNA complex across the limiting membrane requires the onset of mitosis. *PLoS Pathog* **13**, e1006200 (2017).

43. S. DiGiuseppe *et al.*, Incoming human papillomavirus type 16 genome resides in a vesicular compartment throughout mitosis. *Proc Natl Acad Sci U S A* **113**, 6289-6294 (2016).

44. S. DiGiuseppe, M. Bienkowska-Haba, L. G. M. Guion, T. R. Keiffer, M. Sapp, Human Papillomavirus Major Capsid Protein L1 Remains Associated with the Incoming Viral Genome throughout the Entry Process. *J Virol* **91**, (2017).

45. P. M. Day *et al.*, Human Papillomavirus 16 Capsids Mediate Nuclear Entry during Infection. *J Virol* **93**, (2019).

46. K. Xiao, R. G. Oas, C. M. Chiasson, A. P. Kowalczyk, Role of p120-catenin in cadherin trafficking. *Biochim Biophys Acta* **1773**, 8-16 (2007).

47. H. S. Huang, P. F. Lambert, Use of an in vivo animal model for assessing the role of integrin alpha(6)beta(4) and syndecan-1 in early steps in papillomavirus infection. *Virology* **433**, 395-400 (2012).

48. C. Y. Abban, P. I. Meneses, Usage of heparan sulfate, integrins, and FAK in HPV16 infection. *Virology* **403**, 1-16 (2010).

49. C. S. Yoon, K. D. Kim, S. N. Park, S. W. Cheong, alpha(6) Integrin is the main receptor of human papillomavirus type 16 VLP. *Biochem Biophys Res Commun* **283**, 668-673 (2001).

50. A. W. Woodham *et al.*, The S100A10 subunit of the annexin A2 heterotetramer facilitates L2-mediated human papillomavirus infection. *PLoS One* **7**, e43519 (2012).

51. Z. Surviladze, R. T. Sterk, S. A. DeHaro, M. A. Ozbun, Cellular entry of human papillomavirus type 16 involves activation of the phosphatidylinositol 3-kinase/Akt/mTOR pathway and inhibition of autophagy. *J Virol* **87**, 2508-2517 (2013).

52. Z. Surviladze, A. Dziduszko, M. A. Ozbun, Essential roles for soluble virion-associated heparan sulfonated proteoglycans and growth factors in human papillomavirus infections. *PLoS Pathog* **8**, e1002519 (2012).

53. K. D. Scheffer *et al.*, Tetraspanin CD151 mediates papillomavirus type 16 endocytosis. *J Virol* **87**, 3435-3446 (2013).

54. C. M. Cadwell, W. Su, A. P. Kowalczyk, Cadherin tales: Regulation of cadherin function by endocytic membrane trafficking. *Traffic* **17**, 1262-1271 (2016).

55. G. Serban *et al.*, Cadherins mediate both the association between PS1 and beta-catenin and the effects of PS1 on beta-catenin stability. *J Biol Chem* **280**, 36007-36012 (2005).

56. NCI, in *Laboratory of Cellular Oncology Technical Files: Production of Papillomaviral Vectors (Pseudoviruses)*. (Center for Cancer Research, National Cancer Institute, 2015).

CHAPTER 3:
HPV is a Cargo for the COPI Sorting Complex During Virus Entry

With permission from the publisher, this chapter is adapted from a previous publication:

HPV is a cargo for the COPI sorting complex during virus entry

Mara C. Harwood[†], Tai-Ting Woo[†], Yuka Takeo, Daniel DiMaio, and Billy Tsai. (2023).

Science advances, 9(3), eadc9830. https://doi.org/10.1126/sciadv.adc9830;

[†]co-first authors

3.1 Abstract

During entry, human papillomavirus (HPV) traffics from the cell surface to the endosome, and then to the trans-Golgi network (TGN) and Golgi apparatus. HPV must transit across the TGN/Golgi and exit these compartments to reach the nucleus to cause infection, although how these steps are accomplished is unclear. Combining cellular fractionation, unbiased proteomics, and gene-knockdown strategies, we identified COPI—a highly-conserved protein complex that facilitates retrograde trafficking of cellular cargos—as a host factor required for HPV infection. Upon TGN/Golgi arrival, the cytoplasmic segment of HPV L2 binds directly to COPI. COPI depletion causes the accumulation of HPV in the TGN/Golgi, resembling the fate of a COPI binding-defective L2 mutant. We propose that the L2-COPI interaction drives

HPV trafficking through the TGN and Golgi stacks during virus entry. This is the first evidence that an incoming virus is a cargo of the COPI complex.

3.2 Introduction

Human papillomavirus (HPV) accounts for approximately 4.5% of all cancers worldwide (*1*). It is the primary cause of cervical cancer and accounts for a substantial fraction of other anogenital and oropharyngeal cancers (*2*). Additionally, HPV causes a wide variety of warts, including common warts, plantar warts, and anogenital warts (*3*). Due in large part to incomplete understanding of many aspects of HPV infection including entry of the virus into cells, there are no specific anti-viral drugs that target HPV.

The HPV capsid, which encases the ~8 kb DNA genome, consists of 72 pentamers of the major viral capsid protein L1 and up to 72 copies of the minor capsid protein L2 (*4*). When fully assembled, the diameter of the capsid is approximately 55 nm (*5*). To cause infection, L1 binds to heparin sulfate proteoglycans at the plasma membrane of the host cell or in the extracellular matrix. This interaction imparts conformational changes to L1 that allow for cleavage of the N-terminus of L2 by the extracellular protease furin (*6-8*). Subsequent transfer of HPV to an unknown entry receptor (*8, 9*) promotes virus endocytosis, enabling the viral particle to reach the endosome where the low pH induces partial capsid disassembly (*10*).

The partially disassembled HPV in the endosome is targeted to γ-secretase, a transmembrane protease, through the action of the p120 catenin (*11*). γ-secretase then deploys an unconventional chaperone activity to promote the insertion of L2 into the endosome membrane and into the cytoplasm (*12, 13*), a process driven by a C-terminal cell-penetrating peptide (CPP) on L2 (*14, 15*). Membrane insertion allows for the bulk of L2 to protrude into the cytosol and recruit cytosolic trafficking factors, such as the retromer sorting complex that delivers the virus to the trans-Golgi network (TGN) (*16-19*). Several studies report L2-mediated trafficking of incoming viral components to the TGN and Golgi apparatus, and possibly the endoplasmic

reticulum (ER) prior to nuclear entry (*20-22*). An artificial transmembrane protein named JX4 traps incoming HPV in the TGN/Golgi compartment and inhibits infection, implying that transit through these compartments is required for infection (*19*).

How HPV transits the TGN and the Golgi apparatus and exits these compartments to reach the nucleus to cause infection remains unclear. Studies suggest that during transient nuclear envelope breakdown in mitosis (*23, 24*), transport vesicles containing HPV move from the TGN and/or Golgi apparatus to condensed chromosomes in the nucleus in an L2-dependent fashion (*20, 25, 26*). Throughout this transport process, the virus is thought to remain protected within a membrane-bound vesicle, with the viral DNA becoming exposed to the nucleoplasm only after mitosis is complete and the nuclear envelope reforms (*27*).

The retromer-L2 interaction at the endosome membrane generates vesicles that transport the incoming virus to the TGN. The subsequent transport of HPV through the TGN and Golgi stacks (a process we collectively designate here as "Golgi transit") presumably requires other more distal-acting retrograde trafficking factors, but the identity of the host sorting machinery promoting these steps in HPV entry remains unknown. We hypothesize that successful HPV trafficking during entry requires the sequential binding of different cytosolic sorting factors to the L2 segment that protrudes into the cytoplasm. The Sapp laboratory described a mutant HPV16 L2 protein in which two highly conserved arginine residues at position 302 and 305 (located in the cytosol when L2 protrudes into the cytoplasm) are changed to alanine (Figure 3.1A; R302/5A) (*28*). When cells are infected with pseudovirus (PsV) containing this L2 mutant, the mutant L2 protein accumulates in the TGN along with its encapsidated DNA and thus infection is blocked (*28*). Follow-up studies by the Sapp laboratory suggest that the R302/5A mutant may dissociate from the TGN but fails to associate with mitotic chromatin and is

subsequently reabsorbed into the TGN compartment (*27*). The segment of L2 that contains R302/R305 has also been identified as a nuclear retention signal and a chromatin binding domain (*29, 30*).

We hypothesized that L2 plays a central role in passage through the Golgi stacks separate from chromatin binding and nuclear entry and that the R302/5A mutant is defective for binding a cellular factor required for this process. Here, utilizing a combination of a cellular fractionation method, an unbiased proteomics approach, and a gene-knockdown strategy, our data reveal that the multi-subunit COPI protein complex is a critical host factor during HPV infection. COPI is a major cytosolic sorting protein complex that functions to transport cellular cargos within the TGN/Golgi compartments and out of the Golgi and into the ER (*31, 32*). We find that upon arrival of the incoming virion to the TGN, HPV L2 directly binds to a cargo recognition subunit of COPI (*33*). We further show that a short peptide from L2 containing R302/R305 is sufficient to bind COPI and that COPI depletion causes the accumulation of HPV16 in the TGN/Golgi. In addition, the R302/5A L2 mutant HPV that accumulates in the TGN/Golgi is defective for COPI binding. These results indicate that the L2-COPI interaction is required for trafficking of HPV through the TGN and Golgi stacks during entry and identify an incoming virus as a cargo for this vesicle sorting complex.

3.3 Results

3.3.1 Cell fractionation identifies COPI as an HPV-interacting host factor at the TGN/Golgi

We studied HPV entry using a well-established HPV pseudovirus (PsV) system that is composed of assembled viral capsid proteins L1 and L2, along with a reporter plasmid expressing a reporter protein such as green fluorescent proteins (GFP) instead of the viral genome (*34-36*). This PsV system allows us to study wild-type (WT) HPV16 as well as L2 mutants including R302/5A. Furthermore, the PsVs contain a 3xFLAG epitope tag appended to the C-terminus of L2 (called "L2F"), allowing us to use an anti-FLAG antibody to immunoprecipitate and detect the virus throughout the entry process (*20*). Because key intracellular trafficking steps of the HPV PsV resemble that of HPV generated by stratified keratinocyte raft cultures (*37*), insights from the study of HPV PsV entry continue to illuminate bona fide HPV infection events.

To elucidate the mechanism of Golgi transit, we hypothesized that during entry HPV binds to a Golgi-associated factor that sorts HPV out of the TGN or between Golgi stacks and that the R302/5A L2 mutant is unable to undergo Golgi transit because it cannot interact with this putative factor. To explore these hypotheses, we first confirmed that WT HPV16.L2F infects HeLa and HaCaT cells [via a pathway sensitive to the γ-secretase inhibitor XXI, as expected (*28, 38*)], but the R302/5A HPV16.L2F mutant virus is defective (Supplementary Figure 3.1A–B). We then used the proximity ligation assay (PLA) to assess if R302/5A HPV16 indeed accumulates in the TGN/Golgi [previous studies used immunofluorescence colocalization and did not examine Golgi stack markers (*27, 28*)]. PLA is an antibody-based assay in which a fluorescent signal is generated when two target proteins are proximal (~40 nm) to each other. If one of the proteins is a cellular organelle marker and the other is an HPV structural protein,

appearance of a fluorescent signal indicates arrival of HPV to (or near) that organelle (*39*). Accordingly, HeLa cells were infected with WT HPV16.L2F or R302/5A HPV16.L2F for different times, fixed, incubated with anti-L1 antibody and antibodies recognizing TGN46 and GM130 (widely used as TGN and cis-/medial-Golgi stack markers, respectively) and subjected to PLA to detect localization of HPV in the TGN or Golgi apparatus. In PLA assays, we used PsV containing a reporter plasmid expressing luciferase or red fluorescent protein instead of GFP to prevent possible interference with the green fluorescent signals generated by PLA.

In HeLa cells infected with either WT HPV16.L2F or R302/5A HPV16.L2F, similar levels of L1-TGN46 PLA signals were observed at 24 h post-infection (hpi) (Supplementary Figure 3.1C, top row of panels; quantified in Supplementary Figure 3.1D), indicating that the R302/5A virus can enter host cells and reach the TGN. In contrast, at 30 hpi when wild-type virus had largely exited the TGN/Golgi compartment en route to the nucleus, we observed an approximately 4.7-fold increased L1-TGN46 PLA signal in cells infected with the mutant compared to wild-type (Supplementary Figure 3.1C, bottom row of panels; quantified in Supplementary Figure 3.1D). However, there is not an absolute block to departure of the mutant from the TGN, because we also detected L1-GM130 PLA signal at 24 hpi in cells infected with wild-type or R302/5A HPV16.L2F PsV (Supplementary Figure 3.1E–F). At 30 hpi the mutant PsV displayed approximately 2-fold accumulation in the GM130-positive compartment compared to wild-type PsV. As expected, only a low background level of PLA signal was detected in uninfected cells at any timepoint examined (Supplementary Figure 3.1C–F). These data confirm that the R302/5A virus accumulates in the TGN/Golgi, consistent with previous reports that showed increased co-localization of TGN46 with reporter plasmid DNA and L2 (*27, 28*).

To identify TGN/Golgi-associated host factors that bind to WT but not R302/5A L2 during infection, we used a cellular fractionation/proteomics approach. Cells were infected with WT HPV16.L2F or R302/5A HPV16.L2F PsV. At 22 hpi (before the mutant PsV accumulates in TGN), cells were mechanically homogenized and the resulting extract was subjected to ultracentrifugation over a discontinuous sucrose gradient (Figure 3.1B; Steps 1 and 2). After centrifugation, gradient fractions were collected (Figure 3.1B; Step 3), and a portion of each fraction was subjected to sodium dodecyl-sulfate polyacrylamide gel electrophoresis (SDS-PAGE) followed by immunoblotting with antibodies that mark different cellular compartments, HPV L1, or HPV L2 (FLAG). Our analysis showed that fractions 3–5 in infected (Figure 3.1C) and uninfected (Supplementary Figure 3.1G) cells contained the TGN and Golgi organelle markers TGN46 and GM130. In infected cells, these fractions also contained a pool of HPV16 L1 and L2. The TGN/Golgi-containing fractions of infected cells were then combined, lysed, and subjected to FLAG immunoprecipitation (Figure 3.1B; Step 4), which isolated similar levels of L2 from either WT or R302/5A infected cells (Supplementary Figure 3.1H). The precipitated material was analyzed by mass-spectrometry to identify potential virus-interacting host components that co-precipitated with L2F in each condition (Figure 3.1B, Step 5). As a control, TGN/Golgi-containing fractions derived from uninfected cells were mixed with purified WT HPV16.L2F PsV prior to immunoprecipitation and processed as above (“control” lane, Supplementary Figure 3.1H). We presume that any host factors that interact with L2 under this condition are cellular components that bound to HPV post-homogenization, instead of during infectious cellular entry of HPV.

As expected, the mass-spectrometry results identified comparable levels of peptides corresponding to HPV L1 and L2 in samples derived from cells infected with WT HPV16.L2F,

R302/5A HPV16.L2F, or from the control sample (Supplementary Figure 3.1I). Peptides corresponding to five of the seven subunits of the COPI protein-sorting complex (α, β, β', δ, and γ; with the exception of ε and ζ) were found in the sample derived from cells infected with WT but not from the control sample with admixed PsV (Figure 3.1D). Importantly, the COPI peptides were not recovered from the immunoprecipitates from cells infected with R302/5A HPV16.L2F PsV. (The entire mass-spectrometry data are available in Supplementary Table 3.1.)

COPI is a multi-subunit cytosolic sorting complex (Figure 3.1E) that facilitates cargo trafficking within the TGN/Golgi and between the Golgi and ER [reviewed in (*31-33*)]. COPI is generally considered a retrograde sorting complex, but it can also sort proteins in an anterograde direction (see discussion). This protein-sorting complex displays several features consistent with being a Golgi transit factor for HPV: it associates with wild-type HPV localized to the TGN/Golgi during entry, it fails to associate with an L2 mutant HPV defective for Golgi transit, and it is known to display intrinsic sorting activity with cellular retrograde cargos.

A

```
                                  **  ::      :* **:* : *: ****  **::
      WT HPV5   L2  328  GRPQYSTTPAGYVRVSRLGTRATIRTRSGAQIGSQ  362
      WT HPV18  L2  283  HRPALTS-RRGTVRFSRLGQRATMFTRSGTQIGAR  316
      WT HPV16  L2  290  HRPALTS-RRTGIRYSRIGNKQTLRTRSGKSIGAK  323
R302/5A HPV16 L2  290  HRPALTS-RRTGIAYSAIGNKQTLRTRSGKSIGAK  323
```

B

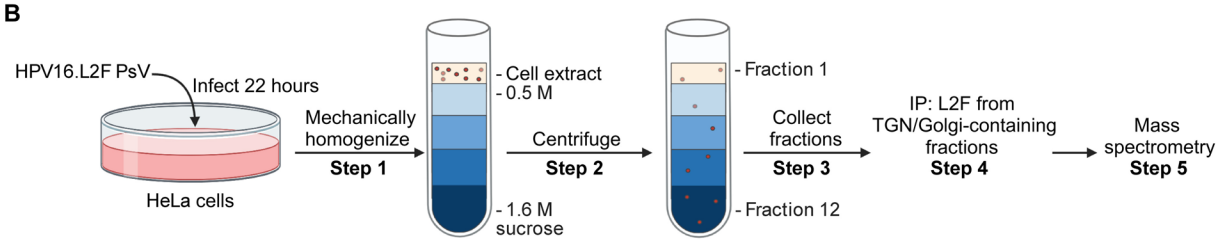

C

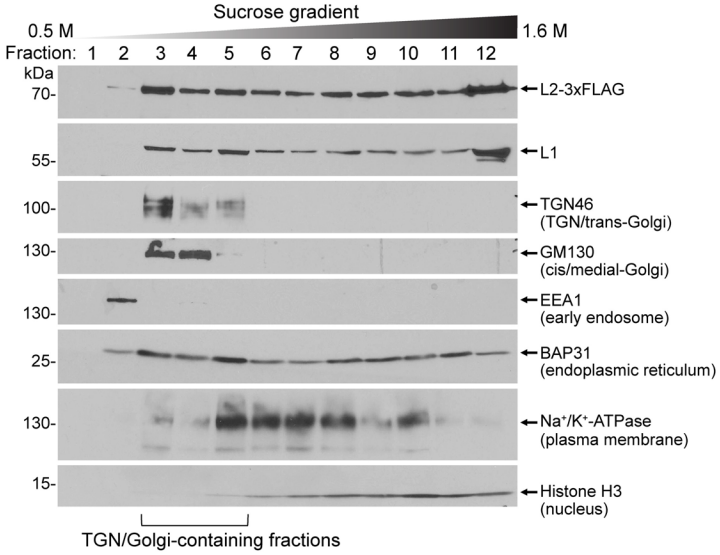

D

Mass spec total number of peptides

Gene symbol	Control WT HPV16.L2F	WT HPV16.L2F	R302/5A HPV16.L2F
COPA (α)	0	11	0
COPB1 (β)	0	1	0
COPB2 (β')	0	2	0
COPD (δ)	0	1	0
COPG1 (γ1)	0	1	0

E

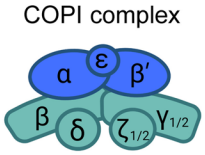

Figure 3.1: Cell fractionation identifies COPI as an HPV-interacting host factor at the TGN/Golgi
A. *Sequence alignment of the L2 protein of various HPV types. Two conserved arginine residues (magenta) are mutated to alanine (red) in R302/5A HPV16 L2. Asterisks indicate fully conserved residues. Colons indicate conservation between groups of strongly similar properties. Multiple sequence alignment of full-length L2 was performed with Clustal Omega, and the fragments containing the di-arginine motif are shown.*
B. *Overview of cellular fractionation to isolate material for mass spectrometry analysis. See the main text for details. Figure created with BioRender.com.*
C. *Representative blots from fractionated extract obtained after step 3. Extracts were subjected to SDS-PAGE followed by immunoblotting with the indicated antibodies. Fractions 3 to 5 containing TGN46 and GM130 were pooled before FLAG-immunoprecipitation (step 4) and mass spectrometry (step 5).*
D. *Total number of peptides corresponding to subunits of the COPI complex identified by mass spectrometry (step 5). WT, material obtained from cells infected with WT HPV16.L2F PsV; R302/5A, material obtained from cells infected with R302/5A HPV16.L2F PsV; control, material obtained from cells that were uninfected but mixed with WT HPV16.L2F PsV between steps 3 and 4. See table S1 for a complete list of peptides identified by mass spectrometry.*
E. *Simplified diagram of the COPI complex. Blue and green represent the two subcomplexes of COPI (32). Figure created with BioRender.com.*

3.3.2 The di-arginine motif in the L2 protein mediates binding between HPV16 and COPI upon TGN/Golgi arrival

To verify the mass-spectrometry findings, we performed co-immunoprecipitation (co-IP) and immunoblotting experiments. Extracts derived from uninfected cells or cells infected for 22 h with WT HPV16.L2F or R302/5A HPV16.L2F were subjected to immunoprecipitation using an antibody against the β-COP subunit, and the precipitated material was analyzed by SDS-PAGE followed by immunoblotting. We found that precipitation of β-COP selectively pulled down L2-3xFLAG from cells infected with WT but not the mutant PsV (Figure 3.2A, top panel); as a negative control, an IgG antibody did not pull down L2-3xFLAG from the WT-infected cells because β-COP was not precipitated. Similar findings were found when antibodies recognizing β'-COP (Figure 3.2B, top panel) or γ-COP (Figure 3.2C, top panel) were used for immunoprecipitation. Combined with the mass-spectrometry data in the preceding section, these data demonstrate that HPV engages the COPI complex in cells in a manner that requires arginine residues that are mutated in the trafficking defective R302/5A mutant.

To assess whether a short segment of the L2 protein containing the arginine residues at positions 302 and 305 is sufficient to bind to COPI, we performed pull-down experiments with 14-residue peptides consisting of HPV16 L2 positions 299 to 312 (Figure 3.1A). Peptides consisting of the wild-type HPV16 L2 sequence (TGI**R**YS**R**IGNKQTL) or the corresponding mutant sequence in which arginine 302 and arginine 305 are substituted with alanine (TGI**A**YS**A**IGNKQTL, with the mutated amino acids in bold) were synthesized with an N-terminal biotin tag. Peptides were incubated with extracts of uninfected HeLa cells for 2 h. Peptides and associated proteins were then pulled down with streptavidin beads and subjected to SDS-PAGE and immunoblotting. As shown in Figure 3.2D, lanes 3 and 4, the wild-type but not

the mutant peptide bound to α-COP and γ-COP. As expected, neither peptide bound the VPS35 subunit of retromer, which binds to a different sequence near the C-terminus of L2 (*18*). This experiment demonstrates that a short segment derived from the middle of the L2 protein is sufficient to bind COPI and that a conserved di-arginine motif within this segment is required for the L2-COPI interaction.

To determine when the HPV-COPI interaction occurs during entry, we performed a time-course experiment. Extracts derived from HeLa cells infected with WT HPV16.L2F for various times were subjected to immunoprecipitation using an antibody against γ-COP, and the precipitated material analyzed by SDS-PAGE and immunoblotting using a FLAG (L2) antibody. L2-3xFLAG co-immunoprecipitated with γ-COP starting at 16 hpi (Figure 3.2E, top panel), a time point when HPV reaches the TGN (*12, 17, 18, 20*). Moreover, impairing HPV arrival to the TGN by inhibiting the upstream host factor γ-secretase with the chemical XXI prevented co-immunoprecipitation between γ-COP and HPV L2 (Figure 3.2F, top panel); as expected, XXI blocked γ-secretase-mediated cleavage of L2 (Figure 3.2F, input). Together, these biochemical data suggest that HPV interacts with COPI upon arrival in the TGN.

To assess the COPI-HPV interaction in intact cells, we performed PLA with antibodies recognizing γ-COP and HPV L1. At 24 hpi, PLA signals between γ-COP and HPV16 L1 were observed. Consistent with co-IP results, PLA signals were inhibited by treating cells with XXI, which prevents HPV trafficking to the TGN (*20*) (Figure 3.2G; quantified in 3.2H). These imaging data suggest that transport of HPV to the TGN positions the virus proximal to the COPI complex, in agreement with our biochemical findings that HPV physically engages COPI when the virus reaches the TGN.

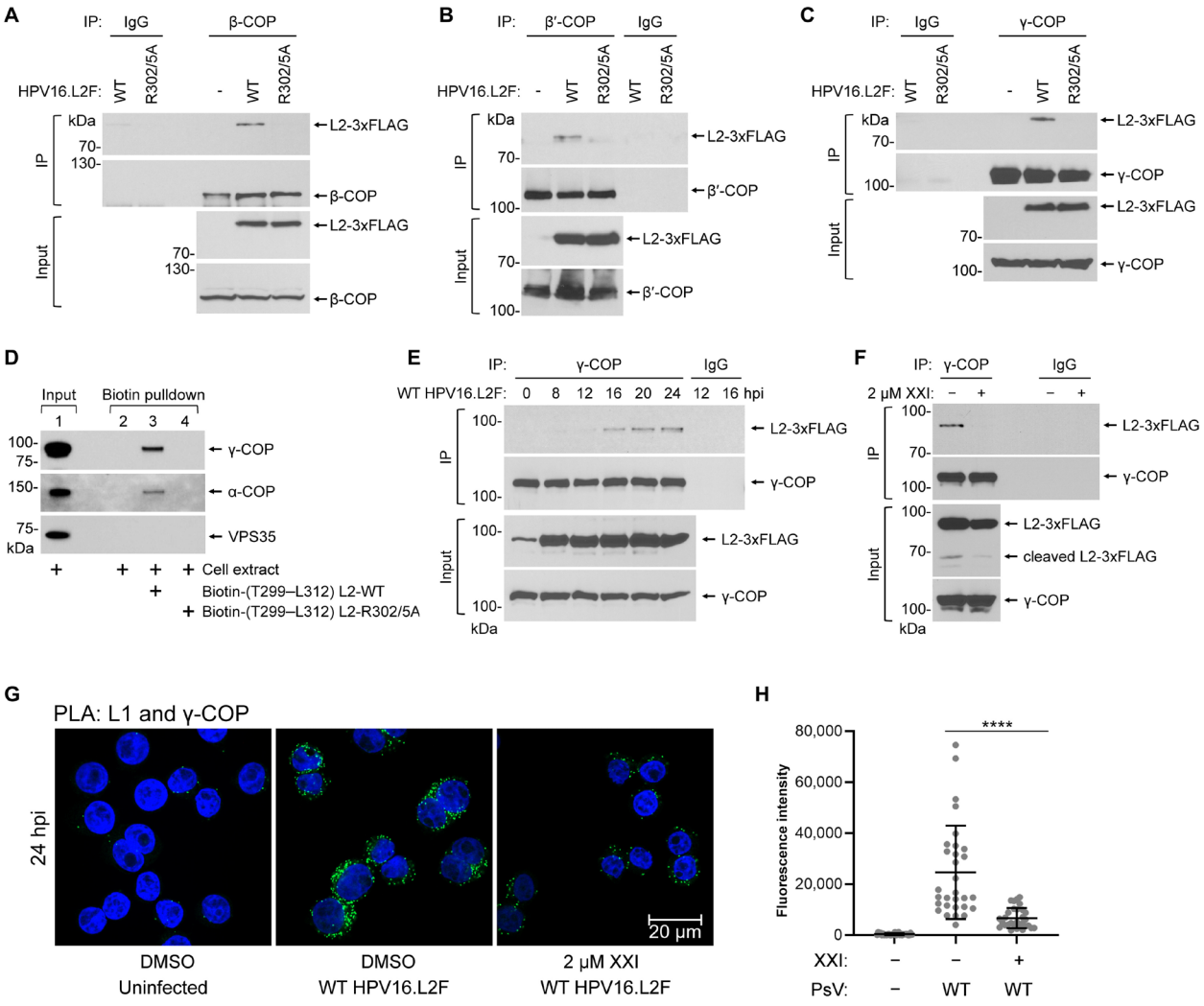

Figure 3.2: The di-arginine motif in the L2 protein mediates binding between HPV16 and COPI upon TGN/Golgi arrival

A. *Whole-cell extracts of HeLa cells uninfected or infected with WT or R302/5A HPV16.L2F for 22 hours were subjected to immunoprecipitation with an anti–β-COP antibody or a rabbit normal IgG as a negative control. Immunoprecipitated samples were analyzed with anti-FLAG and anti–β-COP antibodies.*

B. *As in (A), except an anti-β'-COP antibody was used.*

C. *As in (A), except an anti–γ-COP antibody was used.*

D. *Whole-cell extracts of uninfected HeLa cells were incubated with biotin-tagged peptides containing residues T299 to L312 of the WT HPV16 L2 (lane 3) or the corresponding R302/5A mutant (lane 4). Samples precipitated with streptavidin-beads were analyzed with antibodies recognizing α-COP, γ-COP, or retromer subunit VPS35.*

E. *WT HPV16.L2F–infected HeLa cells were lysed at different hpi for immunoprecipitation experiments as in (C).*

F. *HeLa cells were infected with WT HPV16.L2F for 20 hours in the presence of dimethyl sulfoxide (DMSO) or 2 μM XXI and subjected to immunoprecipitation experiments as in (C).*

G. *HeLa-S3 cells were uninfected or infected with WT HPV16.L2F in the presence of DMSO or 2 μM XXI. At 24 hpi, PLA (signals shown in green) was performed with antibodies recognizing HPV16 L1 and γ-COP. Nuclei were stained with 4',6-diamidino-2-phenylindole (DAPI; blue). Similar results were obtained in two independent experiments.*

H. *PLA fluorescence intensity per cell in multiple images as in (G) was measured, and the individual cell fluorescence intensity values, means, and SDs of 30 cells are shown. A two-tailed, unequal variance t test was used to determine statistical significance. ****$P < 0.0001$.*

3.3.3 COPI directly binds to HPV16 L2 in vitro

To test whether HPV L2 binds directly to COPI, we incubated purified mammalian COPI complex with either purified WT HPV16.L2F PsV or the control protein EGFP-FLAG (Figure 3.3A), and the samples were subjected to FLAG immunoprecipitation. γ-COP co-precipitated with L2-3xFLAG but not EGFP-FLAG (Figure 3.3B, top panel), suggesting that the HPV particle directly interacts with the COPI complex.

To determine if γ-COP, a subunit of the COPI complex that has been shown to bind cellular cargo (*40, 41*), binds directly to L2, we conducted in vitro binding assays with purified FLAG-γ1-COP (lacking the other COPI subunits) and a hemagglutinin (HA)-tagged HPV16 L2-3xFLAG protein lacking the N-terminal 67 amino acids [HA-(Δ1–67) L2-3xFLAG] (Figure 3.3C). The N-terminus of L2 contains a putative transmembrane domain (amino acids 45–67) (*42*). Upon insertion, the C-terminal portion of the L2 (amino acids 68–473) is positioned into the cytosol where binding to COPI could take place. When purified FLAG-γ1-COP was incubated with either EGFP-FLAG or HA-(Δ1–67) L2-3xFLAG and the samples subjected to immunoprecipitation using a γ-COP antibody, only HA-(Δ1–67) L2-3xFLAG but not EGFP-FLAG was pulled down (Figure 3.3D, top panel, compare lanes 2 to 1). Not surprisingly, in the absence of FLAG-γ1-COP, the γ-COP antibody did not pull down HA-(Δ1–67) L2-3xFLAG (Figure 3.3D, top panel, lane 4), indicating that presence of γ1-COP is needed to co-immunoprecipitate L2. These findings demonstrate that γ1-COP directly interacts with the portion of L2 thought to protrude into the cytoplasm.

Because the mutant R302/5A HPV16.L2F PsV did not associate with the COPI complex during viral entry in cells (Figure 3.2A–C) and because a short peptide from L2 containing the R302/5A mutation could not bind to COPI in a cellular extract (Figure 3.2D), we asked if a

purified L2 protein containing the same mutation can engage γ1-COP in the in vitro system. Accordingly, we purified HA-(Δ1–67) L2-R302/5A-3xFLAG (Figure 3.3C) and tested its ability to bind to purified FLAG-γ1-COP as above. Our results showed that the mutant L2 protein displayed significantly reduced efficiency in binding to γ1-COP when compared to the corresponding WT L2 protein (Figure 3.3E, top panel, compare lane 2 to 1; quantified in Figure 3.3F). The requirement and competency of the di-arginine motif for binding to γ-COP was also evident in the peptide-pulldown assay when purified FLAG-γ1-COP instead of the cell extract was used (Figure 3.2D). After incubating the corresponding biotinylated peptides with the purified FLAG-γ1-COP in vitro, the L2 peptide carrying the wild-type di-arginine motif was sufficient to pull down FLAG-γ1-COP, whereas the peptide harboring the R302/5A mutation was defective (Figure 3.3G).

Together, these findings are consistent with our biotin-L2 peptide pull-downs and co-IPs from extracts of infected cells and our mass-spectrometry results, demonstrating that the di-arginine motif of L2 at positions 302 and 305 in HPV16 plays a critical role in mediating direct contact with the COPI complex.

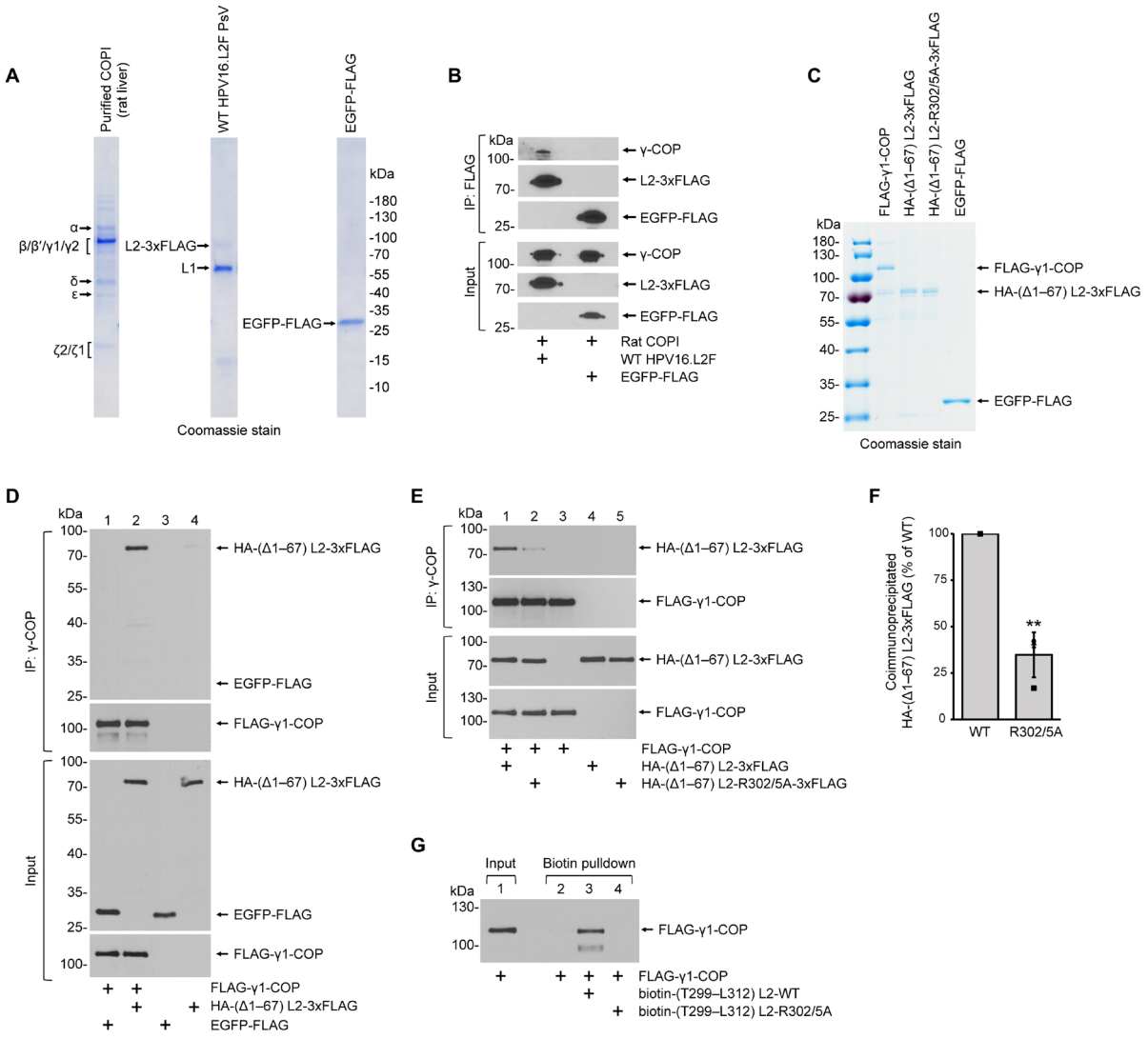

Figure 3.3: COPI directly binds to HPV16 L2 in vitro

A. *Coomassie stain (left to right): purified rat liver COPI with subunits marked left of the gel, WT HPV16.L2F PsV purified from HEK 293T cells, and purified C-terminal FLAG-tagged EGFP.*

B. *The rat COPI complex was incubated with WT HPV16.L2F PsV or EGFP-FLAG. Samples from immunoprecipitation using anti-FLAG beads were analyzed by immunoblotting with antibodies recognizing FLAG or human γ-COP.*

C. *Coomassie stain of purified proteins. FLAG-γ1-COP, N-terminal FLAG-tagged human γ1-COP; HA-(Δ1–67) L2-3xFLAG, HPV16 L2 (amino acids 1 to 67 deleted) tagged with N-terminal HA and C-terminal 3xFLAG; HA-(Δ1–67) L2-R302/5A-3xFLAG, HA-(Δ1–67) L2-3xFLAG with R302/5A mutation.*

D. *FLAG-γ1-COP was incubated with EGFP-FLAG or HA-(Δ1–67) L2-3xFLAG followed by immunoprecipitation using anti–γ-COP antibodies. Coimmunoprecipitated proteins were analyzed by immunoblotting for HA-(Δ1–67) L2-3xFLAG and EGFP-FLAG (anti-FLAG antibody) or FLAG-γ1-COP (anti–γ-COP antibody).*

E. *Same experiments as in (D) except that HA-(Δ1–67) L2-R302/5A-3xFLAG was analyzed for the comparison with HA-(Δ1–67) L2-3xFLAG.*

F. *Quantification of the coimmunoprecipitated proteins shown in top of (E). The protein band intensity of HA-(Δ1–67) L2-3xFLAG (WT) or HA-(Δ1–67) L2-R302/5A-3xFLAG (R302/5A) was normalized to that of FLAG-γ1-COP in the same precipitated sample. Data represents means normalized to WT and SDs (n = 4). A two-tailed, unequal variance t test was used to determine statistical significance. **P < 0.01.*

G. *Biotin peptide pulldown as in (Figure 3.2D), except biotinylated peptides were incubated with the purified FLAG-γ1-COP. Precipitated samples were immunoblotted with an antibody recognizing γ-COP.*

3.3.4 COPI promotes HPV infection

Because we identified COPI as a direct HPV L2-binding partner during entry, we asked if COPI is important during HPV entry. We used siRNA-mediated knockdown (KD) to deplete the individual COPI subunits in HeLa cells and tested the effect on PsV infection. Isoforms of γ-COP and ζ-COP (γ1/γ2 and ζ1/ζ2) (43, 44) were also examined. The transcript levels of all the COPI subunits, with the exception of ζ1-COP, were effectively reduced by their corresponding siRNAs (Supplementary Figure 3.2A). After KD, cells were infected with WT HPV16.L2F PsV containing the GFP reporter plasmid, and virus infection was assessed by flow cytometry to analyze GFP expression as an indication of successful delivery of the pseudoviral genome to the nucleus. WT HPV16.L2F infection was severely impaired by α-COP (COPA), β-COP (COPB1), β'-COP (COPB2), δ-COP (COPD), and γ1-COP (COPG1) KD when compared to control (scrambled siRNA-treated, Scr) cells (Figure 3.4A); a similar pattern was seen when GFP expression was analyzed by immunoblotting (Supplementary Figure 3.2B). Strikingly, these required subunits are the same ones that associate with incoming wild-type HPV as assessed by the proteomics analysis of infected cells (Figure 3.1D). The lack of phenotype in cells depleted of ε-COP may be due to its non-essential role for retrograde transport as reported in prior studies in yeast and human cells (*43, 44*). Of these five COPI subunits required for HPV infection, KD of α-COP and γ1-COP did not affect the level of the other subunits, while KD of β-COP, β'-COP, or δ-COP reduced the level of the others to varying extents (Supplementary Figure 3.2C).

Despite blocking HPV infection (Figure 3.4A), KD of γ1-COP did not affect the localization pattern of the Golgi marker GM130 (Supplementary Figure 3.2D, first column) or β'-COP (Supplementary Figure 3.2D, second column). In addition, γ1-COP KD did not significantly alter cell cycle progression, as measured by the percentage of cells in G1, S, or

G2+M phases compared to control cells (Supplementary Figure 3.2E–F). Membrane integrity and cell viability, as monitored by the ability of cells to exclude DAPI-stain, were also largely unaffected by γ1-COP KD (Supplementary Figure 3.2G). Moreover, γ1-COP KD cells supported infection by another non-enveloped DNA virus, SV40 (Supplementary Figure 3.2H, left panel) despite robust depletion of γ1-COP protein levels (Supplementary Figure 3.2I, left panel). In contrast, KD of SGTA (Supplementary Figure 3.2H, right panel), a host factor important for SV40 infection (*45*), reduced SV40 infection as expected (Supplementary Figure 3.2I, right panel). These findings demonstrate that depletion of γ1-COP did not globally disrupt cellular integrity, strongly suggesting that COPI plays a specific and critical role during HPV infection.

To establish that the COPI KD phenotype is not due to an off-target effect, we performed a KD-rescue experiment with γ1-COP fused to mCherry to allow monitoring of γ1-COP expression. Cells transfected with the Scr or COPG1 siRNA were co-transfected with the control plasmid HA-mCherry or the siRNA-resistant rescue construct HA-γ1-COP-mCherry (Supplementary Figure 3.2J), and then infected with WT HPV16.L2F PsV. Flow cytometry analyses revealed that most cells expressed the exogenous mCherry-fusion proteins and that expression levels were similar in each condition (Supplementary Figure 3.2K). In cells expressing HA-mCherry, KD of γ1-COP blocked infection, as expected (Figure 3.4B; compare second to first bar). However, if HA-γ1-COP-mCherry is expressed in cells depleted of γ1-COP, infection was largely restored (Figure 3.4B, compare fourth to second bar), while expression of HA-γ1-COP-mCherry in cells transfected with control siRNA did not increase HPV infection (Figure 3.4B, compare third to first bar). Moreover, this restoration of infection in γ1-COP KD cells was not observed in cells not expressing HA-γ1-COP-mCherry (i.e., mCherry-negative) (Figure 3.4C, compare fourth to second bar). These results demonstrate that the block in HPV

infection from the COPG1 siRNA is due to loss of γ1-COP and not to unintended off-target effects, firmly establishing a crucial function of the COPI complex in HPV infection.

We next evaluated if COPI is used as an entry factor by different HPV types. Depletion of γ1-COP attenuated infection by HPV5 (Figure 3.4D) or HPV18 (Figure 3.4E) PsVs. When different siRNAs (pooled) were used to KD γ1-COP in human HaCaT skin keratinocytes (Supplementary Figure 3.2L), HPV16 infection was blunted as well (Figure 3.4F). Thus, COPI is used by divergent HPV types to support infection in cell types relevant to HPV infection.

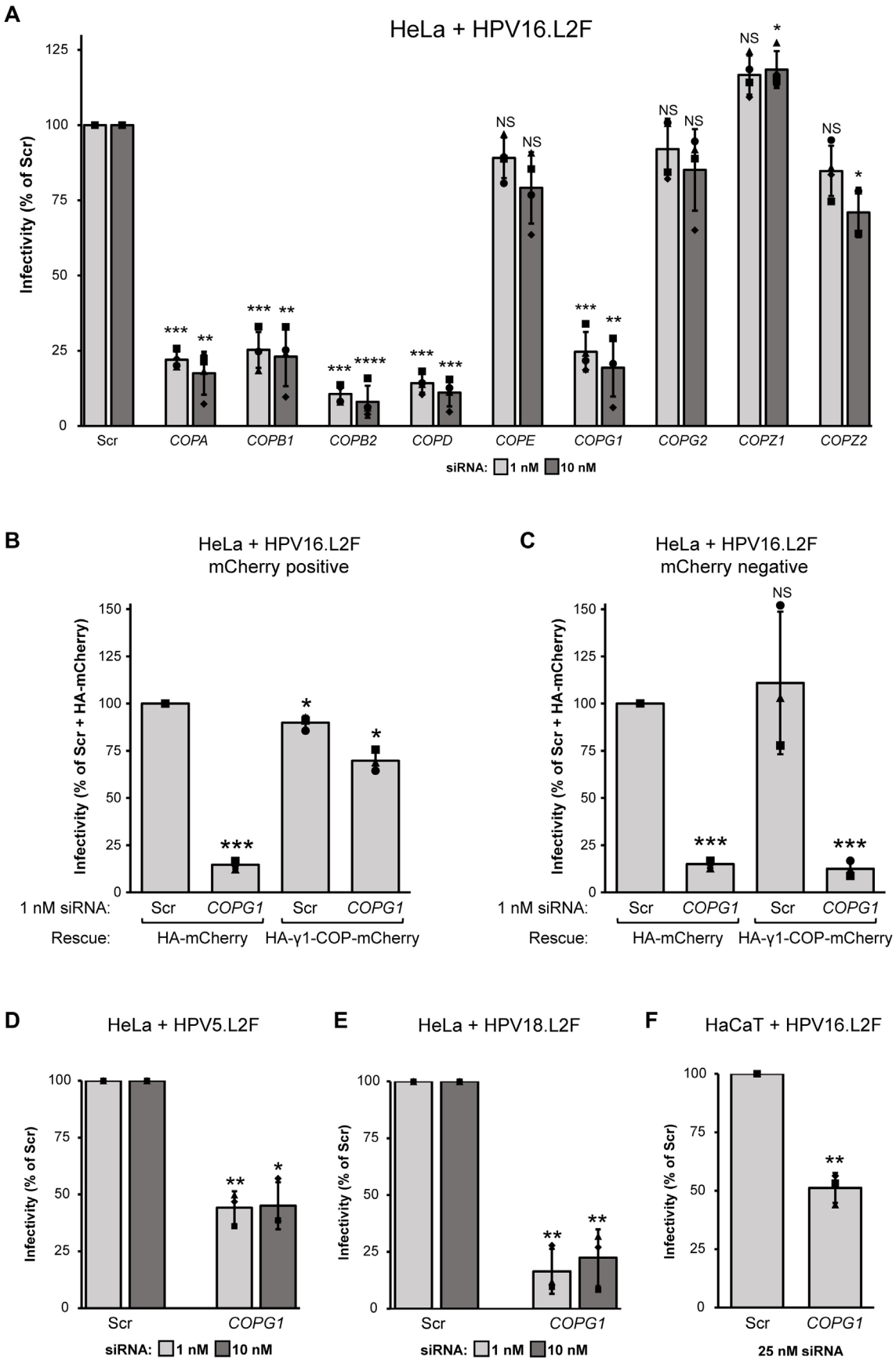
A
HeLa + HPV16.L2F
Infectivity (% of Scr)
Scr
COPA
COPB1
COPB2
COPD
COPE
COPG1
COPG2
COPZ1
COPZ2
siRNA: 1 nM 10 nM
B
HeLa + HPV16.L2F
mCherry positive
Infectivity (% of Scr + HA-mCherry)
1 nM siRNA:
Rescue:
HA-mCherry
HA-γ1-COP-mCherry
C
HeLa + HPV16.L2F
mCherry negative
D
HeLa + HPV5.L2F
E
HeLa + HPV18.L2F
F
HaCaT + HPV16.L2F
25 nM siRNA
NS

Figure 3.4: COPI promotes HPV infection

A. *HeLa cells transfected with the indicated siRNA for 24 hours were infected with WT HPV16.L2F PsV containing a GFP reporter plasmid. At 48 hpi, flow cytometry was used to determine the fraction of GFP-expressing cells. The results were normalized to the infected fraction of cells treated with Scr siRNA. The means and SDs are shown (n = 3). A two-tailed, unequal variance t test was used to determine statistical significance compared to Scr siRNA–treated cells. NS, not significant; *P < 0.05, **P < 0.01, ***P < 0.001, and ****P < 0.0001.*

B. *HeLa cells were transfected with Scr or COPG1 siRNAs for 9 hours, followed by another transfection with DNA constructs for 15 hours for the expression of HA-γ1-COP-mCherry or the control HA-mCherry. The transfected cells were then infected with WT HPV16.L2F PsV containing a GFP reporter plasmid. At 48 hpi, flow cytometry was used to measure GFP and mCherry fluorescence. The fraction of cells expressing GFP in the mCherry-positive population is graphed. The results were normalized to the infected fraction of cells cotransfected with Scr siRNA and HA-mCherry–expressing plasmid. Data from three independent experiments were analyzed and presented as in (A).*

C. *As in (B), except the fraction of cells expressing GFP in the mCherry-negative population is graphed.*

D. *As in (A), except WT HPV5.L2F PsV was used.*

E. *As in (A), except WT HPV18.L2F PsV was used.*

F. *As in (A), except HaCaT cells were transfected with pooled Scr or COPG1 siRNAs for 48 hours before infection with WT HPV16.L2F PsV.*

3.3.5 Arf1-dependent COPI recruitment to the TGN/Golgi is critical for HPV infection

Our model thus far posits that HPV—via the L2 protein protruding in the cytosol—captures COPI when the virus reaches the TGN/Golgi to promote virus infection. This model presumes that HPV L2 binds to COPI at the cytosolic surface of TGN/Golgi membranes. To test if proper targeting of COPI to these membranes is required for HPV infection, we disrupted COPI recruitment to the TGN/Golgi membrane by inhibiting the small GTPase Arf1. Arf1 cycles between a GDP or GTP bound state, a process regulated by nucleotide exchange factors and GTPase-activating proteins (GEFs and GAPs) (Figure 3.5A) (*46*). When a GEF replaces GDP with GTP on cytosolic Arf1, the resulting Arf1-GTP is directed to the TGN/Golgi membrane; this in turn recruits COPI to the membrane (*47*). The chemical inhibitor NAV-2729 (NAV) inhibits nucleotide exchange on Arf1 (*48, 49*), thus preventing Arf1 from binding to the TGN/Golgi membrane and subsequent recruitment of COPI.

In untreated cells, γ1-COP displayed a concentrated, asymmetric perinuclear distribution that was slightly more disperse than the GM130 distribution, consistent with a TGN/Golgi localization (Figure 3.5B, top row). As expected, NAV treatment resulted in a diffuse distribution of γ-COP, while leaving the Golgi structure intact as assessed by GM130 staining (Figure 3.5B, bottom row). In addition, the levels of the individual COPI subunits (as well as Arf1) were unaffected by inhibitor treatment as assessed by western blotting (Figure 3.5C). These results confirm that NAV treatment prevents the localization of γ1-COP to the TGN/Golgi membrane, without disrupting cellular levels of COPI or Arf1.

Importantly, NAV-treatment prevented COPI (γ-COP) from binding to HPV16 L2 in infected cells as assessed by co-immunoprecipitation (Figure 3.5D, top panel), suggesting that proper localization of COPI to the TGN/Golgi membrane is important for the HPV L2-COPI

interaction. Of note, NAV-treatment did not block formation of the cleaved form of L2 (Figure 3.5D, input, long exposure), indicating that this inhibitor did not disrupt endocytosis of HPV to the endosomes where γ-secretase typically cleaves L2. NAV-treatment also blocked WT HPV16.L2F infection in a concentration-dependent manner in both HeLa and HaCaT cells, as analyzed by flow cytometry (Supplementary Figure 3.3A) or immunoblotting for reporter gene expression (Supplementary Figure 3.3B), but membrane integrity was not perturbed by NAV-treatment (Supplementary Figure 3.3C). Our findings are consistent with prior studies that reported chemical inhibition of Arf1-GTPase reduces HPV infection (*21, 50*). However, we did observe that NAV-treatment affected cell cycle progression (Supplementary Figure 3.3D), making the infection data difficult to interpret. To evaluate the role of Arf1 without disrupting mitosis, we directly depleted Arf1 itself using two different siRNAs (Figure 3.5E) and found that infection was consistently reduced (Figure 3.5F) while leaving membrane integrity (Supplementary Figure 3.3E) and cell cycle progression unperturbed (Supplementary Figure 3.3F–G). Together, these findings indicate that COPI recruitment to the TGN/Golgi membrane, a step regulated by the Arf1-GTPase, is critical for COPI-dependent HPV infection.

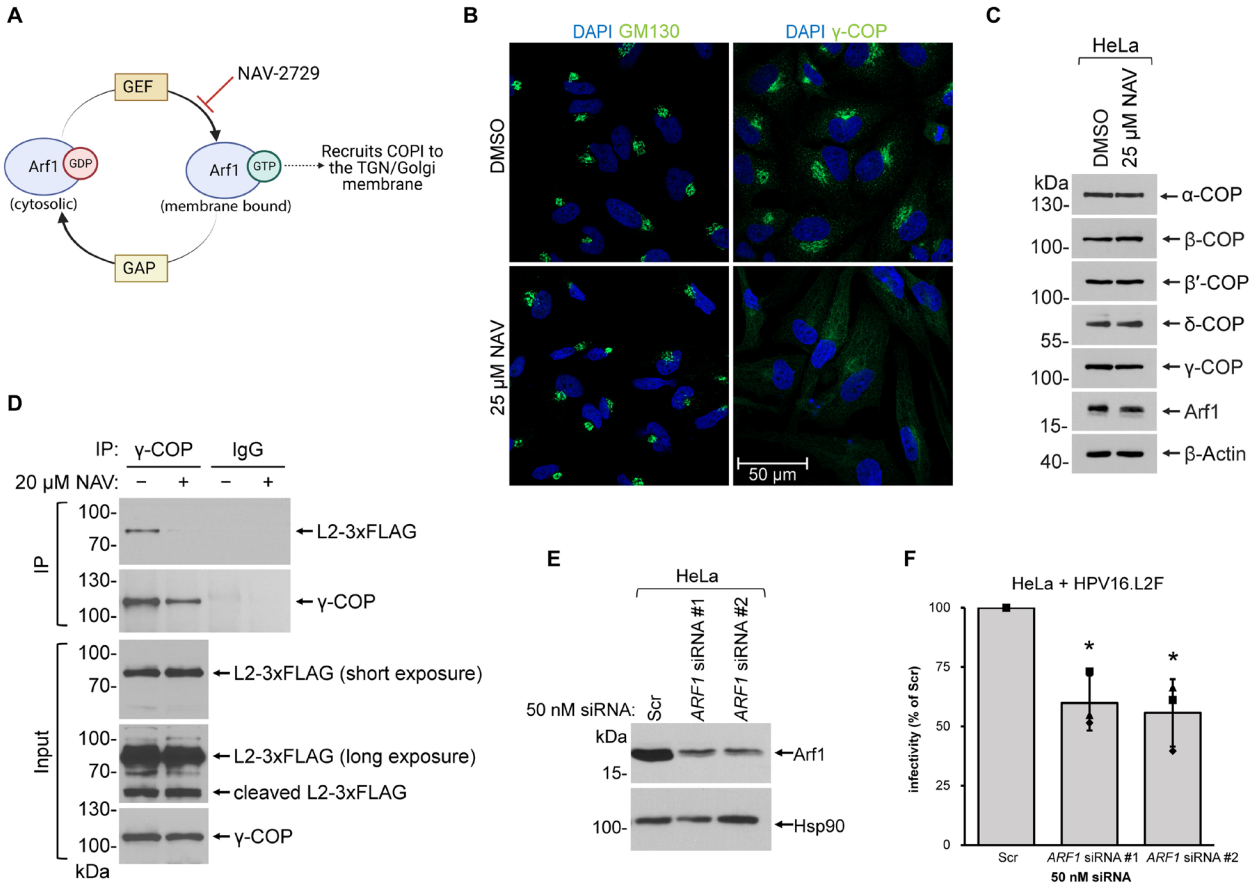

Figure 3.5. Arf1-dependent COPI recruitment to the TGN/Golgi is critical for HPV infection

A. *Overview of COPI recruitment to the Golgi membrane by the small GTPase Arf1. The chemical inhibitor NAV disrupts Arf1 nucleotide exchange. Figure created with BioRender.com.*

B. *HeLa cells treated with DMSO or 25 μM of NAV for 48 hours were subjected to immunofluorescence staining with antibodies recognizing GM130 (green, first column) or γ-COP (green, second column). Nuclei were stained with DAPI (blue). Representative images of a single, medial Z plane taken by confocal microscopy are shown.*

C. *HeLa cells treated with DMSO or 25 μM NAV for 48 hours were lysed, and the resulting whole-cell extract was analyzed by immunoblotting with the indicated antibodies. β-Actin, loading control.*

D. *HeLa cells were infected with WT HPV16.L2F for 22 hours in the presence of DMSO or 20 μM NAV. Immunoprecipitation experiments followed by immunoblotting were carried out as in (Figure 3.2C).*

E. *HeLa cells treated with the indicated siRNA for 72 hours were lysed, and the resulting whole-cell extract was analyzed by immunoblotting with antibodies recognizing Arf1 or Hsp90 as a loading control.*

F. *Infectivity analysis as in (Figure 3.4A) except cells were treated with Scr or ARF1 siRNA before infection (n = 3). A two-tailed, unequal variance t test was used to determine statistical significance compared to Scr siRNA–treated cells. *P < 0.05.*

3.3.6 The COPI complex drives TGN/Golgi-transit of HPV

What role does the HPV L2-COPI interaction play during virus entry? The COPI complex normally binds to a cellular transmembrane cargo at the TGN/Golgi, triggering a budding process that generates a COPI-coated vesicle harboring the cargo, which is then transported to the target membrane where fusion occurs (*31-33*). Given that COPI vesicles with a typical outer diameter 60–100 nm (*51, 52*) are large enough to carry a partially disassembled HPV particle (diameter ≦ 55 nm), we hypothesize that the membrane-inserted L2 protein mimics a transmembrane protein, deploying its cytosolic region to bind to COPI associated with the TGN/Golgi membrane. After budding, the ensuing formation of an HPV-containing vesicle enables trafficking of incoming HPV beyond the TGN.

To test if COPI is required for HPV trafficking, we probed the fate of HPV under COPI knockdown. At 30 hpi in cells infected with WT HPV16.L2F, we found that knockdown of α-COP and γ1-COP significantly increased the PLA signal between L1 and TGN46 compared to cells treated with scrambled siRNA (Figure 3.6A; quantified in 3.6B), much like the effect of the R302/5A mutation in L2. Similarly, there was a significant increase of L1-GM130 PLA signal at this time point in the knockdown cells (Figure 3.6C; quantified in 3.6D). Importantly, knockdown of α-COP and γ1-COP did not affect cell cycle progression (Figure 3.6E–F). These findings demonstrate that without functional COPI, HPV is impaired for passage through the TGN/Golgi compartment, indicating that COPI functions during entry to support trafficking from the TGN and within the Golgi stacks. This idea is consistent with the finding that the R302/5A mutant HPV which cannot interact with COPI also accumulates in the TGN and GM130 compartments (Supplementary Figure 3.1C–F). Hence, the COPI complex engages HPV L2 as a cargo, driving Golgi-transit of the HPV particle to enable infection.

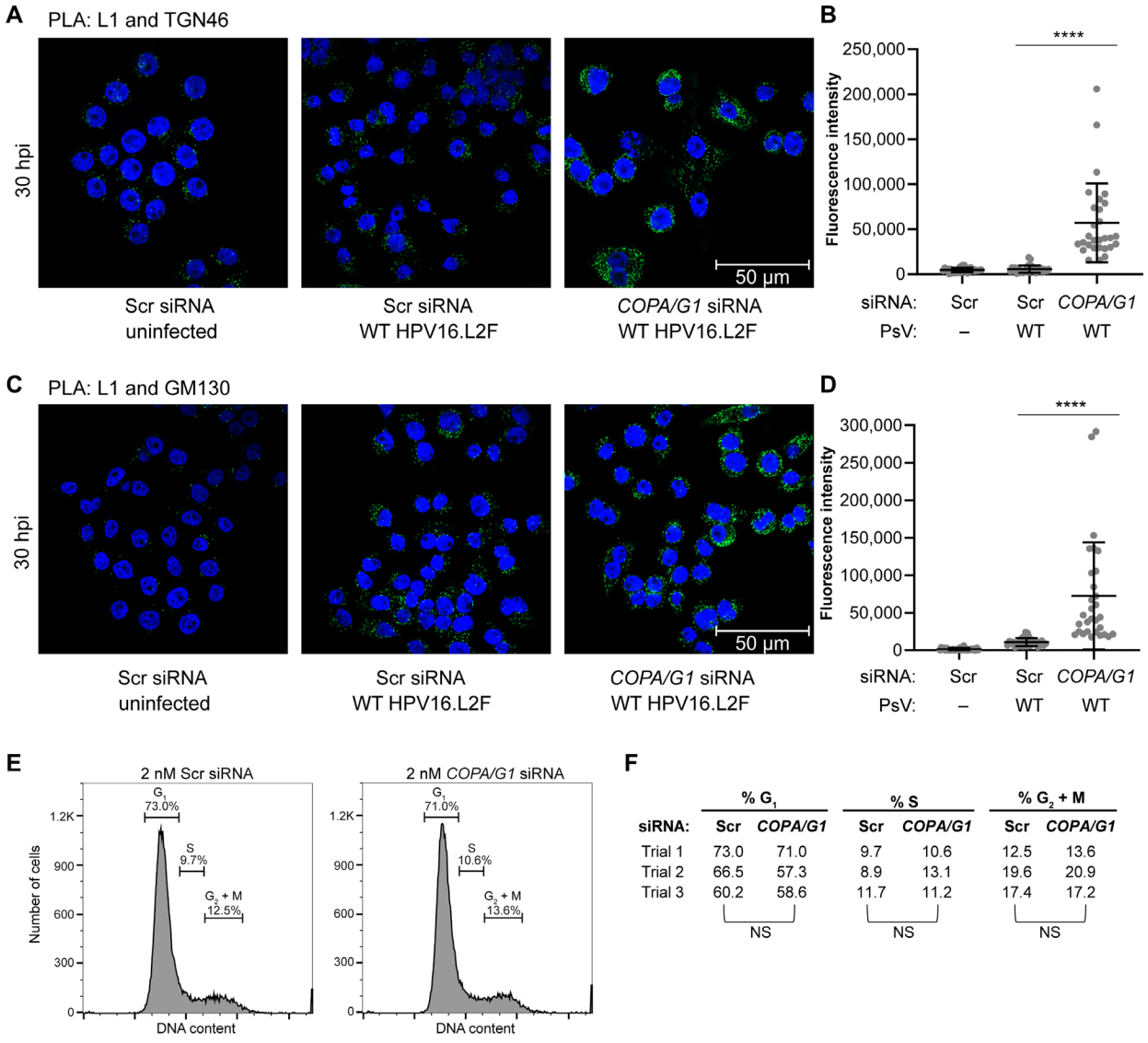

Figure 3.6: The COPI complex drives TGN/Golgi transit of HPV

A. *HeLa-S3 cells treated with 2 nM Scr or a mixture of 1 nM COPA and 1 nM COPG1 (COPA/G1) siRNA for 18 hours were uninfected or infected with WT HPV16.L2F PsV. At 30 hpi, PLA was performed with antibodies recognizing HPV16 L1 and TGN46 (PLA signals shown in green). Nuclei were stained with DAPI (blue).*

B. *Multiple images as in (A) were analyzed and presented as in (Figure 3.2H). ****$P < 0.0001$. Similar results were obtained in three independent experiments.*

C. *As in (A), except PLA was performed with antibodies recognizing HPV16 L1 and GM130.*

D. *As in (B), except images as in (C) were analyzed. Similar results were obtained in three independent experiments.*

E. *HeLa cells transfected with the indicated siRNA for 48 hours were incubated with Hoechst 33342 and analyzed by flow cytometry to measure relative Hoechst 33342 fluorescence (DNA content). The percentage of cells in each phase is indicated. The representative histograms of three independent experiments are shown.*

F. *Summary of cell cycle phase distributions as in (E). Statistical significance for each phase was determined by a two-tailed, paired t test. NS, not significant ($P > 0.05$).*

3.4 Discussion

Given the widespread distribution of HPV infection and the global burden of HPV-associated cancers (*53*), there is pressing need to elucidate the cellular infection mechanisms of this important human pathogen. During entry, HPV is transported from the cell surface to the TGN and Golgi apparatus on its journey to the nucleus, but it is not known how HPV transits the TGN and the Golgi stacks prior to nuclear entry. We show here that the COPI cellular protein-sorting complex directly engages the HPV L2 capsid protein to mediate transit of HPV through the Golgi during virus entry.

Specifically, using a combination of an unbiased proteomics approach, cell-based and in vitro binding studies, along with gene-silencing and chemical inhibitor experiments, we identified the COPI retrograde sorting complex as a host factor essential for HPV infection. COPI-knockdown significantly reduced HPV infection; inhibition appears to be a specific result of impaired L2-COPI binding and not due to a global disruption of the TGN/Golgi compartment, based on Golgi-marker staining, cell viability and cell cycle analysis, and on the lack of effect on SV40 infection, another non-enveloped DNA virus. We note that knockdown conditions for COPI and Arf1 that we used in this study are mild and do not disrupt the cell cycle, but are sufficient to inhibit HPV infection; whereas harsh knockdown treatments such as high concentration of siRNAs or longer periods of knockdown of these protein-sorting components would raise concerns about toxicity and thus their effects on HPV entry would not be possible to interpret. Nevertheless, the inhibition of infectivity caused by the R302/5A mutation that inhibits L2-COPI binding provides additional evidence that the inhibition of infection is due to impaired L2-COPI binding but not overall cell dysfunction.

Our results support a model in which incoming HPV, via its L2 capsid protein protruding into the cytoplasm, directly binds the COPI complex upon TGN-arrival to mediate subsequent trafficking steps during virus entry. γ-COP, an established cargo-binding subunit of the multi-subunit COPI sorting complex (*33*), can interact in vitro with the segment of the L2 protein that is exposed in the cytoplasm after membrane protrusion during entry. In addition, we identified a conserved di-arginine motif located at position 302 and 305 in the cytoplasmic segment of the HPV16 L2 protein that is required for binding to COPI. Like COPI knockdown, a mutation in the di-arginine motif that blocks COPI binding caused HPV accumulation in the TGN and Golgi. Although the COPI complex usually binds to di-lysine K(X)KXX motifs at the C-terminal tail of cellular transmembrane cargos (*54*), non-canonical di-arginine motifs in some cellular cargos can also interact with COPI and mediate trafficking (*55*-*57*).

Previous studies showed that HPV is directed from the endosome to the TGN by the retromer, a cytosolic protein-sorting complex that binds to L2 at the endosome membrane by eight hours after infection (*17*), whereas we show here that COPI, a distinct protein-sorting complex, binds L2 later (16 hpi) when the virus reaches the TGN. Both retromer and COPI normally bind to cellular transmembrane proteins. Although HPV is a non-enveloped virus and lacks classic transmembrane proteins, the virus utilizes a unique strategy to bind to cytoplasmic protein-sorting complexes. Namely, incoming HPV inserts a segment of the L2 protein through the membranes of vesicular compartments to expose short, discrete protein binding sites in the cytoplasm, thus mimicking classic transmembrane cargos. Early during trafficking, retromer interacts with HPV L2 at a retromer binding site located near the cell-penetrating peptide at the C terminus of L2 (*18*). Dissociation of retromer from L2 is required for exit of HPV from the endosome and entry into the TGN (*58*), at which time COPI binds to L2 at a site ~150 residues

N-terminal to the retromer binding site to mediate the next steps of trafficking through the TGN/Golgi. It is possible that the same L2 molecule can sequentially bind to different host cell trafficking complexes as more of the L2 protein protrudes into the cytoplasm, but because each HPV capsid can contain up to 72 copies of L2, it is also possible that different molecules of L2 within an individual viral particle may recruit the retromer or COPI at different stages of entry.

How does the L2/COPI interaction support HPV infection, and more generally, what is the role of the L2 segment encompassing the R302/R305 di-arginine motif? The segment of L2 that contains the COPI binding site (amino acid segment 188–332) can function as a "chromatin-binding region" (*30*), and mutations in this region including R302/5A abrogated the ability of an ectopically expressed L2-EGFP fusion protein to be retained in the nucleus and colocalize with mitotic chromosomes. As we show here, L2 binds directly to γ-COP, and the COPI binding defect of the of R302/5A mutant is evident in vitro with purified proteins, in peptide pull-down experiments, and in infected cells as measured by co-IP. Thus, the impaired binding of R302/5A HPV PsV to COPI is due to a direct inhibition of binding and is not an indirect effect due to impaired binding of L2 to chromatin.

It is difficult to ascribe a precise trafficking defect to the loss of the L2-COPI interaction without further experiments, but it is clear that in the absence of the interaction HPV accumulates in TGN and GM130-positive compartments and infection is inhibited. There are two broad not necessarily exclusive models that may explain this observation. In infection studies with PsV containing mutations in the central segment of L2, the viral genome and L2 accumulated in the TGN46 compartment at a time when the wild-type virus had exited the TGN, and microtubule-associated virus trafficking and chromosome association during the late stages of mitosis were inhibited (*27, 28*). These results suggest that the chromatin-binding region of L2

tethers L2 to host chromosomes during mitosis for L2/vDNA to exit the Golgi compartment and be retained in the nucleus in association with chromosomes. In the absence of such tethering, mitotic Golgi fragments containing L2 appear to coalesce back into Golgi upon completion of mitosis, resulting in a phenotype of "Golgi retention" (*27*). Therefore, the phenotypes of the R302/5A mutant and COPI knockdown may be due to impaired chromatin association and the attendant resorption of the incoming virus into Golgi compartments and the TGN. However, this model does not readily account for our discoveries that COPI, a protein-sorting complex normally active in and around the Golgi apparatus, binds directly to L2 upon TGN entry and is a required HPV entry factor, whose absence causes HPV to accumulate in the TGN/Golgi compartments.

Given our results and the known role of COPI in mediating trafficking of transmembrane proteins between different subcellular compartments, we propose that COPI directly mediates trafficking of HPV-containing vesicles within the TGN/Golgi compartment via its canonical sorting activity acting on the cytoplasmic segment of L2. This interpretation is consistent with the original suggestion of Sapp and colleagues that the R302/R305 segment is required "for interacting with a TGN egress factor that is required to carry the pseudogenome to a subsequent compartment" (*28*). It is also possible that the segment of L2 that contains the R302/R305 di-arginine motif plays multiple roles during viral entry. It might both bind to COPI to mediate passage through the Golgi, as well as tether the virus to mitotic chromosomes to mediate nuclear retention. Further work is required to determine whether the coalescence of the R302/5A mutant virus back into the TGN is due to impaired COPI binding, reduced chromatin binding, or to some other effect of the mutation.

Neither COPI knockdown nor the R302/5A mutation blocks arrival of HPV into the GM130 compartment, implying that these manipulations cause an incomplete block to exit from the TGN. It is possible that the level of knockdown achieved does not cause complete functional depletion of COPI or that COPI retains low level binding to the mutant L2 protein, possibly to secondary binding sites in L2. Consistent with the latter idea, residual binding of γ-COP to mutant L2 is apparent in the in vitro binding experiments (Figure 3.3E–F), although such an interaction is too weak or transient to observe in co-IPs from cell extracts. Alternatively, there may be minor COPI-independent mechanisms that allow HPV to progress beyond the TGN, but that are not sufficient to support departure of the virus from the Golgi. If defective L2-COPI interaction causes the virus to accumulate in Golgi compartments distal to the TGN by restricting passage of HPV through the Golgi or out of the Golgi, ongoing anterograde trafficking would redistribute this virus back into the more TGN-proximal compartments. In addition, at later times more incoming virus arrives in the TGN and Golgi without efficient means to exit. A combination of these factors may cause the observed accumulation of HPV in multiple Golgi compartments at late stages of entry.

Prior studies also found that COPI is located at ER-exit sites and may play a role in anterograde cargo trafficking from the ER to the Golgi as well (*59-61*). We propose that COPI facilitates HPV trafficking between multiple compartments along the TGN-Golgi stack-ER axis, possibly in both a retrograde and anterograde direction. As noted above, such a broad action of COPI coupled with incomplete inhibition at any individual step would cause HPV to accumulate throughout the various compartments along this axis. Another intriguing possibility is that COPI-dependent Golgi transit of HPV might target the virus directly to the nucleus—bypassing the ER— to promote infection. Indeed, there are reports of a COPI-mediated pathway linking the

Golgi and nucleus (*62, 63*). A recent study also suggests that a RanBP10/importin/dynein-motor complex facilitates trafficking of HPV from the Golgi into the nucleus during mitosis (*64*). Moreover, COPI-coated vesicles are involved in Golgi-vesiculation during mitosis (*65*), a process that also requires active Arf1 (*66*). Clearly, additional experiments are needed to decipher the precise role of COPI in vesicular transport of HPV through the Golgi, the infectious route of HPV after the COPI-dependent step(s), and the mechanism of HPV nuclear entry and retention.

Although earlier studies found that brefeldin A (BFA) and golgicide A (GCA), drugs that inhibit GDP-GTP exchange on Arf1 (*67-70*), reduced HPV infection (*21, 50*), a specific role for COPI during HPV entry was not examined in these studies. The findings reported here identify a role of COPI in directly engaging the incoming HPV particle, supporting trafficking through the Golgi leading to infection. Moreover, although COPI has been shown to support the life cycle of many viruses, such as vaccinia, polio, influenza, and hepatitis C viruses (*71-73*), the mechanism by which COPI is exploited by these viruses during infection remains unclear. By contrast, our data identify an incoming viral particle that is recognized as a direct cargo for the COPI sorting complex during virus entry.

3.5 Materials & Methods

3.5.1 Antibodies & Inhibitors

Antibodies and inhibitors used in this study are as follows:

Table 3.1: List of Antibodies & Inhibitors

Antibodies			
Antigen	**Species**	**Cat # / Source**	**Application**
FLAG	Mouse	F3165; Millipore Sigma	WB, IP
HPV16 L1	Mouse	MAB885; Millipore Sigma	WB
α-COP	Rabbit	HPA028024; Millipore Sigma	WB
β-COP	Rabbit	A304-724A; Fisher Scientific	WB, IP
β'-COP	Rabbit	PA5-96557; Invitrogen	WB, IP, IF
γ-COP	Rabbit	12393-1-AP; Proteintech	WB, IP, IF, PLA
δ-COP	Rabbit	23843-1-AP; Proteintech	WB
Arf1	Rabbit	10790-1-AP; Proteintech	WB
TGN46	Rabbit	ab50595; abcam	WB, PLA
GM130	Rabbit	ab52649; abcam	WB, IF, PLA
EEA1	Rabbit	C45B10; Cell Signaling	WB
BAP31	Rat	MA3-002; Invitrogen	WB
Na^+/K^+-ATPase	Rabbit	ab76020; abcam	WB
Histone H3	Rabbit	9715S; Cell Signaling	WB
GFP	Mouse	632380; Takara Bio Clontech	WB
SGTA	Rabbit	11019-2-AP; Proteintech	WB
β-actin	Rabbit	4967S; Cell Signaling	WB
Hsp90	Mouse	sc13119; Santa Cruz Biotech.	WB
HA	Rat	ROAHAHA; Roche	WB
HPV16 L1	Mouse	554171; BD	PLA
SV40 T antigen	Mouse	sc-147; Santa Cruz	IF
VPS35	Rabbit	Ab157220; abcam	WB

Other antibodies	**Species**	**Cat # / Source**	**Application**
anti-mouse IgG peroxidase	Goat	A4416; Millipore Sigma	WB
anti-rabbit IgG peroxidase	Goat	A4914; Millipore Sigma	WB
anti-rat IgG peroxidase	Rabbit	A5795; Millipore Sigma	WB
anti-rabbit Alexa Fluor 488	Goat	A11008; Thermo Fisher	IF
anti-mouse Alexa Fluor 594	Goat	A11032; Thermo Fisher	IF
Normal rabbit IgG	Rabbit	NI01; Millipore Sigma	IP
Inhibitors			
Compound	**Solvent**	**Cat # / Source**	**Concentration**
XXI	DMSO	565790; Millipore Sigma	1–2 μM
NAV-2729	DMSO	SML2238; Millipore Sigma	10–25 μM

IP, immunoprecipitation; WB, Western blot; IF, immunofluorescence; PLA, proximity ligation assay

3.5.2 DNA constructs

The p16sheLL, p5sheLL, and p18sheLL plasmids were gifts from Dr. John Schiller (National Cancer Institute, Rockville, MD; Addgene plasmids #37320, #46953, and #37321) and were modified into p5sheLL.L2F, p16sheLL.L2F, and p18sheLL.L2F, respectively, which consist of WT L1 and 3xFLAG-tagged L2 of corresponding HPV types as previously described (*12*). The R302/5A mutation in L2 was introduced to p16sheLL.L2F by site-directed mutagenesis. The pcDNA3.1 plasmids expressing GFP with a C-terminal S-tag were used as pseudoviral genomes (reporter plasmids) as previously described (*11*). The Gaussia luciferase

coding sequence from phGluc (Addgene plasmid #22522) was cloned into pCINeo-EGFP (obtained from Dr. Christopher Buck, National Cancer Institute, Rockville, MD; Addgene plasmid #46949), replacing the EGFP sequence and the resulting construct was used as the reporter of HPV16 PsV for the PLA assay. Alternatively, HPV16 PsV packaging a reporter plasmid pCAG-HcRed (Addgene plasmid #11152) was used for PLA. The COPG1 coding sequence was amplified from cDNA of HEK 293T cells and cloned into the pFLAG-CMV2 vector in frame with the 5' FLAG for FLAG-γ1-COP recombinant protein production. Site-directed mutagenesis was used to introduce siRNA-resistant/synonymous mutations on COPG1 siRNA target site. To generate pCMVTNT-HA-COPG1-mCherry construct, siRNA-resistant COPG1 was cloned into the pCMVTNT-HA-KPNA2 plasmid, a gift from Dr. Bryce Paschal (University of Virginia, Charlottesville, VA), replacing KPNA2 and an mCherry sequence was inserted before the stop codon of COPG1. COPG1 coding sequence was further removed to generate pCMVTNT-HA-mCherry, which was used as the control vector. HPV16 L2 fragment (amino acids 68–473) with 3xFLAG epitope tag was amplified from p16sheLL.L2F and cloned into this pCMVTNT-HA vector to generate the pCMVTNT-HA-(Δ1–67) L2-3xFLAG construct and the R302/5A mutation was further introduced by site-directed mutagenesis. pcDNA3.1(-)-EGFP-FLAG was described before (*74*). All plasmids constructed in this study were verified by sequencing.

3.5.3 Cell culture

HEK 293T (ATCC, Cat# CRL-3216), HeLa (ATCC, Cat# CCL-2), and HeLa-S3 (ATCC, Cat# CCL-2.2) cells were obtained from American Type Culture Collection. HeLa-Sen2 cells, a HeLa derivative, were generated as described in (*75*). HaCaT cells were purchased from AddexBio Technologies. HEK 293TT cells were obtained from Dr. Christopher Buck (National

Cancer Institute, Rockville, MD). All cell lines were cultured in Dulbecco's modified Eagle's medium (DMEM) supplemented with 10% fetal bovine serum and penicillin/streptomycin and incubated at 37°C and 5% CO2. HeLa cells (ATCC, Cat# CCL-2) were used throughout this study unless otherwise specified.

3.5.4 HPV PsV production

HPV PsV were produced by co-transfecting HEK 293TT cells with indicated reporter plasmid and p16sheLL.L2F (WT or R302/5A), p5sheLL.L2F, or p18sheLL.L2F using polyethyleneimine (PEI, Polysciences Inc.). Packaged PsVs were purified by density gradient centrifugation in OptiPrep (Millipore Sigma) as described (*34, 35*). The purified PsVs were subjected to SDS-PAGE followed by Coomassie staining for L1 and L2 to assess the quality. Encapsidated reporter plasmids of equivalent amount of WT and R302/5A HPV16.L2F PsV were quantified by qPCR using primers for the reporter gene to validate that equivalent numbers of plasmid were encapsidated.

3.5.5 Sucrose gradient fractionation

The protocol for sucrose gradient fractionation to isolate TGN/Golgi-containing cellular fractions was kindly shared by Dr. Yanzhuang Wang (University of Michigan) (*76*) and adapted for our purposes. HeLa cells were plated in 15-cm plates and grown to ~80% confluency. Cells were then infected with equivalent amounts of WT HPV16.L2F PsV (~100 μg PsV per 15 cm plate, MOI ~4), R302/5A HPV16.L2F PsV, or left uninfected. A total of twelve 15-cm plates per condition were processed as follows. At 22 hpi, cells were washed once with 500 mM NaCl to remove residual virus followed by three ice-cold PBS washes. Cells were resuspended in HBS buffer (10 mM HEPES pH 7.2, 1 mM Mg(OAc)2, 0.25 M sucrose, 1 mM EDTA, 1 mM DTT, 1

mM PMSF), and homogenized by passing 20 times through an 8-µm clearance ball bearing homogenizer (Isobiotech). The homogenate was centrifuged at 1,000 g for 10 min, and the resulting supernatant was layered over a sucrose gradient comprised of 1 mL 1.6 M, 1 mL 1.4 M, 2 mL 1.2 M, 3 mL 1.0 M, 2 mL 0.8 M, and 1 mL 0.5 M sucrose in MEB buffer (50 mM Tris-HCl pH 7.4, 50 mM KCl, 20 mM beta-glycerol phosphate, 15 mM EGTA, 10 mM MgCl2, 1 mM DTT) supplemented with 250 mM KCl. The sucrose gradients were ultracentrifuged at 30,000 rpm in a SW40Ti swinging-bucket rotor (Beckman) at 4°C for 20 h. After centrifugation, 12 fractions were collected from top-to-bottom. A portion of each fraction was analyzed by SDS-PAGE followed by immunoblotting to identify the TGN/Golgi-containing fractions.

3.5.6 Immunoprecipitation and Mass-Spectrometry using pooled sucrose fractions

Samples from fractions 3–5 (TGN/Golgi-containing fractions) were pooled, incubated with 1% Triton X-100 on ice for 10 min, and centrifuged 16,100 g for 10 min. The resulting supernatants were collected, and ~150 ng WT HPV16.L2F PsV was added per 1 mL of the uninfected sample lysate (called "control"). The samples were then incubated with anti-FLAG M2 antibody (~8 µg antibody per 1 mL of lysate) (F3165; Millipore Sigma) at 4°C overnight, and the immune complex was captured with protein G-coated magnetic beads (Invitrogen, 10003D) at 4°C for 1 h. Beads were washed four times with 0.1% Triton X-100 in HBS buffer. Bound proteins were eluted with 1% SDS in HN buffer (50 mM HEPES, 150 mM NaCl) and denatured by incubating at 90°C for 10 min. A portion of eluate was analyzed by SDS-PAGE followed by immunoblotting to confirm equivalent amounts of L2-3xFLAG were precipitated from WT or R302/5A infected conditions or control. The remaining eluate was treated with 10% trichloroacetic acid (TCA) and incubated on ice for 10 min. The sample was subjected to centrifugation, and the precipitated material washed twice with acetone. The precipitate was

subject to mass-spectrometry analysis at the Taplin Mass-Spectrometry Core Facility (Harvard Medical School). LC/MS/MS was performed using an Orbitrap mass spectrometer (ThermoFisher).

3.5.7 Proximity ligation assay (PLA)

5 x 10^4 HeLa-Sen2 or HeLa-S3 cells were seeded onto glass coverslips in a 24-well plate. After overnight incubation, the cells were infected with equivalent amounts of WT (MOI ~100) or R302/5A HPV16.L2F PsV, or left uninfected. In Figure 3.2G, cells were treated with 2 μM XXI or an equivalent volume of dimethyl sulfoxide (DMSO) (as a vehicle control) 0.5 h before infection with HPV16.L2F PsV. In Figure 3.6A–D, cells were transfected with 2 nM siRNA 18 h before infection with HPV16.L2F PsV. At 24 or 30 hpi, cells were fixed with 4% paraformaldehyde (PFA), permeabilized with 0.1% saponin, and incubated with mouse anti-L1 antibody (1:1000–2500 dilution) and with rabbit anti-TGN46 antibody (1:200–1000 dilution), rabbit anti-γ-COP antibody (1:2000 dilution), or rabbit anti-GM130 antibody (1:100 dilution) at 4°C overnight. PLA was performed with Duolink reagents (Millipore Sigma) as described before (39). In brief, cells were incubated with PLA probes in a humidified chamber for 1 h at 37°C. Ligation was performed for 45 min at 37°C, and amplification was performed for 3 h at 37°C. Coverslips were mounted with mounting medium containing 4',6-diamidino-2-phenylindole (DAPI, Abcam ab104139) and visualized by confocal fluorescence microscopy. Images were processed by ZEN software (Zeiss) and quantitatively analyzed by Fiji software (*77*) to measure the total fluorescence intensity per cell in each sample. All PLA experiments were performed independently at least two (in most cases three) times with similar results. Because it is difficult to directly compare the quantitative results between experiments, data points are shown with the

means and standard deviations from one representative independent experiment. A two-tailed, unequal variance t-test was used to determine statistical significance.

3.5.8 siRNA transfection

siRNA oligos used in this study are listed in the Table 3.2. 6- or 12-well plates were seeded with 1–3 x 10^5 HeLa or HaCaT cells per well and simultaneously reverse-transfected with indicated siRNA using Lipofectamine RNAi MAX (Thermo Fisher Scientific) according to the manufacturer's instructions.

Table 3.2: List of siRNAs

siRNA	**Sequence**	**Supplier**
Scr	predesigned	QIAGEN; Cat. # 1027281
COPA	CCAUUGAUCCCACUGAGUUCA	Sigma
COPB1	UACGUUAAUUAACGUGCCAAU	Sigma
COPB2	CCCAUUAUGUUAUGCAGAU	Sigma
COPD (*ARCN1*)	GAAAGUUGUUUGUCCGUAU	Sigma
COPE	ACGAGCUGUUCGACGUAAA	Sigma
COPG1	CUUGUAAUCUGGAUCUGGA	Sigma
COPG2	CCGAAUUGCCAGUCGCUUA	Sigma
COPZ1	GGGAAUAGUUCAUAGGGAA	Sigma
COPZ2	GGGCUCAUCCUACGAGAAU	Sigma
Pooled *COPG1*	GAGGGUGGCUUUGAGUAUA; GCAAACACGCCGUCCUUAU; GAAGAGGCUGUGGGUAAUA; GGAGGCCCGUGUAUUUAAU	Dharmacon
Pooled Scr	UAAGGCUAUGAAGAGAUAC; AUGUAUUGGCCUGUAUUAG; AUGAACGUGAAUUGCUCAA; UGGUUUACAUGUCGACUAA	Dharmacon

siRNA	Sequence	Supplier
SGTA	CAGCCUACAGCAAACUCGGCAACUA	Sigma
ARF1 #1	GGCUUUAGAGCUGUGUUGA	Sigma
ARF1 #2	GCCUGAUCCUUCGUGGUGGA	Sigma

3.5.9 DNA transfections

For knockdown-rescue experiments, 2.1 x 10^5 HeLa cells per well were reverse-transfected with 1 nM siRNA of Scr or COPG1 in 6-well plates for 9 h. Attached cells were washed with PBS twice and then transfected with 0.7 μg of pCMVTNT-HA-mCherry or 1 μg of pCMVTNT-HA-COPG1-mCherry plasmids for 15 h using the transfection reagent FuGENE HD (Promega). Transfected cells were washed with PBS twice and infected with WT HPV16.L2F for 48 h. Infectivity was analyzed by flow cytometry to determine the fraction of GFP-expressing cells among mCherry-expressing or mCherry-negative cells in the same culture. Alternatively, before infection, whole-cell extract of cells with the same treatment was collected for immunoblot analyses. For recombinant protein production, HEK 293T cells were seeded in 10-cm plates for 24 h to reach ~80% confluency and then transfected with 3 μg of indicated plasmids for 48 h using the transfection reagent PEI.

3.5.10 RT-qPCR

qPCR primers used in this study are listed in the Table 3.3. 3 x 10^5 HeLa cells per well were seeded in 6-well plates and simultaneously reverse-transfected with the indicated siRNA. 24 h later, cells were harvested and RNA was isolated using RNeasy Mini Kit (Qiagen) according to the manufacturer's instructions. 1 μg of RNA from each condition was reverse-transcribed to cDNA using iScript cDNA Synthesis Kit (Bio-Rad) according to the

manufacturer's instructions. qPCR was performed using SsoAdvanced Universal SYBR Green Supermix (Bio-Rad) in CFX Connect Real-Time PCR Detection System (Bio-Rad).

Table 3.3: DNA primers used for qPCR analysis

Target	**Sequence**
COPA	Fwd: CGTGGAGACAGAAAGGAAGAAG Rev: AGGTTTGAGTGGGTGAAATAGG
COPB1	Fwd: CCTGATGCTCCTGAACTGATAC Rev: CTCGATCCTGATCTGCATGAAT
COPB2	Fwd: AGCTATTCCCTGCTGGTTTC Rev: CAACTCTGGTCCTCTGTTCTTT
COPD	Fwd: CATGAGGAGAAGGTGTTCAGAG Rev: CTCTTCGGGCCTGTTGTAAT
COPE	Fwd: CCTGAGGTGACAAACCGATAC Rev: AGCCTGTCAAAGTCGTTCTC
COPG1	Fwd: GAAGAGGGTGGCTTTGAGTATAA Rev: TCGATGAACTCGCACAGATG
COPG2	Fwd: CCATGTGAGAGGTCCGATAAAG Rev: GCCTGGACCTCACCAATAAA
COPZ1	Fwd: TCTTGCAGTTCTGGGAGTAAAG Rev: AGGGAGCATGTGAGCATAATC
COPZ2	Fwd: TTGGTGCTGGACGAGATTG Rev: CGCCATCATCTGCCCTAAA
GAPDH	Fwd: CCCTTCATTGACCTCAACTACA Rev: ATGACAAGCTTCCCGTTCTC

3.5.12 HPV infectivity

To quantify HPV infectivity by flow cytometry, HeLa or HaCaT cells were treated as indicated and infected with HPV16.L2F, HPV5.L2F, or HPV18.L2F PsV (MOI < 1) containing a GFP reporter construct. Where indicated, inhibitors (XXI or NAV-2729) were added at time of

infection. An equivalent volume of the carrier DMSO was added to the control cultures. At 48 hpi, cells were washed with PBS, harvested by trypsinization, and resuspended in PBS containing 2% FBS and 0.1 μg/mL of DAPI. For knockdown-rescue experiments, trypsin without phenol red was used to prevent interference of mCherry signal. Flow cytometry was performed with a Bio-Rad ZE5 cell analyzer (University of Michigan Flow Cytometry Core Facility). After gating for size and singlets, the population of DAPI-negative cells (~2 x 10^4 cells) was analyzed for GFP or mCherry fluorescence. Data are presented as the means and standard deviations of three independent experiments. A two-tailed, unequal variance t-test was used to determine statistical significance.

To analyze HPV infectivity by immunoblotting, HeLa or HaCaT cells were treated as indicated and infected with HPV16.L2F PsV containing a GFP reporter construct. At 48 hpi, cells were washed with PBS, harvested by scraping, and lysed in HN buffer containing 1% Triton X-100 for 10 min on ice. Cells were centrifuged at 16,100 g for 10 min. The resulting supernatant was incubated with SDS sample buffer containing 2-mercaptoethanol, denatured by incubating at 90 °C for 10 min, and analyzed by SDS-PAGE followed by immunoblotting for GFP.

3.5.13 Membrane integrity

DAPI-exclusion as measured by flow cytometry was used to assess membrane integrity. Non-permeabilized cells were washed with PBS, harvested by trypsinization, and resuspended in PBS containing 2% FBS and 0.1 μg/mL of DAPI. Flow cytometry was performed with a Bio-Rad ZE5 cell analyzer (University of Michigan Flow Cytometry Core Facility). After gating for size and singlets, the percentage of DAPI-negative cells was calculated. Data are presented as the

means and standard deviations of three independent experiments. A two-tailed, unequal variance t-test was used to determine statistical significance.

3.5.14 Cell cycle analysis

DNA content was measured using Hoechst 33342 staining and flow cytometry analysis. Non-permeabilized cells were incubated with 10 μg/mL Hoechst 33342 (Bio-Techne) at 37°C for 1 h. Cells were then washed with PBS, harvested by trypsinization, and resuspended in PBS containing 2% FBS. Flow cytometry was performed with a Bio-Rad ZE5 cell analyzer (University of Michigan Flow Cytometry Core Facility). The percentage of cells in G1, S, or G2+M phases was visibly determined from control cell cultures using FlowJo software (BD). Data from three independent experiments are presented as the percentage of cells in each phase. A two-tailed, paired t-test was used to determine statistical significance between the knockdown and control cells for each cell cycle phase.

3.5.15 SV40 infection

1 x 10^5 HeLa cells were seeded onto glass coverslips in a 12-well plate and simultaneously reverse-transfected with siRNA for 24 h. Cells were then infected with SV40 (MOI ~0.1) for 24 h to reach ~10% infection, fixed with 4% PFA for 15 min, permeabilized with 0.2% Triton X-100/TBS/3% BSA for 20 min, and blocked with 0.2% Tween-20/TBS/3% BSA for 1 h at room temperature. Primary antibody recognizing SV40 large T antigen was diluted in 0.2% Tween-20/TBS/3% BSA and incubated with cells overnight at 4°C. Secondary antibody was also diluted in 0.2% Tween-20/TBS/3% BSA and incubated at room temperature for 1 h. Coverslips were mounted with mounting medium containing DAPI (Abcam ab104139) and visualized by fluorescence microscopy. The number of cells expressing SV40 large T antigen

was scored relative to the total number of cells. Data are presented as the means and standard deviations of three independent experiments. A two-tailed, unequal variance t-test was used to determine statistical significance.

3.5.16 Immunofluorescence

1 x 10^5 HeLa cells were seeded onto glass coverslips in a 12-well plate and treated as indicated. Cells were fixed with 4% PFA for 15 min, permeabilized with 0.2% Triton X-100/TBS/3% BSA for 20 min, and blocked with 0.2% Tween-20/TBS/3% BSA for one hour at room temperature. Primary antibodies were diluted in 0.2% Tween-20/TBS/3% BSA and incubated overnight at 4°C. Secondary antibodies were also diluted in 0.2% Tween-20/TBS/3% BSA and incubated at room temperature for 1 h. Coverslips were mounted with mounting medium containing DAPI (Abcam ab104139) and visualized by confocal fluorescence microscopy (Zeiss LSM 800 confocal laser scanning microscope with a Plan-Apochromat 40×/1.4 oil differential interference contrast M27 objective). Representative images were chosen out of two independent experiments.

3.5.17 Immunoprecipitation

HeLa cells were grown to ~80% confluency in 10-cm plates and infected with equivalent amounts of WT HPV16.L2F (MOI < 1) or R302/5A HPV16.L2F PsV or left uninfected. For HPV inhibitor experiments, XXI (2 μM) or NAV (20 μM) were added at time of infection. An equivalent volume of the carrier DMSO was added to the control cultures. At the indicated time after infection, cells from one 10-cm plate were washed with PBS three times and lysed in 400 μL of 1% Triton X-100 in HN buffer containing 1 mM PMSF and were incubated on ice for 10 min. For time-course immunoprecipitation experiments, the second PBS-wash was

supplemented with 300 mM NaCl to reduce cell surface-bound HPV before cell lysis. After centrifugation at 16,100 g for 10 min, the resulting supernatant was incubated with indicated antibodies (~2.5 μg/mL) at 4°C overnight. The immune complex was captured with protein G-coated magnetic beads (Thermo Fisher Scientific, 10003D) at 4°C for 1 h. Beads were washed with lysis buffer and incubated at 95°C for 10 min in SDS sample buffer with 2-mercaptoethanol.

3.5.18 Biotin-peptide pull-down assay

Peptides consisting of the wild-type HPV16 L2 sequence (TGIRYSRIGNKQTL) or the R302/5A HPV16 L2 sequence (TGIAYSAIGNKQTL) were synthesized with an N-terminal biotin tag (GenScript). Peptides were dissolved in DMSO, and peptide stocks (5 mg/mL) were aliquoted and stored at -80°C. 1 x 10^6 HeLa cells were plated in 6-cm dishes. 24 h later, cells were collected by trypsinization, washed with PBS, and lysed with 165 μL HEPES buffer (1% Triton X-100, 20 mM HEPES [pH 7], 50 mM NaCl, 5 mM MgCl2, 1mM DTT) supplemented with Halt protease and phosphatase inhibitor cocktail (Thermo Fisher). The lysate was incubated on ice for 45 min followed by centrifugation at 14,000 g for 15 min. The resulting supernatant was incubated with 10 μg of biotinylated peptide for 2 h at 4°C. 50 μL of streptavidin magnetic beads (Pierce, 88817) were pre-washed three times with HEPES buffer then added to the lysates and incubated for 1 h at 4°C. The beads were captured and washed three times with HEPES buffer and incubated at 100°C for 10 min in 2X SDS sample buffer with 2-mercaptoethanol. For the biotin-peptide pull-down assay using purified FLAG-γ1-COP, same conditions were applied except that ~100 ng FLAG-γ1-COP instead of cellular extracts was incubated with 10 μg of biotinylated peptide and captured with 30 μL of streptavidin magnetic beads.

3.5.19 Preparation of recombinant proteins

Two 10-cm plates of HEK 293T cells transfected with indicated plasmid for 48 h were harvested and lysed in 1.2 mL of HN buffer containing 1% Triton X-100 and 1 mM PMSF on ice for 20 min. Following centrifugation at 16,100 g for 10 min, the resulting supernatant was incubated with anti-FLAG M2 antibody-conjugated agarose beads (Millipore Sigma, A2220) at 4°C overnight. The beads were recovered by centrifugation and washed once with HN buffer containing 1% Triton X-100 and 1 mM PMSF, twice with HN buffer containing 1% Triton X-100 and 1 mM PMSF supplemented with 300 mM NaCl and 2 mM ATP, and then once with HN buffer containing 0.1% Triton X-100 and 1 mM PMSF. The recombinant proteins were eluted twice with 150 μg/mL 3xFLAG peptide (Millipore Sigma) in HN buffer containing 0.1% Triton X-100 and 1 mM PMSF at room temperature for 30 min. A portion of the sample was analyzed alongside with BSA in standard concentrations by SDS-PAGE followed by SimplyBlue SafeStain (Invitrogen) to assess the quality and quantity of purified recombinant proteins.

3.5.20 In vitro binding assay

For in vitro binding assay with rat COPI complex, the reconstituted COPI complex purified from rat liver as described in (*76*) was a gift from Dr. Yanzhuang Wang (University of Michigan); WT HPV16.L2F PsV particle was prepared as described in "HPV PsV production"; EGFP-FLAG was purified from HEK 293T cells with anti-FLAG M2 antibody-conjugated agarose beads and Amicon Ultracel-10K Centrifugal Filters (Millipore Sigma) was applied to remove 3xFLAG peptide from the EGFP-FLAG eluate. ~1250 ng rat COPI was incubated with ~300 ng WT HPV16.L2F PsV or ~300 ng EGFP-FLAG in the reaction buffer (HN buffer containing 0.1% Triton X-100) at 37°C for 45 min with mild agitation. Anti-FLAG M2 antibody-conjugated magnetic beads (Millipore Sigma, M8823) were added to the reaction for a further incubation at room temperature for 30 min with mild agitation. Beads were recovered and

washed with reaction buffer and eluted with SDS sample buffer (without reducing agent) at 95°C for 5 min. Eluate was separated from beads and supplemented with 1% 2-mercaptoethanol and incubated at 95°C for another 5 min and then analyzed by SDS-PAGE followed by immunoblotting.

For the in vitro binding assay using purified recombinant proteins, ~100 ng FLAG-γ1-COP was incubated with ~80 ng of HA-(Δ1–67) L2-3xFLAG, ~80 ng of HA-(Δ1–67) L2-R302/5A-3xFLAG, or ~800 ng of EGFP-FLAG in the reaction buffer (HN buffer containing 0.1% Triton X-100 and 1 mM PMSF) at 37°C for 1 h with mild agitation. Anti-γ-COP antibodies were added into reactions for a further incubation at 37°C for 30 min with mild agitation. The immune complex was captured with protein G-coated magnetic beads (Thermo Fisher Scientific, 10003D) at 37°C for 20 min. Beads were washed with reaction buffer and incubated at 95°C for 10 min in SDS sample buffer with 2-mercaptoethanol.

3.6 Statistical Analysis

3.6.1 Quantitation of HPV infectivity by flow cytometry

Flow cytometry data was processed by Everest software (Bio-Rad). After gating for size and singlets, the population of DAPI-negative cells (~2 x 10^4 cells per condition) was analyzed for GFP or mCherry fluorescence. Data are presented as the means and standard deviations of three independent experiments. A two-tailed, unequal variance t-test was used to determine statistical significance.

3.6.2 Quantitation of cell cycle by flow cytometry

DNA content was measured by Hoechst 33342 staining. The percentage of cells in G1, S, or G2+M phases was visibly determined from control cell cultures using FlowJo software (BD). Data from three independent experiments are presented as the percentage of cells in each phase. A two-tailed, paired t-test was used to determine statistical significance between the knockdown and control cells for each cell cycle phase.

3.6.3 Quantitation of PLA

Images were analyzed by Fiji software (*77*) to measure the total fluorescence intensity per cell in each sample. Approximately 30 cells from 10 representative images were quantified for each condition. All PLA experiments were performed independently at least two times with similar results. Because it is difficult to directly compare the quantitative results between experiments, data points are shown with the means and standard deviations from one representative independent experiment. A two-tailed, unequal variance t-test was used to determine statistical significance.

3.6.4 Quantitation of SV40 infectivity

Images were analyzed by Fiji software (*77*) to count the number of cells expressing SV40 large T antigen out of the total number of cells. Approximately 5 x 10^3 cells were analyzed for each condition. Data are presented as the means and standard deviations of three independent experiments. A two-tailed, unequal variance t-test was used to determine statistical significance.

3.6.5 Western blot quantification

In Figure 3.3F, western blots from three independent experiments were quantified using ImageJ software (NIH). The protein band intensity of HA-(Δ1–67) L2-3xFLAG (WT) or HA-(Δ1–67) L2-R302/5A-3xFLAG (R302/5A) was normalized to that of FLAG-γ1-COP in the same precipitated sample. Data represents means normalized to WT and standard deviations of four independent experiments. A two-tailed, unequal variance t-test was used to determine statistical significance.

3.7 Acknowledgements

This work was funded by grants from the National Institutes of Health (R01AI150897 and AI064296) to BT, and R01AI150897 to DD. MCH was funded by F31AI152365.

With permission from the publisher, this chapter is adapted from an original publication: *HPV is a cargo for the COPI sorting complex during virus entry. Mara C. Harwood†, Tai-Ting Woo†, Yuka Takeo, Daniel DiMaio, and Billy Tsai. (2023). Science advances, 9(3), eadc9830. https://doi.org/10.1126/sciadv.adc9830; †co-first authors*.

3.8 Author Contributions

Contributions for each figure are as follows:

Mara C. Harwood

- Figures 3.1A, 3.1B, 3.1C, 3.1D, 3.1E, 3.3A, 3.3B, 3.4A, 3.4D, 3.4E, 3.4F, 3.5A, 3.5B, 3.5C, 3.5E, 3.5F, 3.6E, 3.6F
- Supplementary Figures 3.1A, 3.1B, 3.1G, 3.1H, 3.1I, 3.2A, 3.2B, 3.2C, 3.2D, 3.2E, 3.2F, 3.2G, 3.2H, 3.2I, 3.2L, 3.3A, 3.3B, 3.3C, 3.3D, 3.3E, 3.3F, 3.3G
- Supplementary Table 3.1

Tai-Ting Woo

- Figures 3.2A, 3.2B, 3.2C, 3.2E, 3.2F, 3.3C, 3.3D, 3.3E, 3.3F, 3.3G, 3.4B, 3.4C, 3.5D
- Supplementary Figures 3.2J, 3.2K

Yuka Takeo

- Figures 3.2D, 3.2G, 3.2H, 3.6A, 3.6B, 3.6C, 3.6D
- Supplementary Figures 3.1C, 3.1D, 3.1E, 3.1F

3.9 Supplemental Material

3.9.1 Supplementary Figures

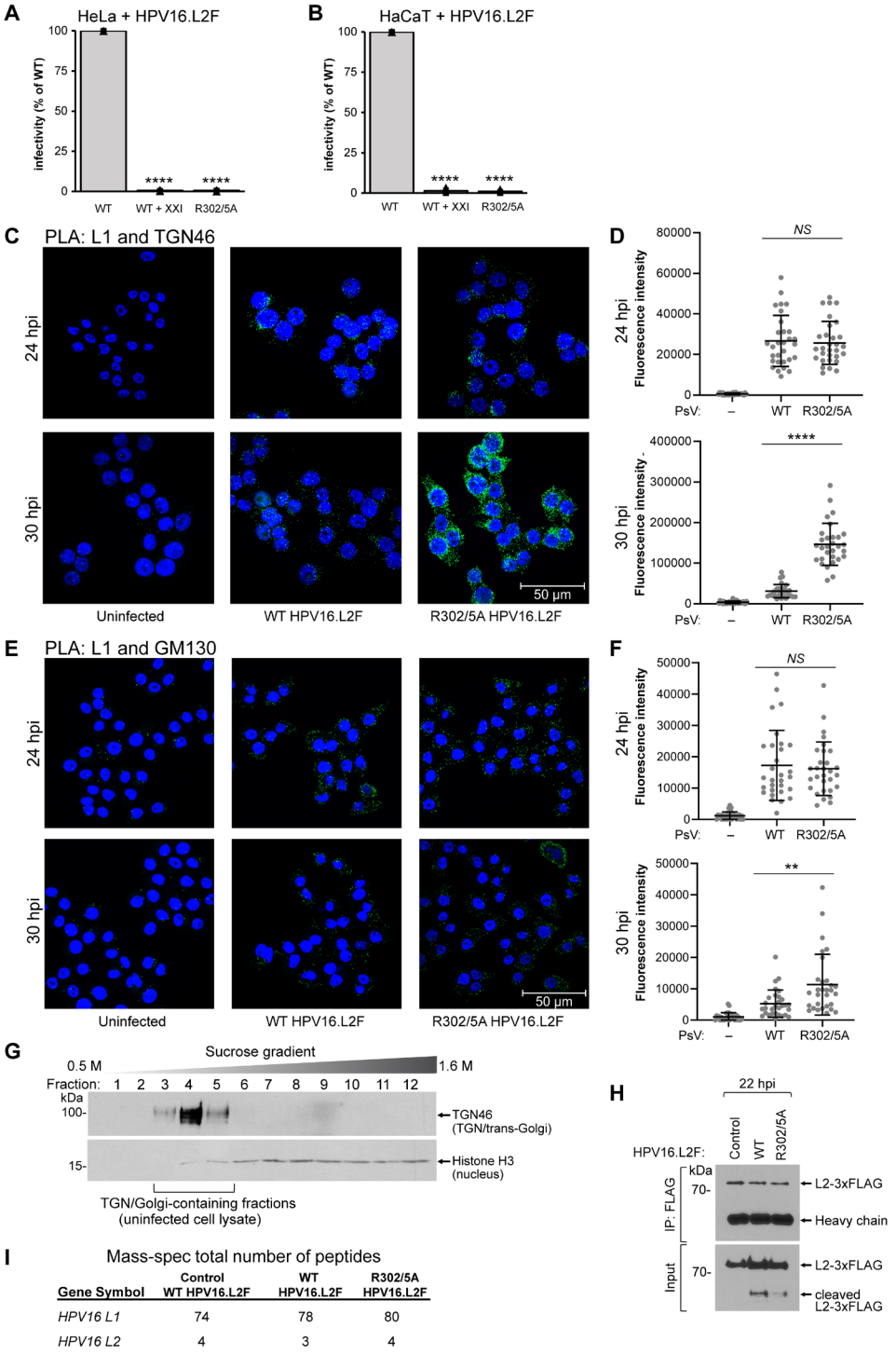

I Mass-spec total number of peptides

Gene Symbol	Control WT HPV16.L2F	WT HPV16.L2F	R302/5A HPV16.L2F
HPV16 L1	74	78	80
HPV16 L2	4	3	4

Supplementary Figure 3.1: Characterization of wild-type and R302/5A HPV16.L2F used for mass-spectrometry analysis (related to Figure 3.1)

A. *HeLa cells were infected with wild-type (WT) or mutant (R302/5A) HPV16.L2F PsV containing a GFP reporter plasmid. 1 μM of γ-secretase inhibitor (XXI) or dimethyl sulfoxide (DMSO) was added to cells as indicated at time of infection. At 48 hours post-infection (hpi), flow cytometry for GFP fluorescence was used to determine the fraction of GFP-expressing cells. The results were normalized to the fraction of cells infected by wild-type PsV without XXI-treatment. The means and standard deviations of three independent experiments are shown. A two-tailed, unequal variance t-test was used to determine statistical significance compared to cells infected with WT HPV16.L2F PsV without XXI-treatment. ****P < 0.0001.*

B. *As in (A), except HaCaT cells were used.*

C. *HeLa-Sen2 cells were uninfected or infected with WT or R302/5A HPV16.L2F PsV. At 24 or 30 hpi, cells were fixed and proximity ligation assay (PLA) was performed with antibodies recognizing HPV16 L1 and TGN46. PLA signals are shown in green. Nuclei were stained with 4',6-diamidino-2-phenylindole (DAPI, blue). Representative images of a single, medial Z-plane taken by confocal microscopy are shown.*

D. *Multiple images as in (C) were processed with Fiji software to measure the PLA fluorescence intensity per cell. The individual cell fluorescence intensity values, means, and standard deviations of 30 cells measured from one representative experiment are shown. A two-tailed, unequal variance t-test was used to determine statistical significance compared to cells infected with WT HPV16.L2F. NS, not significant (P >0.05); ****P < 0.0001. Similar results were obtained in two (24 hpi) or four (30 hpi) independent experiments.*

E. *As in (C), except PLA was performed in HeLa-S3 cells with antibodies recognizing HPV16 L1 and GM130.*

F. *As in (D), except images as in (E) were analyzed. Similar results were obtained in two (24 hpi) or three (30 hpi) independent experiments. NS, not significant (P > 0.05); **P < 0.01.*

G. *Representative immunoblots from fractionated extract obtained from uninfected cells.*

H. *Representative blots from immunoprecipitated material obtained after Step 4 (described in Figure 3.1B). The TGN/Golgi-containing fractions from Step 3 were combined and subjected to FLAG immunoprecipitation of HPV16 L2-3xFLAG. The resulting precipitate was subjected to SDS-PAGE followed by immunoblotting with an anti-FLAG antibody. "WT" indicates material obtained from cells infected with WT HPV16.L2F PsV for 22 h. "R302/5A" indicates material obtained from cells infected with R302/5A HPV16.L2F PsV for 22 h. "Control" indicates material obtained from uninfected cells that was mixed with WT HPV16.L2F PsV between Steps 3 and 4.*

I. *Total number of peptides corresponding to L1 and L2 proteins of HPV16 identified by mass-spectrometry. See Table S1 for a complete list of peptides identified by mass-spectrometry.*

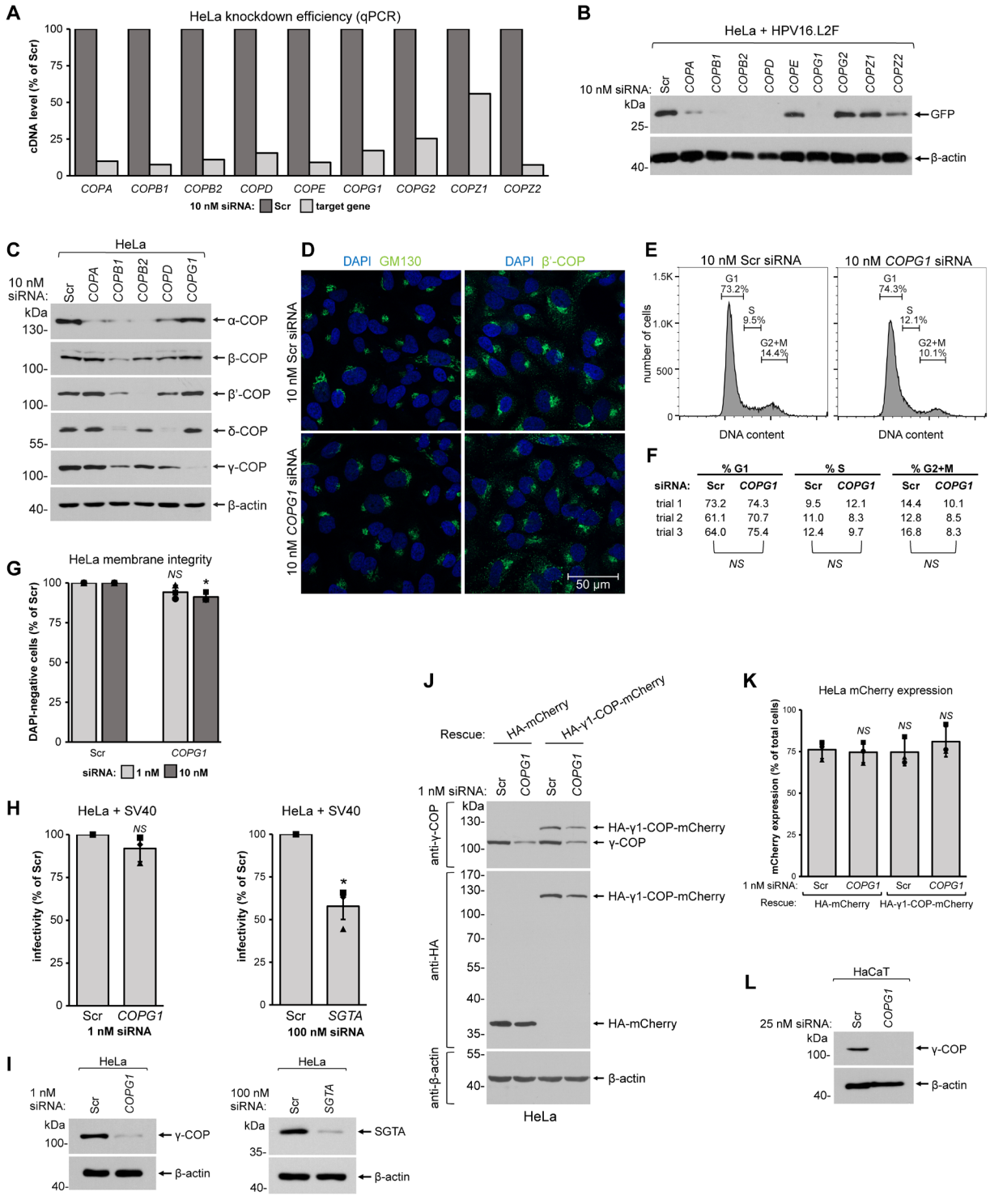
A
HeLa knockdown efficiency (qPCR)
cDNA level (% of Scr)
COPA COPB1 COPB2 COPD COPE COPG1 COPG2 COPZ1 COPZ2
10 nM siRNA: Scr target gene
B
HeLa + HPV16.L2F
10 nM siRNA: Scr COPA COPB1 COPB2 COPD COPE COPG1 COPG2 COPZ1 COPZ2
kDa
GFP
β-actin
C
HeLa
10 nM siRNA: Scr COPA COPB1 COPB2 COPD COPG1
α-COP
β-COP
β'-COP
δ-COP
γ-COP
β-actin
D
DAPI GM130
DAPI β'-COP
10 nM Scr siRNA
10 nM COPG1 siRNA
50 μm
E
10 nM Scr siRNA
10 nM COPG1 siRNA
number of cells
G1 73.2%
S 9.5%
G2+M 14.4%
G1 74.3%
S 12.1%
G2+M 10.1%
DNA content
F
% G1 % S % G2+M
siRNA: Scr COPG1 Scr COPG1 Scr COPG1
trial 1 73.2 74.3 9.5 12.1 14.4 10.1
trial 2 61.1 70.7 11.0 8.3 12.8 8.5
trial 3 64.0 75.4 12.4 9.7 16.8 8.3
NS
G
HeLa membrane integrity
DAPI-negative cells (% of Scr)
NS
*
Scr COPG1
siRNA: 1 nM 10 nM
H
HeLa + SV40
infectivity (% of Scr)
NS
Scr COPG1
1 nM siRNA
HeLa + SV40
infectivity (% of Scr)
*
Scr SGTA
100 nM siRNA
I
HeLa
1 nM siRNA: Scr COPG1
γ-COP
β-actin
HeLa
100 nM siRNA: Scr SGTA
SGTA
β-actin
J
Rescue: HA-mCherry HA-γ1-COP-mCherry
1 nM siRNA: Scr COPG1 Scr COPG1
anti-γ-COP
HA-γ1-COP-mCherry
γ-COP
anti-HA
HA-γ1-COP-mCherry
HA-mCherry
anti-β-actin
β-actin
HeLa
K
HeLa mCherry expression
mCherry expression (% of total cells)
NS NS NS
1 nM siRNA: Scr COPG1 Scr COPG1
Rescue: HA-mCherry HA-γ1-COP-mCherry
L
HaCaT
25 nM siRNA: Scr COPG1
γ-COP
β-actin

Supplementary Figure 3.2: Cellular effects of COPI-knockdown during HPV infection (related to Figure 3.4)
A. *RT-qPCR was used to analyze the knockdown efficiency of COPI subunits. HeLa cells were transfected with control siRNA or siRNAs targeting indicated genes for 24 h, followed by mRNA isolation and cDNA synthesis. The cDNA levels of the siRNA target genes were normalized to those of scrambled (Scr) siRNA-treated cells. All samples were further normalized to their GAPDH cDNA levels.*
B. *HeLa cells transfected with the indicated siRNA for 24 h were infected with WT HPV16.L2F PsV containing a GFP reporter plasmid. At 48 hpi, cells were lysed and the resulting whole-cell extract was subjected to SDS-PAGE followed by immunoblotting with antibodies recognizing GFP or β-actin as a loading control.*
C. *HeLa cells transfected with the indicated siRNA for 48 h were lysed and the resulting whole-cell extract was subjected to SDS-PAGE followed by immunoblotting with antibodies recognizing the indicated COPI subunit or β-actin as a loading control.*
D. *HeLa cells transfected with the indicated siRNA for 24 h were fixed, permeabilized, and subjected to immunofluorescence staining with antibodies recognizing GM130 (green, first column) or β'-COP (green, second column). Nuclei were stained with DAPI (blue). Representative images of a single, medial Z-plane taken by confocal microscopy are shown.*
E. *HeLa cells transfected with the indicated siRNA for 72 h were incubated with Hoechst 33342 to stain cellular DNA. Cells were then trypsinized and flow cytometry was used to measure relative Hoechst 33342 fluorescence (DNA content). The percentage of cells in G1, S, or G2+M phases for each condition is indicated. One set of representative histograms is shown. Similar results were obtained in three independent experiments.*
F. *Summary of cell cycle phase distributions as in (E). Data from three independent experiments are presented as the percentage of cells in each phase. A two-tailed, paired t-test was used to determine statistical significance between the Scr and COPG1 siRNA treated cells for each cell cycle phase. NS, not significant ($P > 0.05$).*
G. *HeLa cells transfected with Scr or COPG1 siRNA for 72 h were trypsinized and incubated in a buffer containing DAPI. Flow cytometry was used to determine the fraction of cells that excluded DAPI (DAPI-negative cells) as those with an intact membrane. The results were normalized to the DAPI-negative fraction of cells treated with Scr siRNA. The means and standard deviations of three independent experiments are shown. A two-tailed, unequal variance t-test was used to determine statistical significance compared to Scr siRNA-treated cells. NS, not significant; $*P < 0.05$.*
H. *HeLa cells transfected with COPG1 or SGTA siRNA for 24 h were infected with SV40. At 24 hpi, cells were fixed, permeabilized, and subjected to immunofluorescence staining using an antibody recognizing SV40 large T antigen. Data are the percent of cells expressing large T antigen, as assessed by fluorescence microscopy, normalized to SV40-infected cells treated with Scr siRNA. The means and standard deviations of three independent experiments are shown. A two-tailed, unequal variance t-test was used to determine statistical significance compared to Scr siRNA-treated cells. NS, not significant; $*P < 0.05$.*
I. *HeLa cells transfected with COPG1 or SGTA siRNA for 24 h were lysed and the resulting whole-cell lysate was subjected to SDS-PAGE followed by immunoblotting with the indicated antibodies. β-actin, loading control.*
J. *HeLa cells transfected with Scr or COPG1 siRNA for 9 h were then co-transfected with the control plasmid HA-mCherry or the rescue construct HA-γ1-COP-mCherry for another 15 h. Cells were lysed and the resulting whole-cell extract was subjected to SDS-PAGE followed by immunoblotting with the indicated antibodies. β-actin, loading control.*
K. *HeLa cells were transfected with Scr or COPG1 siRNAs for 9 h, followed by another transfection with DNA constructs for 15 h for the expression of HA-γ1-COP-mCherry or the control HA-mCherry. The transfected cells were then infected with WT HPV16.L2F PsV containing a GFP reporter plasmid. At 48 hpi, flow cytometry was used to determine the fraction of mCherry-expressing cells. The means and standard deviations of three independent experiments are shown. A two-tailed, unequal variance t-test was used to determine statistical significance compared to cells co-transfected with Scr siRNA and HA-mCherry-expressing plasmid. NS, not significant ($P > 0.05$).*
L. *HaCaT cells transfected with pooled Scr or COPG1 siRNAs for 48 h were lysed and the resulting whole-cell extract was subjected to SDS-PAGE followed by immunoblotting with antibodies recognizing γ-COP or β-actin as a loading control.*

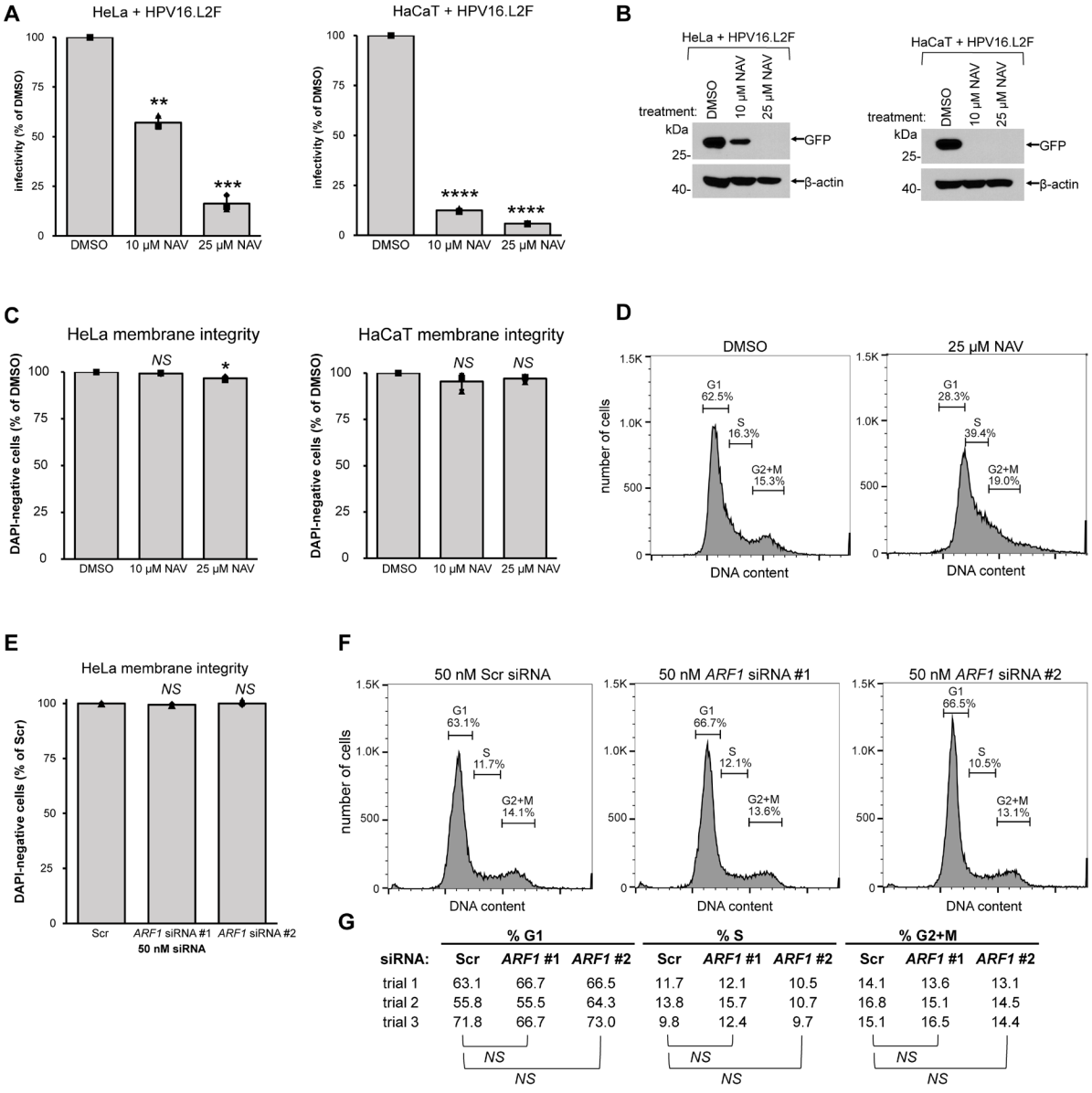

	% G1			% S			% G2+M		
siRNA:	**Scr**	***ARF1* #1**	***ARF1* #2**	**Scr**	***ARF1* #1**	***ARF1* #2**	**Scr**	***ARF1* #1**	***ARF1* #2**
trial 1	63.1	66.7	66.5	11.7	12.1	10.5	14.1	13.6	13.1
trial 2	55.8	55.5	64.3	13.8	15.7	10.7	16.8	15.1	14.5
trial 3	71.8	66.7	73.0	9.8	12.4	9.7	15.1	16.5	14.4
	NS		*NS*	*NS*		*NS*	*NS*		*NS*

Supplementary Figure 3.3: Cellular effects of Arf1-inhibition during HPV infection (related to Figure 3.5)
A. *HeLa (left) or HaCaT (right) cells were infected with WT HPV16.L2F PsV. DMSO, 10 μM, or 25 μM NAV-2729 (NAV) was added to cells at time of infection. At 48 hpi, infection was measured by flow cytometry. The results were normalized to the infected fraction of cells treated with DMSO. The means and standard deviations are shown (n = 3). A two-tailed, unequal variance t-test was used to determine statistical significance compared to DMSO treated cells. **P < 0.01; ***P < 0.001; ****P < 0.0001.*
B. *HeLa (left) or HaCaT (right) cells treated with DMSO, 10 μM, or 25 μM NAV for 48 h were lysed and the resulting whole-cell extract was subjected to SDS-PAGE followed by immunoblotting with the antibodies recognizing GFP or β-actin as a loading control.*
C. *HeLa (left) or HaCaT (right) cells treated with DMSO, 10 μM, or 25 μM NAV for 48 h were trypsinized and incubated in a buffer containing DAPI. Flow cytometry was used to determine the fraction of cells that excluded DAPI (DAPI-negative cells) as those with an intact membrane. The results were normalized to the DAPI-negative fraction of cells treated with DMSO. The means and standard deviations of three independent experiments are shown. A two-tailed, unequal variance t-test was used to determine statistical significance compared to DMSO treated cells. NS, not significant; *P < 0.05.*
D. *HeLa cells treated with DMSO (left) or 25 μM NAV (right) for 48 h were incubated with Hoechst 33342 to stain cellular DNA. Cells were then trypsinized and flow cytometry was used to measure relative Hoechst 33342 fluorescence (DNA content). The percentage of cells in G1, S, or G2+M phases for each condition is indicated.*
E. *HeLa cells treated with the indicated siRNA for 72 h were subjected to membrane integrity assay as in (C) except that the results were normalized to the DAPI-negative fraction of cells treated with Scr siRNA.*
F. *HeLa cells transfected with the indicated siRNA for 72 h were incubated with Hoechst 33342 to stain cellular DNA. Cells were then trypsinized and flow cytometry was used to measure relative Hoechst 33342 fluorescence (DNA content). The percentage of cells in G1, S, or G2+M phases for each condition is indicated. One set of representative histograms is shown. Similar results were obtained in three independent experiments.*
G. *Summary of cell cycle phase distributions as in (F). Data from three independent experiments are presented as the percentage of cells in each phase. A two-tailed, paired t-test was used to determine statistical significance between the Scr and ARF1 siRNA #1 or ARF1 siRNA #2 treated cells for each cell cycle phase. NS, not significant (P > 0.05).*

3.9.2 Supplementary Tables

Supplementary Table 3.1: Mass-spectrometry results
Download complete table (PDF):
https://www.science.org/doi/suppl/10.1126/sciadv.adc9830/suppl_file/sciadv.adc9830_sm.pdf

3.10 References

1. C. de Martel, M. Plummer, J. Vignat, S. Franceschi, Worldwide burden of cancer attributable to HPV by site, country and HPV type. *Int J Cancer* **141**, 664-670 (2017).

2. CDC, "Cancers Associated with Human Papillomavirus, United States—2015–2019," *USCS Data Brief, no. 31* (Atlanta, GA: Centers for Disease Control and Prevention, US Department of Health and Human Services, 2022).

3. J. C. Cardoso, E. Calonje, Cutaneous manifestations of human papillomaviruses: a review. *Acta Dermatovenerol Alp Pannonica Adriat* **20**, 145-154 (2011).

4. C. B. Buck *et al.*, Arrangement of L2 within the papillomavirus capsid. *J Virol* **82**, 5190-5197 (2008).

5. D. M. Belnap *et al.*, Conserved features in papillomavirus and polyomavirus capsids. *J Mol Biol* **259**, 249-263 (1996).

6. R. M. Richards, D. R. Lowy, J. T. Schiller, P. M. Day, Cleavage of the papillomavirus minor capsid protein, L2, at a furin consensus site is necessary for infection. *Proc Natl Acad Sci U S A* **103**, 1522-1527 (2006).

7. P. M. Day, D. R. Lowy, J. T. Schiller, Heparan sulfate-independent cell binding and infection with furin-precleaved papillomavirus capsids. *J Virol* **82**, 12565-12568 (2008).

8. R. C. Kines, C. D. Thompson, D. R. Lowy, J. T. Schiller, P. M. Day, The initial steps leading to papillomavirus infection occur on the basement membrane prior to cell surface binding. *Proc Natl Acad Sci U S A* **106**, 20458-20463 (2009).

9. M. Becker, L. Greune, M. A. Schmidt, M. Schelhaas, Extracellular Conformational Changes in the Capsid of Human Papillomaviruses Contribute to Asynchronous Uptake into Host Cells. *J Virol* **92**, (2018).

10. J. L. Smith, S. K. Campos, A. Wandinger-Ness, M. A. Ozbun, Caveolin-1-dependent infectious entry of human papillomavirus type 31 in human keratinocytes proceeds to the endosomal pathway for pH-dependent uncoating. *J Virol* **82**, 9505-9512 (2008).

11. M. C. Harwood, A. J. Dupzyk, T. Inoue, D. DiMaio, B. Tsai, p120 catenin recruits HPV to gamma-secretase to promote virus infection. *PLoS Pathog* **16**, e1008946 (2020).

12. T. Inoue *et al.*, gamma-Secretase promotes membrane insertion of the human papillomavirus L2 capsid protein during virus infection. *J Cell Biol* **217**, 3545-3559 (2018).

13. M. Crite, D. DiMaio, Human Papillomavirus L2 Capsid Protein Stabilizes gamma-Secretase during Viral Infection. *Viruses* **14**, (2022).

14. P. Zhang, G. Monteiro da Silva, C. Deatherage, C. Burd, D. DiMaio, Cell-Penetrating Peptide Mediates Intracellular Membrane Passage of Human Papillomavirus L2 Protein to Trigger Retrograde Trafficking. *Cell* **174**, 1465-1476 e1413 (2018).

15. N. Kamper *et al.*, A membrane-destabilizing peptide in capsid protein L2 is required for egress of papillomavirus genomes from endosomes. *J Virol* **80**, 759-768 (2006).

16. S. DiGiuseppe *et al.*, Topography of the Human Papillomavirus Minor Capsid Protein L2 during Vesicular Trafficking of Infectious Entry. *J Virol* **89**, 10442-10452 (2015).

17. A. Lipovsky *et al.*, Genome-wide siRNA screen identifies the retromer as a cellular entry factor for human papillomavirus. *Proc Natl Acad Sci U S A* **110**, 7452-7457 (2013).

18. A. Popa *et al.*, Direct binding of retromer to human papillomavirus type 16 minor capsid protein L2 mediates endosome exit during viral infection. *PLoS Pathog* **11**, e1004699 (2015).

19. J. Xie, P. Zhang, M. Crite, C. V. Lindsay, D. DiMaio, Retromer stabilizes transient membrane insertion of L2 capsid protein during retrograde entry of human papillomavirus. *Sci Adv* **7**, (2021).

20. W. Zhang, T. Kazakov, A. Popa, D. DiMaio, Vesicular trafficking of incoming human papillomavirus 16 to the Golgi apparatus and endoplasmic reticulum requires gamma-secretase activity. *mBio* **5**, e01777-01714 (2014).

21. P. M. Day, C. D. Thompson, R. M. Schowalter, D. R. Lowy, J. T. Schiller, Identification of a role for the trans-Golgi network in human papillomavirus 16 pseudovirus infection. *J Virol* **87**, 3862-3870 (2013).

22. A. V. Morante, D. D. Baboolal, X. Simon, E. C. Pan, P. I. Meneses, Human Papillomavirus Minor Capsid Protein L2 Mediates Intracellular Trafficking into and Passage beyond the Endoplasmic Reticulum. *Microbiol Spectr* **10**, e0150522 (2022).

23. S. Guttinger, E. Laurell, U. Kutay, Orchestrating nuclear envelope disassembly and reassembly during mitosis. *Nat Rev Mol Cell Biol* **10**, 178-191 (2009).

24. I. Aydin *et al.*, Large scale RNAi reveals the requirement of nuclear envelope breakdown for nuclear import of human papillomaviruses. *PLoS Pathog* **10**, e1004162 (2014).

25. C. M. Calton *et al.*, Translocation of the papillomavirus L2/vDNA complex across the limiting membrane requires the onset of mitosis. *PLoS Pathog* **13**, e1006200 (2017).

26. P. M. Day *et al.*, Human Papillomavirus 16 Capsids Mediate Nuclear Entry during Infection. *J Virol* **93**, (2019).

27. S. DiGiuseppe *et al.*, Incoming human papillomavirus type 16 genome resides in a vesicular compartment throughout mitosis. *Proc Natl Acad Sci U S A* **113**, 6289-6294 (2016).

28. S. DiGiuseppe, M. Bienkowska-Haba, L. Hilbig, M. Sapp, The nuclear retention signal of HPV16 L2 protein is essential for incoming viral genome to transverse the trans-Golgi network. *Virology* **458-459**, 93-105 (2014).

29. S. Mamoor *et al.*, The high risk HPV16 L2 minor capsid protein has multiple transport signals that mediate its nucleocytoplasmic traffic. *Virology* **422**, 413-424 (2012).

30. I. Aydin *et al.*, A central region in the minor capsid protein of papillomaviruses facilitates viral genome tethering and membrane penetration for mitotic nuclear entry. *PLoS Pathog* **13**, e1006308 (2017).

31. M. C. Lee, E. A. Miller, J. Goldberg, L. Orci, R. Schekman, Bi-directional protein transport between the ER and Golgi. *Annu Rev Cell Dev Biol* **20**, 87-123 (2004).

32. V. Popoff, F. Adolf, B. Brugger, F. Wieland, COPI budding within the Golgi stack. *Cold Spring Harb Perspect Biol* **3**, a005231 (2011).

33. J. Bethune, F. T. Wieland, Assembly of COPI and COPII Vesicular Coat Proteins on Membranes. *Annu Rev Biophys* **47**, 63-83 (2018).

34. C. B. Buck, D. V. Pastrana, D. R. Lowy, J. T. Schiller, Efficient intracellular assembly of papillomaviral vectors. *J Virol* **78**, 751-757 (2004).

35. C. B. Buck, C. D. Thompson, Y. Y. Pang, D. R. Lowy, J. T. Schiller, Maturation of papillomavirus capsids. *J Virol* **79**, 2839-2846 (2005).

36. C. B. Buck, C. D. Thompson, Production of papillomavirus-based gene transfer vectors. *Curr Protoc Cell Biol* **Chapter 26**, Unit 26 21 (2007).

37. J. Biryukov, C. Meyers, Papillomavirus Infectious Pathways: A Comparison of Systems. *Viruses* **7**, 4303-4325 (2015).

38. Y. Li *et al.*, Structural interactions between inhibitor and substrate docking sites give insight into mechanisms of human PS1 complexes. *Structure* **22**, 125-135 (2014).

39. A. Lipovsky, W. Zhang, A. Iwasaki, D. DiMaio, Application of the proximity-dependent assay and fluorescence imaging approaches to study viral entry pathways. *Methods Mol Biol* **1270**, 437-451 (2015).

40. C. Harter *et al.*, Nonclathrin coat protein gamma, a subunit of coatomer, binds to the cytoplasmic dilysine motif of membrane proteins of the early secretory pathway. *Proc Natl Acad Sci U S A* **93**, 1902-1906 (1996).

41. C. Harter, F. T. Wieland, A single binding site for dilysine retrieval motifs and p23 within the gamma subunit of coatomer. *Proc Natl Acad Sci U S A* **95**, 11649-11654 (1998).

42. M. P. Bronnimann, J. A. Chapman, C. K. Park, S. K. Campos, A transmembrane domain and GxxxG motifs within L2 are essential for papillomavirus infection. *J Virol* **87**, 464-473 (2013).

43. R. Duden, L. Kajikawa, L. Wuestehube, R. Schekman, epsilon-COP is a structural component of coatomer that functions to stabilize alpha-COP. *EMBO J* **17**, 985-995 (1998).

44. A. Steiner *et al.*, Deficiency in coatomer complex I causes aberrant activation of STING signalling. *Nat Commun* **13**, 2321 (2022).

45. C. P. Walczak, M. S. Ravindran, T. Inoue, B. Tsai, A cytosolic chaperone complexes with dynamic membrane J-proteins and mobilizes a nonenveloped virus out of the endoplasmic reticulum. *PLoS Pathog* **10**, e1004007 (2014).

46. T. Serafini *et al.*, ADP-ribosylation factor is a subunit of the coat of Golgi-derived COP-coated vesicles: a novel role for a GTP-binding protein. *Cell* **67**, 239-253 (1991).

47. D. J. Palmer, J. B. Helms, C. J. Beckers, L. Orci, J. E. Rothman, Binding of coatomer to Golgi membranes requires ADP-ribosylation factor. *J Biol Chem* **268**, 12083-12089 (1993).

48. S. Benabdi *et al.*, Family-wide Analysis of the Inhibition of Arf Guanine Nucleotide Exchange Factors with Small Molecules: Evidence of Unique Inhibitory Profiles. *Biochemistry* **56**, 5125-5133 (2017).

49. J. H. Yoo *et al.*, ARF6 Is an Actionable Node that Orchestrates Oncogenic GNAQ Signaling in Uveal Melanoma. *Cancer Cell* **29**, 889-904 (2016).

50. V. Laniosz, S. A. Dabydeen, M. A. Havens, P. I. Meneses, Human papillomavirus type 16 infection of human keratinocytes requires clathrin and caveolin-1 and is brefeldin a sensitive. *J Virol* **83**, 8221-8232 (2009).

51. P. A. Pellett, F. Dietrich, J. Bewersdorf, J. E. Rothman, G. Lavieu, Inter-Golgi transport mediated by COPI-containing vesicles carrying small cargoes. *Elife* **2**, e01296 (2013).

52. L. Orci, B. S. Glick, J. E. Rothman, A new type of coated vesicular carrier that appears not to contain clathrin: its possible role in protein transport within the Golgi stack. *Cell* **46**, 171-184 (1986).

53. E. Farmer, M. A. Cheng, C. F. Hung, T. C. Wu, Vaccination Strategies for the Control and Treatment of HPV Infection and HPV-Associated Cancer. *Recent Results Cancer Res* **217**, 157-195 (2021).

54. W. Ma, J. Goldberg, Rules for the recognition of dilysine retrieval motifs by coatomer. *EMBO J* **32**, 926-937 (2013).

55. D. J. Shiwarski, S. E. Crilly, A. Dates, M. A. Puthenveedu, Dual RXR motifs regulate nerve growth factor-mediated intracellular retention of the delta opioid receptor. *Mol Biol Cell* **30**, 680-690 (2019).

56. P. Sharma *et al.*, Endoplasmic reticulum protein targeting of phospholamban: a common role for an N-terminal di-arginine motif in ER retention? *PLoS One* **5**, e11496 (2010).

57. K. Michelsen, H. Yuan, B. Schwappach, Hide and run. Arginine-based endoplasmic-reticulum-sorting motifs in the assembly of heteromultimeric membrane proteins. *EMBO Rep* **6**, 717-722 (2005).

58. J. Xie, E. N. Heim, M. Crite, D. DiMaio, TBC1D5-Catalyzed Cycling of Rab7 Is Required for Retromer-Mediated Human Papillomavirus Trafficking during Virus Entry. *Cell Rep* **31**, 107750 (2020).

59. M. Aridor, S. I. Bannykh, T. Rowe, W. E. Balch, Sequential coupling between COPII and COPI vesicle coats in endoplasmic reticulum to Golgi transport. *J Cell Biol* **131**, 875-893 (1995).

60. A. V. Weigel *et al.*, ER-to-Golgi protein delivery through an interwoven, tubular network extending from ER. *Cell* **184**, 2412-2429 e2416 (2021).

61. O. Shomron *et al.*, COPII collar defines the boundary between ER and ER exit site and does not coat cargo containers. *J Cell Biol* **220**, (2021).

62. J. Liu, A. J. Prunuske, A. M. Fager, K. S. Ullman, The COPI complex functions in nuclear envelope breakdown and is recruited by the nucleoporin Nup153. *Dev Cell* **5**, 487-498 (2003).

63. S. Y. Bednarek *et al.*, COPI- and COPII-coated vesicles bud directly from the endoplasmic reticulum in yeast. *Cell* **83**, 1183-1196 (1995).

64. K. Y. Lai *et al.*, A Ran-binding protein facilitates nuclear import of human papillomavirus type 16. *PLoS Pathog* **17**, e1009580 (2021).

65. T. Misteli, G. Warren, COP-coated vesicles are involved in the mitotic fragmentation of Golgi stacks in a cell-free system. *J Cell Biol* **125**, 269-282 (1994).

66. Y. Xiang, J. Seemann, B. Bisel, S. Punthambaker, Y. Wang, Active ADP-ribosylation factor-1 (ARF1) is required for mitotic Golgi fragmentation. *J Biol Chem* **282**, 21829-21837 (2007).

67. J. G. Donaldson, D. Finazzi, R. D. Klausner, Brefeldin A inhibits Golgi membrane-catalysed exchange of guanine nucleotide onto ARF protein. *Nature* **360**, 350-352 (1992).

68. J. B. Helms, J. E. Rothman, Inhibition by brefeldin A of a Golgi membrane enzyme that catalyses exchange of guanine nucleotide bound to ARF. *Nature* **360**, 352-354 (1992).

69. J. Lippincott-Schwartz *et al.*, Brefeldin A's effects on endosomes, lysosomes, and the TGN suggest a general mechanism for regulating organelle structure and membrane traffic. *Cell* **67**, 601-616 (1991).

70. J. B. Saenz *et al.*, Golgicide A reveals essential roles for GBF1 in Golgi assembly and function. *Nat Chem Biol* **5**, 157-165 (2009).

71. E. Sun, J. He, X. Zhuang, Dissecting the role of COPI complexes in influenza virus infection. *J Virol* **87**, 2673-2685 (2013).

72. R. Konig *et al.*, Human host factors required for influenza virus replication. *Nature* **463**, 813-817 (2010).

73. J. A. Thompson, J. C. Brown, Role of Coatomer Protein I in Virus Replication. *J Virol Antivir Res* **1**, (2012).

74. P. Bagchi, M. Torres, L. Qi, B. Tsai, Selective EMC subunits act as molecular tethers of intracellular organelles exploited during viral entry. *Nat Commun* **11**, 1127 (2020).

75. E. C. Goodwin *et al.*, Rapid induction of senescence in human cervical carcinoma cells. *Proc Natl Acad Sci U S A* **97**, 10978-10983 (2000).

76. D. Tang, Y. Xiang, Y. Wang, Reconstitution of the cell cycle-regulated Golgi disassembly and reassembly in a cell-free system. *Nat Protoc* **5**, 758-772 (2010).

77. J. Schindelin *et al.*, Fiji: an open-source platform for biological-image analysis. *Nat Methods* **9**, 676-682 (2012).

CHAPTER 4:
Conclusion and Future Directions

To initiate infection, DNA viruses must enter host cells, traverse a complex intracellular environment, and in most cases deliver their viral genomic DNA to the nucleus for replication – all without detection by host cell defense mechanisms. In the case of HPV, the virus remains largely protected behind various subcellular membranes as it traverses the intracellular space. However, targeting of a virus along its productive infectious pathway often necessitates exposure of a viral protein to the cytosol that provides the essential instructional cues for proper trafficking. This scenario poses a conundrum – how does HPV ensure it is directed towards the nucleus for infection rather than along a non-productive pathway, while also remaining hidden behind subcellular membranes? This dissertation provides mechanistic understanding to how HPV achieves transport through the endosomal and Golgi membrane systems to achieve infection, and highlights the next critical areas of research for future investigation.

4.1 Endosomal trafficking and cytosolic exposure of HPV

Upon endocytosis, HPV is delivered to the endosome where its capsid proteins L1 and L2 partially disassemble (*1-3*). The virus is then targeted to γ-secretase localized on the endosomal membrane (*4, 5*). This transmembrane protease harbors a novel chaperone-like activity that promotes insertion of the C-terminus of L2 across the endosomal membrane (*4*) in a process aided by the presence of a cell-penetrating peptide on L2 (*6*). Membrane insertion of L2 exposes the C-terminus of this viral protein to the cytosol where it recruits host trafficking factors that direct the virus along an infectious route.

Prior to my research, a major gap in our understanding of HPV entry was *how HPV is targeted from the cell surface to endosome-localized γ-secretase*. This is a critical step for HPV entry; without properly associating with γ-secretase, the virus does not reach the Golgi and infection is inhibited (*4, 5, 7*). However, HPV is an unusual cargo for γ-secretase, which typically cleaves endogenous transmembrane proteins such as cadherin, notch, and amyloid precursor protein (*8*). How then is HPV recruited to this host protease to facilitate membrane insertion of a viral protein?

4.1.1 Key findings: p120 catenin recruits HPV to γ-secretase for membrane insertion

p120 was first identified as a potential HPV interacting factor in a previously published proteomics dataset (*4*). As a known γ-secretase interacting factor (*9, 10*), p120 stood out as a viable candidate to pursue. Subsequent immunoprecipitation studies revealed that p120 does indeed interact with the capsid proteins of HPV, and that p120 is required for infection with multiple HPV types in multiple cell types.

What role is p120 playing in HPV infection? The mechanistic data in Chapter 2 support a model in which p120 targets the virus to γ-secretase (see Figure 4.1). In the absence of p120, HPV reaches the endosome but cannot associate with γ-secretase or become membrane-inserted. A previous report demonstrated that p120 can directly bind to a defined region of γ-secretase (*9*). Not surprisingly, a p120 binding-defective γ-secretase mutant cannot support HPV infection, likely because the virus cannot be recruited to γ-secretase in a p120-dependent manner. Although these findings illuminated the molecular mechanism by which HPV is targeted to γ-secretase, they raised an enigma centered on the topological state of the host protein and HPV L2: because p120 is in the cytosol and L2 remains in the endosomal lumen (prior to engaging γ-secretase), how can the two proteins interact? At present, the most plausible explanation is that the HPV L2-p120 interaction is indirect and bridged by an additional cellular transmembrane factor whose identity remains unknown (see Figure 4.1, further discussion in section 4.3.1).

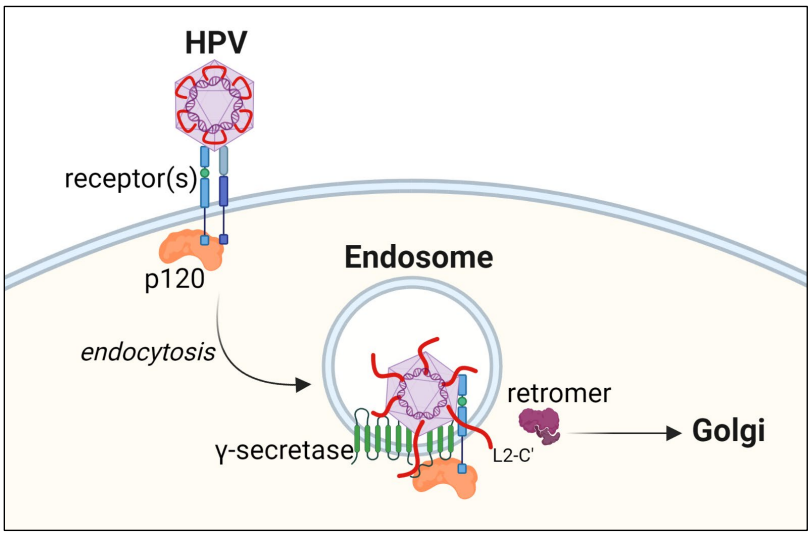

Figure 4.1: p120 recruits HPV to γ-secretase to enable insertion of L2 across the endosome membrane
See text for details. Figure created with BioRender.com

4.2 Golgi transit and nuclear arrival of HPV

After endocytosis and insertion of L2 across the endosomal membrane, HPV is sorted to the Golgi apparatus by the cellular sorting complex retromer (*11, 12*). HPV then moves from the Golgi towards the nucleus in membrane-bound vesicles (*13*), and these intact vesicles containing HPV enter the nucleus during mitotic nuclear envelope breakdown. Only once mitosis is complete and the nuclear envelope reforms does the viral genome of HPV become exposed to the nucleoplasm. The viral genome is then able to replicate using host machinery, thus completing the cellular entry phase of HPV infection.

Despite the steps depicted above, the molecular basis by which HPV traffics through the Golgi remains mysterious. In fact, little is known about the function of the Golgi during HPV infection beyond serving as a temporary "pit-stop" where the virus hides in this compartment until the onset of mitosis. Why does HPV traffic to the Golgi, how does it traverse the Golgi stacks, and how does the virus ultimately exit this organelle? Moreover, what are the characteristics of the Golgi-derived transport vesicle harboring HPV that is targeted to the nucleus for infection?

4.2.1 Key findings: HPV directly binds to the COPI sorting complex to facilitate Golgi transit

To identify host factors responsible for promoting transit of HPV across the Golgi membranes, I initiated an unbiased proteomics approach. In this strategy, I first fractionated HPV-infected cells to enrich for HPV in the Golgi, followed by immunoprecipitation of the virus in this fraction and mass-spectrometry to identify HPV-associated Golgi factors. From this list, I decided to further examine COPI because this retrograde protein sorting complex is known to

function at the Golgi where it promotes retrograde transport of cellular cargos across the Golgi and into the ER (*14-16*) (see Figure 4.2).

Indeed, our binding experiments revealed that HPV not only associates with multiple subunits of the COPI complex, but a highly conserved motif of L2 is sufficient to directly bind to the γ1-COP subunit (an established cargo-binding subunit of COPI) (*16*). Specifically, this binding is facilitated by a di-arginine motif on L2 (RXXR); similar di-arginine motifs have been previously shown to act as a non-canonical COPI binding motifs (*17-19*). Importantly, genetic depletion of COPI robustly blocked HPV infection in multiple cell lines with many HPV types, demonstrating a critical role of COPI during HPV infection. Furthermore, COPI-L2 binding and efficient HPV infection both require that COPI be properly recruited to the Golgi membrane by the small GTPase Arf1. Mutation of the COPI binding motif of L2 similarly blocked HPV infection, firmly establishing a functional link between COPI and HPV entry. Microscopy experiments revealed that when COPI is depleted (or the COPI-binding site on L2 is mutated), HPV becomes trapped and accumulates in the Golgi. Together, these data support a model whereby COPI is required for HPV to transit across the Golgi en route for the nucleus (see Figure 4.2).

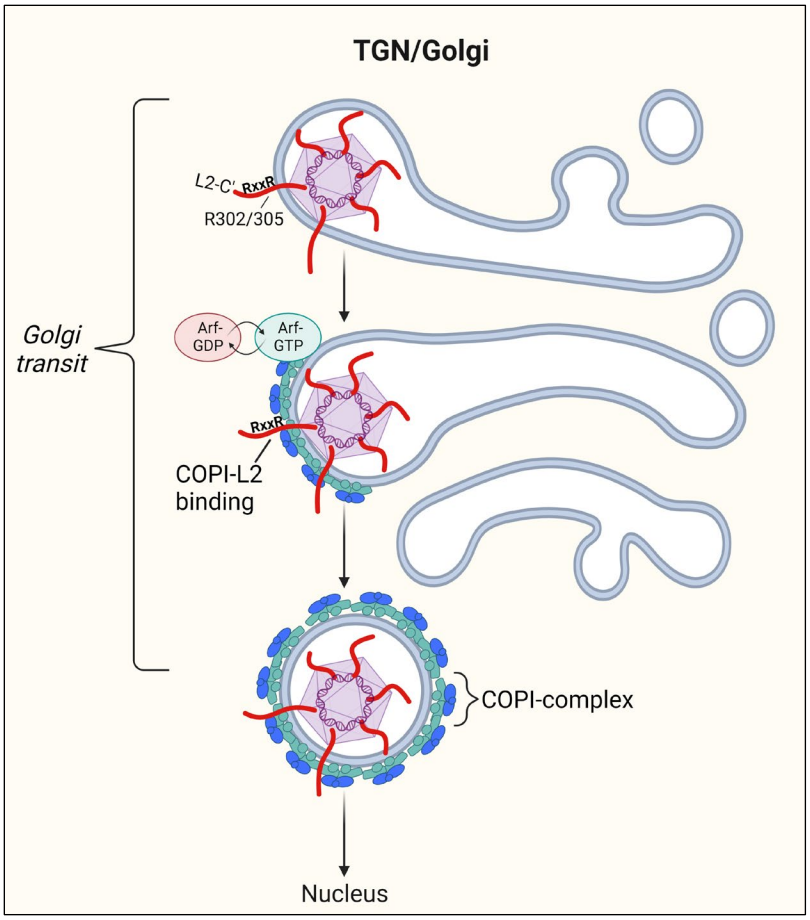

Figure 4.2: COPI directly binds a di-arginine motif on HPV-L2 to facilitate Golgi transit during viral entry
See text for details. Figure created with BioRender.com

4.3 Future directions

4.3.1 Identifying the entry receptor

Perhaps the most obvious enigma in the field of HPV infection is the identity of the virus entry receptor (Figure 4.3, number 1). Various cell surface-localized membrane proteins including tetraspanins, epidermal growth factor receptor, integrins, and annexin A2 have all been implicated in HPV entry, although none of them have been conclusively shown to act as the bona fide entry receptor (*20-29*). Indeed, this area of HPV research remains murky, with different putative receptors being reported by different groups. Regardless, a consensus model is emerging in which HPV is thought to bind to a cell surface "entry platform" consisting of several proteins which coordinate actin-dependent HPV endocytosis (*30, 31*). Because Chapter 2 of my thesis demonstrated p120 binding to HPV via an unidentified transmembrane protein, it would be reasonable to test whether p120 associates with the cytosolic side of this entry platform, thereby linking p120 to cell surface-localized HPV.

Alternatively, the aforementioned transmembrane protein bridging HPV and p120 may represent the actual entry receptor. Here a likely candidate is the cell-adhesion protein family cadherins, which are cell surface receptors that are recruited from the plasma membrane to the γ-secretase by p120 (*9, 10, 32, 33*). In this context, our initial (unpublished) studies of cadherin are promising – knockdown of cadherin blocks HPV infection, and immunoprecipitation of HPV shows some association of the virus with cadherin. Further studies will be needed to determine which cadherin type(s) are required for HPV infection in various cell lines, and to characterize the nature of the HPV-cadherin interaction.

4.3.2 Membrane insertion of L2

Upon receptor-mediated entry to the endosome, HPV L2 is inserted into the endosomal membrane so that this viral protein is exposed to the cytosol. Membrane insertion of L2 is a critical step because it recruits cytosolic sorting factors (including COPI, see Chapter 3) that directs the virus along a productive pathway. However, how the insertion state of L2 is maintained throughout viral entry is unclear (Figure 4.3, number 2). Without a classical transmembrane domain, L2 insertion is likely unstable, with the possibility of "backsliding" to the luminal compartment. Yet, stable L2 membrane insertion is required for it to engage cytosolic factors throughout the intracellular trafficking process. One possibility is that these cytosolic factors function to lock the C-terminus of L2 in the cytosol, thus stabilizing its membrane-spanning conformation. In agreement with this model, a recent study finds that the cytosolic retromer complex stabilizes L2 insertion across the endosomal membrane. If retromer is depleted, L2 is initially inserted, but then backslides over time (*34*). Thus, binding retromer helps stabilize L2 in a transmembrane conformation. However, retromer must also *release* L2 for the virus to continue trafficking beyond the endosome (*35*). How then does L2 remain membrane-inserted after retromer is released from this viral protein?

This question led to a model where different cytosolic factors sequentially bind to L2, stabilize the transmembrane topology, route the virus towards its next destination, then release from L2 to enable binding of the next cytosolic factor. This highly-coordinated process may serve as a template for understanding HPV's intracellular trafficking mechanisms. Beyond HPV L2, our studies also raise the intriguing possibility that other soluble cellular (and even viral) proteins may adopt a stable membrane spanning-topology using this mechanism in order to execute their biological functions.

4.3.3 The role of the endoplasmic reticulum during HPV entry

Although Chapter 3 of my thesis demonstrates that HPV binds to COPI to transit the Golgi en route to the nucleus for infection, this study nonetheless raises several questions that remain unanswered. Classically, COPI shuttles cargo from the Golgi to the ER, not to the nucleus. A logical question is if COPI also transports HPV to the ER (Figure 4.3, number 3). While there is evidence that a subset of HPV particles can reach the ER during viral entry (*5, 36*), it is unclear if ER transport represents the infectious route. One study demonstrated that siRNA-mediated depletion of PDI and ERp72, two ER-localized cellular reductases, moderately inhibited HPV16 infection (*37*), although there is no clear explanation to account for this inhibition. One approach to determine if HPV traverses the ER prior to nuclear arrival is the use the biotinylation proximity labeling technique. For example, cells containing an ER-localized biotin ligase could be infected with HPV. Following infection, nuclear-localized HPV is then isolated and analyzed for biotinylation to determine if the virus passed through the ER en route for the nucleus.

Alternatively, if HPV is *not* routed through the ER before nuclear arrival, the cytosol-exposed portion of L2 could bind to a cellular sorting factor that redirects the COPI-coated vesicle exiting the Golgi (that carries the virus) directly towards the nucleus, thereby bypassing the ER completely. In support of this model, there is evidence suggesting the dynein motor complex helps transport HPV from the Golgi into the nucleus (*38*). A potential role for dynein here is intriguing as dynein was another highly-enriched cellular factor identified in the Golgi enriched mass-spectrometry dataset (Chapter 3, Supplementary Table 3.1). Further studies are needed to determine if dynein can directly engage L2 during Golgi exit. Perhaps dynein actively reroutes the virus away from the ER, thus allowing for transport of HPV from the Golgi directly to the nucleus.

4.3.4 Nuclear entry

In the current model of HPV nuclear entry, the virus buds from the Golgi in a vesicle, and this vesicle enters the nucleus during mitotic nuclear envelope breakdown (Figure 4.3, number 4). Though this model precludes the use of nuclear pore complexes (due to size limitations), nuclear import machinery could still play a role in actively targeting the HPV-containing vesicle towards the nucleus. In fact, several pieces of data suggest that importins, a family of nuclear import proteins, may be involved in HPV nuclear entry.

My Golgi-enriched mass-spectrometry dataset (Chapter 3, Supplementary Table 3.1) identified the α-importin KPNA2 as a potential HPV-interacting host protein, and proteomics analysis by Inoue et al. (*4*) also identified the α-importin KPNA1 as a possible HPV-interacting factor. Moreover, siRNA screens revealed that knockdown of the β-importins IPO9 (*11*) and IPO5 (*39*) reduced HPV infection. A more recent study found that depleting KPNA2 appears to trap HPV in the Golgi and blocks nuclear arrival (*38*).

Given these data, a systematic approach is needed to determine the role of importins during HPV infection. Towards this goal, I conducted a preliminary siRNA screen of 7 α-importins and 10 β-importins and found that individual knockdown of IPO5, 7, or 9 (all β-importins) inhibited HPV infection (unpublished data). Consistent with these findings, treating cells with the β-importin inhibitor importazole (*40*) robustly blocked HPV infection in multiple cell types (unpublished data). Follow-up studies are needed to determine if β-importins can directly engage L2 during infection. Indeed, it is possible for β-importins to directly engage cargo without the involvement of α-importins (*41*), and several putative nuclear-localization sequences have been identified on L2 (*42*).

Although presence of a membrane-bound cargo vesicle in the nuclei of cells is atypical, electron microscopy images provide clear evidence of intact HPV particles surrounded by a vesicular membrane in the nucleus of cells (*43*). Given my findings that COPI is required for the Golgi-escape of HPV prior to nuclear entry, this result begs the question: is the HPV-containing vesicle in the nucleus a COPI-coated vesicle? High-resolution microscopy, such as cryo-electron tomography or correlative light electron microscopy, may help to visualize these vesicles containing HPV and determine if they are indeed COPI coated. Biochemical approaches may also be useful – a simple immunoprecipitation of HPV from the nuclear fraction of infected cells could determine if the virus is still COPI-bound in the nucleus.

4.3.5 Viral genome exposure

Once the HPV-containing transport vesicle arrives in the nucleus, an outstanding question remains as to how the viral DNA ultimately becomes exposed to the nucleoplasm (Figure 4.3, number 5). This process appears to be intimately tied to mitosis: semi-permeabilized cell-based studies demonstrate that the viral genome is not exposed to the nucleoplasm until mitosis is complete (*13*). Is there a cell-cycle linked signal that triggers viral genome exposure, and how is this achieved? A very recent study found evidence for phosphorylation of L2 by the mitotic kinases CDK1 and PLK1, and provides evidence that phosphorylation is required for viral DNA to efficiently reach the nucleus and associate with host chromatin (*44*). This raises the possibility that L2 phosphorylation during mitosis is the signal for viral DNA exposure, although it is unclear how the translocation of the viral DNA across the limiting membrane would be mechanistically achieved.

One possibility is that L2 associates with a nuclear-localized chaperone that "pulls" the viral DNA out of the vesicle, analogous to the mechanism by which chaperones pull SV40 into the cytosol from the ER (*45-47*). Alternatively, the limiting membrane surrounding HPV in the nucleus could be ruptured by nuclear-localized phospholipases. In fact, two prior siRNA screens (*11, 48*) found that knockdown of phospholipase PLCD3 reduced HPV infection, warranting further investigation of this lipolytic enzyme during HPV viral-genome exposure.

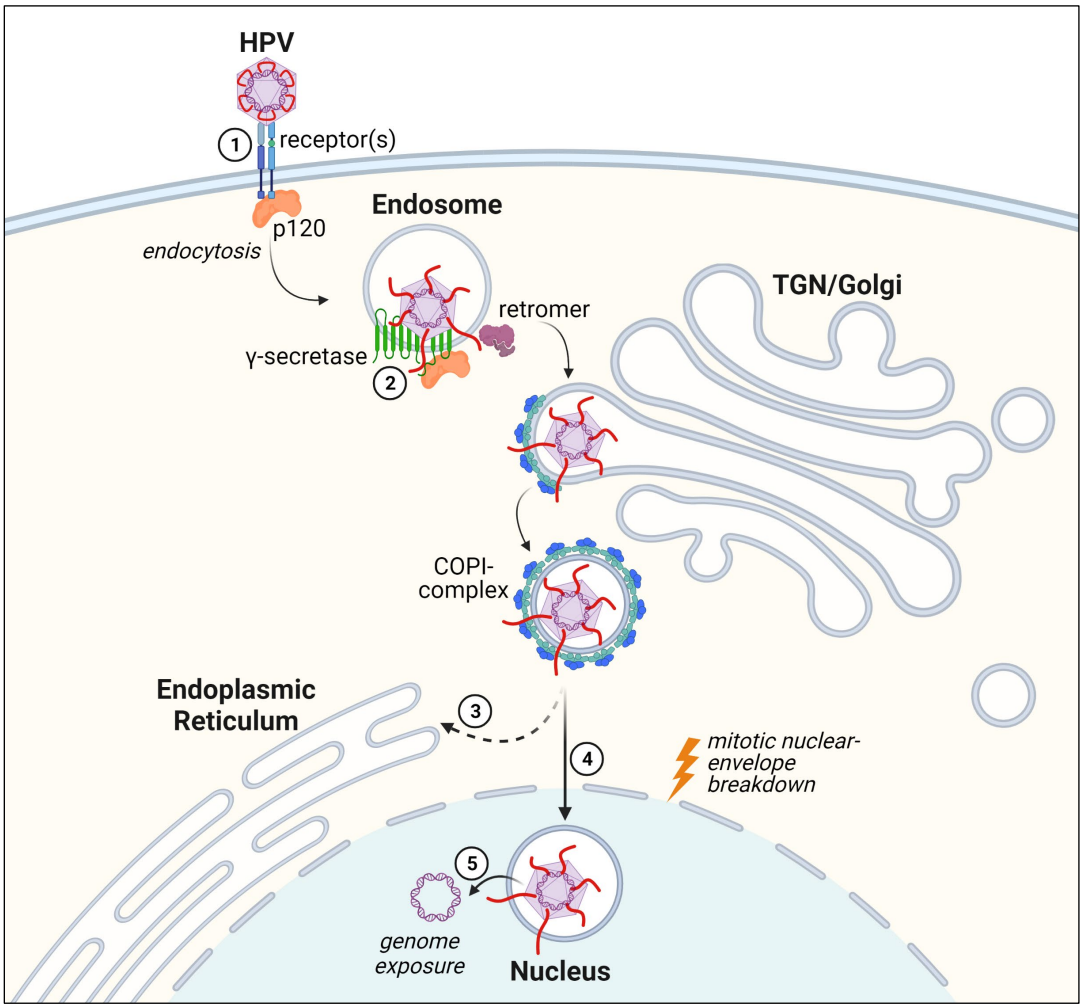

Figure 4.3: Current model of HPV entry and outstanding questions
1. *What is the identity of the cell surface entry receptor(s)?*
2. *How is membrane insertion of L2 maintained?*
3. *Does HPV entry require trafficking through the ER?*
4. *What targets HPV to the nucleus?*
5. *How does the viral genome become exposed to the nucleoplasm?*
Figure created with BioRender.com

4.4 Broader implications in cell biology and biomedical development

HPV is an extremely common human pathogen, infecting the majority of U.S. individuals by age 45 (*49, 50*). While most HPV infections clear spontaneously within 2 years, persistent infection with certain types of HPV may cause life threatening cancers (*51, 52*). Alas, HPV is the primary cause of cervical, anogenital, and oropharyngeal cancers (*53*) – the latter of which is on an unprecedented rise in the U.S (*54*). HPV also causes a wide variety of bothersome warts, including plantar warts, anogenital warts, and common warts of the hands and body (*55*).

Although prophylactic multivalent HPV vaccines are highly effective, vaccine uptake is low (*56*) and much of the U.S. population remains susceptible to HPV-related cancers (*57*). On a global level, widespread vaccination has not been implemented (*58*). While vaccination is an excellent first-line of defense, it is only preventative and there are no therapeutic options to help clear pre-existing HPV infections, nor does vaccination prevent all types of HPV infection. For these reasons, identifying targets for anti-viral therapy remains an important objective in combating HPV-induced disease.

Small-molecule antivirals classically target enzymes encoded by the viral genome that help the virus to replicate upon nuclear arrival (*59, 60*). Some small molecules have been studied in their ability to inhibit HPV replication once the virus has reached the nucleus (*61, 62*). However, this is a difficult approach because HPV only encodes for one helicase of its own, relying instead on host replication machinery. For this reason, targeting the viral entry pathway may be a good alternative for therapeutic development. Although this approach would not clear pre-existing infections, it could help prevent spread of the virus through close contact or autoinoculation.

One such area of therapeutic opportunity is in designing peptides that specifically disrupt the interaction between the HPV and its host trafficking machinery. As a proof-of-principle, experiments with small peptides were found to inhibit HPV infection in both cell culture and mouse models (*63*). In these studies, a 29-residue peptide was synthesized to contain the cell-penetrating peptide (CPP) sequence of L2 and the retromer binding site of L2. When cultured with cells, the synthetic peptide efficiently enters the cells (likely via the action of the CPP) and robustly blocks subsequent HPV infection. Mechanistically, this is likely achieved because the peptide is able to bind and sequester retromer in a manner outcompeting HPV. The virus becomes trapped in the endosome, thus blocking infection. In mouse models, the same peptide moderately but significantly prevented HPV infection. In a similar approach, infection by the human polyomavirus BKV (a small non-enveloped DNA virus) was inhibited using a synthetic 13-residue peptide derived from a sequence of the polyomavirus capsid protein VP2/3 (*64*). Rather than binding a cellular factor, as the HPV-inhibiting peptide does with retromer, the polyomavirus-inhibiting peptide associates with the VP1 capsid protein of incoming polyomavirus. Consequently, the virus becomes trapped in the ER and infection is blocked.

Could a synthetic peptide containing the COPI binding region of L2 show similar antiviral properties towards HPV? Because the COPI binding motif is highly conserved on multiple HPV types, this could serve as a pan-HPV antiviral target. The fact that the RXXR COPI-binding motif on L2 is *not* canonical could serve as an advantage – perhaps the HPV-COPI interaction could be specifically targeted without disrupting COPI's interaction with other important cellular cargo. Combining the retromer and the COPI binding peptides, using either a chimera or a cocktail approach, might further enhance the antiviral properties. Moreover, the use

of the CPP from L2 may aid the cytosolic delivery of diverse peptides in a wide range of therapeutic contexts.

γ-secretase is another intriguing target for therapeutic development, and may have applications beyond HPV infection. γ-secretase inhibitors have long been the subject of therapeutic development; but with nearly 100 cellular substrates, γ-secretase inhibitors run the risk of broadly disrupting cellular function (*65*). γ-secretase is well-known to interact with and cleave cellular transmembrane substrates. In the case of Notch and amyloid precursor protein (APP), aberrant cleavage by γ-secretase has mechanistic consequences such as cancer and plaque formation, respectively (*66, 67*). Although γ-secretase is required for HPV infection, proteolytic cleavage of L2 by γ-secretase is not. Rather, it is the ability of γ-secretase to bind and insert L2 that is functionally important for HPV infection (*4*). Intriguingly, there is evidence that L2 binding to γ-secretase actually stabilizes the γ-secretase complex (*68*). Given this information, could an L2-derived peptide be used to bind and stabilize γ-secretase, thus preventing deviant cleavage of other cellular substrates? The lessons learned from L2's interaction with γ-secretase will help us understand the functional and structural interactions of γ-secretase with its different cargos, and could aid in developing more selective and efficient γ-secretase inhibitors.

4.5 Final remarks

In sum, my dissertation illuminates the strategy employed by HPV to overcome the challenges of intracellular trafficking, including how the virus exposes itself to the cytosol so that it can hijack host sorting factors essential for nuclear entry. My work provides a roadmap for how HPV transits two distinct organelles – the endosome and Golgi – en route for the nucleus to establish infection. Furthermore, my dissertation research illustrates how viruses can teach us concepts fundamental to cell biology. By investigating the HPV entry mechanism, we learn how a virus hijacks cellular machinery to perform atypical functions (via p120/γ-secretase-mediated membrane insertion of a viral protein), and how the same virus later transits through the classical retrograde trafficking pathway (by exploiting the COPI retrograde sorting machinery). The intracellular transport mechanisms of HPV are not only fascinating – they are of particular importance to human health. Given the widespread nature of HPV infections on the global level, it is troubling that there are currently no therapeutic treatments for HPV infections. Thus, understanding the fundamentals of how HPV infects cells remains incredibly important to identify novel therapeutic targets and approaches for antiviral development.

4.6 References

1. J. L. Smith, S. K. Campos, A. Wandinger-Ness, M. A. Ozbun, Caveolin-1-dependent infectious entry of human papillomavirus type 31 in human keratinocytes proceeds to the endosomal pathway for pH-dependent uncoating. *J Virol* **82**, 9505-9512 (2008).

2. M. Bienkowska-Haba, C. Williams, S. M. Kim, R. L. Garcea, M. Sapp, Cyclophilins facilitate dissociation of the human papillomavirus type 16 capsid protein L1 from the L2/DNA complex following virus entry. *J Virol* **86**, 9875-9887 (2012).

3. M. C. Harwood, A. J. Dupzyk, T. Inoue, D. DiMaio, B. Tsai, p120 catenin recruits HPV to gamma-secretase to promote virus infection. *PLoS Pathog* **16**, e1008946 (2020).

4. T. Inoue *et al.*, gamma-Secretase promotes membrane insertion of the human papillomavirus L2 capsid protein during virus infection. *J Cell Biol* **217**, 3545-3559 (2018).

5. W. Zhang, T. Kazakov, A. Popa, D. DiMaio, Vesicular trafficking of incoming human papillomavirus 16 to the Golgi apparatus and endoplasmic reticulum requires gamma-secretase activity. *mBio* **5**, e01777-01714 (2014).

6. P. Zhang, G. Monteiro da Silva, C. Deatherage, C. Burd, D. DiMaio, Cell-Penetrating Peptide Mediates Intracellular Membrane Passage of Human Papillomavirus L2 Protein to Trigger Retrograde Trafficking. *Cell* **174**, 1465-1476 e1413 (2018).

7. H. S. Huang, C. B. Buck, P. F. Lambert, Inhibition of gamma secretase blocks HPV infection. *Virology* **407**, 391-396 (2010).

8. G. Barthet, A. Georgakopoulos, N. K. Robakis, Cellular mechanisms of gamma-secretase substrate selection, processing and toxicity. *Prog Neurobiol* **98**, 166-175 (2012).

9. Z. Kouchi *et al.*, p120 catenin recruits cadherins to gamma-secretase and inhibits production of Abeta peptide. *J Biol Chem* **284**, 1954-1961 (2009).

10. A. Kiss, R. B. Troyanovsky, S. M. Troyanovsky, p120-catenin is a key component of the cadherin-gamma-secretase supercomplex. *Mol Biol Cell* **19**, 4042-4050 (2008).

11. A. Lipovsky *et al.*, Genome-wide siRNA screen identifies the retromer as a cellular entry factor for human papillomavirus. *Proc Natl Acad Sci U S A* **110**, 7452-7457 (2013).

12. A. Popa *et al.*, Direct binding of retromer to human papillomavirus type 16 minor capsid protein L2 mediates endosome exit during viral infection. *PLoS Pathog* **11**, e1004699 (2015).

13. S. DiGiuseppe *et al.*, Incoming human papillomavirus type 16 genome resides in a vesicular compartment throughout mitosis. *Proc Natl Acad Sci U S A* **113**, 6289-6294 (2016).

14. M. C. Lee, E. A. Miller, J. Goldberg, L. Orci, R. Schekman, Bi-directional protein transport between the ER and Golgi. *Annu Rev Cell Dev Biol* **20**, 87-123 (2004).

15. V. Popoff, F. Adolf, B. Brugger, F. Wieland, COPI budding within the Golgi stack. *Cold Spring Harb Perspect Biol* **3**, a005231 (2011).

16. J. Bethune, F. T. Wieland, Assembly of COPI and COPII Vesicular Coat Proteins on Membranes. *Annu Rev Biophys* **47**, 63-83 (2018).

17. D. J. Shiwarski, S. E. Crilly, A. Dates, M. A. Puthenveedu, Dual RXR motifs regulate nerve growth factor-mediated intracellular retention of the delta opioid receptor. *Mol Biol Cell* **30**, 680-690 (2019).

18. P. Sharma *et al.*, Endoplasmic reticulum protein targeting of phospholamban: a common role for an N-terminal di-arginine motif in ER retention? *PLoS One* **5**, e11496 (2010).

19. K. Michelsen, H. Yuan, B. Schwappach, Hide and run. Arginine-based endoplasmic-reticulum-sorting motifs in the assembly of heteromultimeric membrane proteins. *EMBO Rep* **6**, 717-722 (2005).

20. K. D. Scheffer *et al.*, Tetraspanin CD151 mediates papillomavirus type 16 endocytosis. *J Virol* **87**, 3435-3446 (2013).

21. G. Spoden *et al.*, Clathrin- and caveolin-independent entry of human papillomavirus type 16--involvement of tetraspanin-enriched microdomains (TEMs). *PLoS One* **3**, e3313 (2008).

22. G. Spoden *et al.*, Human papillomavirus types 16, 18, and 31 share similar endocytic requirements for entry. *J Virol* **87**, 7765-7773 (2013).

23. A. Dziduszko, M. A. Ozbun, Annexin A2 and S100A10 regulate human papillomavirus type 16 entry and intracellular trafficking in human keratinocytes. *J Virol* **87**, 7502-7515 (2013).

24. Z. Surviladze, A. Dziduszko, M. A. Ozbun, Essential roles for soluble virion-associated heparan sulfonated proteoglycans and growth factors in human papillomavirus infections. *PLoS Pathog* **8**, e1002519 (2012).

25. Z. Surviladze, R. T. Sterk, S. A. DeHaro, M. A. Ozbun, Cellular entry of human papillomavirus type 16 involves activation of the phosphatidylinositol 3-kinase/Akt/mTOR pathway and inhibition of autophagy. *J Virol* **87**, 2508-2517 (2013).

26. C. Y. Abban, P. I. Meneses, Usage of heparan sulfate, integrins, and FAK in HPV16 infection. *Virology* **403**, 1-16 (2010).

27. P. Aksoy, C. Y. Abban, E. Kiyashka, W. Qiang, P. I. Meneses, HPV16 infection of HaCaTs is dependent on beta4 integrin, and alpha6 integrin processing. *Virology* **449**, 45-52 (2014).

28. C. S. Yoon, K. D. Kim, S. N. Park, S. W. Cheong, alpha(6) Integrin is the main receptor of human papillomavirus type 16 VLP. *Biochem Biophys Res Commun* **283**, 668-673 (2001).

29. A. B. Raff *et al.*, The evolving field of human papillomavirus receptor research: a review of binding and entry. *J Virol* **87**, 6062-6072 (2013).

30. M. A. Ozbun, S. K. Campos, The long and winding road: human papillomavirus entry and subcellular trafficking. *Curr Opin Virol* **50**, 76-86 (2021).

31. J. Finke *et al.*, Anatomy of a viral entry platform differentially functionalized by integrins alpha3 and alpha6. *Sci Rep* **10**, 5356 (2020).

32. C. M. Cadwell, W. Su, A. P. Kowalczyk, Cadherin tales: Regulation of cadherin function by endocytic membrane trafficking. *Traffic* **17**, 1262-1271 (2016).

33. K. Xiao, R. G. Oas, C. M. Chiasson, A. P. Kowalczyk, Role of p120-catenin in cadherin trafficking. *Biochim Biophys Acta* **1773**, 8-16 (2007).

34. J. Xie, P. Zhang, M. Crite, C. V. Lindsay, D. DiMaio, Retromer stabilizes transient membrane insertion of L2 capsid protein during retrograde entry of human papillomavirus. *Sci Adv* **7**, (2021).

35. J. Xie, E. N. Heim, M. Crite, D. DiMaio, TBC1D5-Catalyzed Cycling of Rab7 Is Required for Retromer-Mediated Human Papillomavirus Trafficking during Virus Entry. *Cell Rep* **31**, 107750 (2020).

36. A. V. Morante, D. D. Baboolal, X. Simon, E. C. Pan, P. I. Meneses, Human Papillomavirus Minor Capsid Protein L2 Mediates Intracellular Trafficking into and Passage beyond the Endoplasmic Reticulum. *Microbiol Spectr* **10**, e0150522 (2022).

37. S. K. Campos, J. A. Chapman, M. J. Deymier, M. P. Bronnimann, M. A. Ozbun, Opposing effects of bacitracin on human papillomavirus type 16 infection: enhancement of binding and entry and inhibition of endosomal penetration. *J Virol* **86**, 4169-4181 (2012).

38. K. Y. Lai *et al.*, A Ran-binding protein facilitates nuclear import of human papillomavirus type 16. *PLoS Pathog* **17**, e1009580 (2021).

39. M. Schelhaas *et al.*, Entry of human papillomavirus type 16 by actin-dependent, clathrin- and lipid raft-independent endocytosis. *PLoS Pathog* **8**, e1002657 (2012).

40. J. F. Soderholm *et al.*, Importazole, a small molecule inhibitor of the transport receptor importin-beta. *ACS Chem Biol* **6**, 700-708 (2011).

41. F. K. Kosyna, R. Depping, Controlling the Gatekeeper: Therapeutic Targeting of Nuclear Transport. *Cells* **7**, (2018).

42. S. Mamoor *et al.*, The high risk HPV16 L2 minor capsid protein has multiple transport signals that mediate its nucleocytoplasmic traffic. *Virology* **422**, 413-424 (2012).

43. P. M. Day *et al.*, Human Papillomavirus 16 Capsids Mediate Nuclear Entry during Infection. *J Virol* **93**, (2019).

44. M. Rizzato *et al.*, Master mitotic kinases regulate viral genome delivery during papillomavirus cell entry. *Nat Commun* **14**, 355 (2023).

45. A. Dupzyk, B. Tsai, Bag2 Is a Component of a Cytosolic Extraction Machinery That Promotes Membrane Penetration of a Nonenveloped Virus. *J Virol* **92**, (2018).

46. A. Dupzyk, B. Tsai, How Polyomaviruses Exploit the ERAD Machinery to Cause Infection. *Viruses* **8**, (2016).

47. A. Dupzyk, J. M. Williams, P. Bagchi, T. Inoue, B. Tsai, SGTA-Dependent Regulation of Hsc70 Promotes Cytosol Entry of Simian Virus 40 from the Endoplasmic Reticulum. *J Virol* **91**, (2017).

48. I. Aydin *et al.*, Large scale RNAi reveals the requirement of nuclear envelope breakdown for nuclear import of human papillomaviruses. *PLoS Pathog* **10**, e1004162 (2014).

49. G. McQuillan, D. Kruszon-Moran, L. E. Markowitz, E. R. Unger, R. Paulose-Ram, Prevalence of HPV in Adults Aged 18-69: United States, 2011-2014. *NCHS Data Brief*, 1-8 (2017).

50. H. W. Chesson, E. F. Dunne, S. Hariri, L. E. Markowitz, The estimated lifetime probability of acquiring human papillomavirus in the United States. *Sex Transm Dis* **41**, 660-664 (2014).

51. T. Y. Walker *et al.*, National, Regional, State, and Selected Local Area Vaccination Coverage Among Adolescents Aged 13-17 Years - United States, 2017. *MMWR Morb Mortal Wkly Rep* **67**, 909-917 (2018).

52. E. A. Van Dyne *et al.*, Trends in Human Papillomavirus-Associated Cancers - United States, 1999-2015. *MMWR Morb Mortal Wkly Rep* **67**, 918-924 (2018).

53. CDC, "Cancers Associated with Human Papillomavirus, United States—2015–2019," *USCS Data Brief, no. 31* (Atlanta, GA: Centers for Disease Control and Prevention, US Department of Health and Human Services, 2022).

54. M. Lechner, J. Liu, L. Masterson, T. R. Fenton, HPV-associated oropharyngeal cancer: epidemiology, molecular biology and clinical management. *Nat Rev Clin Oncol* **19**, 306-327 (2022).

55. J. C. Cardoso, E. Calonje, Cutaneous manifestations of human papillomaviruses: a review. *Acta Dermatovenerol Alp Pannonica Adriat* **20**, 145-154 (2011).

56. C. Pingali *et al.*, National, Regional, State, and Selected Local Area Vaccination Coverage Among Adolescents Aged 13-17 Years - United States, 2020. *MMWR Morb Mortal Wkly Rep* **70**, 1183-1190 (2021).

57. C. I. Liao *et al.*, Trends in Human Papillomavirus-Associated Cancers, Demographic Characteristics, and Vaccinations in the US, 2001-2017. *JAMA Netw Open* **5**, e222530 (2022).

58. J. Spayne, T. Hesketh, Estimate of global human papillomavirus vaccination coverage: analysis of country-level indicators. *BMJ Open* **11**, e052016 (2021).

59. K. Zheng *et al.*, The Reservoir of Persistent Human Papillomavirus Infection; Strategies for Elimination Using Anti-Viral Therapies. *Viruses* **14**, (2022).

60. A. Fradet-Turcotte, J. Archambault, Recent advances in the search for antiviral agents against human papillomaviruses. *Antivir Ther* **12**, 431-451 (2007).

61. J. R. Beadle *et al.*, Synthesis and Antiviral Evaluation of Octadecyloxyethyl Benzyl 9-[(2-Phosphonomethoxy)ethyl]guanine (ODE-Bn-PMEG), a Potent Inhibitor of Transient HPV DNA Amplification. *J Med Chem* **59**, 10470-10478 (2016).

62. Y. Liu *et al.*, Current strategies against persistent human papillomavirus infection (Review). *Int J Oncol* **55**, 570-584 (2019).

63. P. Zhang, R. Moreno, P. F. Lambert, D. DiMaio, Cell-penetrating peptide inhibits retromer-mediated human papillomavirus trafficking during virus entry. *Proc Natl Acad Sci U S A* **117**, 6121-6128 (2020).

64. J. R. Kane *et al.*, A polyomavirus peptide binds to the capsid VP1 pore and has potent antiviral activity against BK and JC polyomaviruses. *Elife* **9**, (2020).

65. A. Haapasalo, D. M. Kovacs, The many substrates of presenilin/gamma-secretase. *J Alzheimers Dis* **25**, 3-28 (2011).

66. G. Yang *et al.*, Structural basis of Notch recognition by human gamma-secretase. *Nature* **565**, 192-197 (2019).

67. R. Zhou *et al.*, Recognition of the amyloid precursor protein by human gamma-secretase. *Science* **363**, (2019).

68. M. Crite, D. DiMaio, Human Papillomavirus L2 Capsid Protein Stabilizes gamma-Secretase during Viral Infection. *Viruses* **14**, (2022).